8-2021

A Phenological Model for a Southern Population of Mountain Pine Beetle

Catherine E. Wangen
Utah State University

A PHENOLOGICAL MODEL FOR A SOUTHERN POPULATION OF MOUNTAIN

PINE BEETLE

by

Catherine E. Wangen

A thesis submitted in partial fulfillment
of the requirements for the degree

of

MASTER OF SCIENCE

in

Statistics

Approved:

_____   _____
James Powell, Ph.D.   Barbara Bentz, Ph.D.
Major Professor   Committee Member

_____   _____
John Stevens, Ph.D.   D. Richard Cutler, Ph.D.
Committee Member   Interim Vice Provost of Graduate Studies

UTAH STATE UNIVERSITY
Logan, Utah

2021

ABSTRACT

A PHENOLOGICAL MODEL FOR A SOUTHERN POPULATION OF MOUNTAIN
PINE BEETLE

by

Catherine E. Wangen, Master of Science

Utah State University, 2021

Major Professor: James Powell, Ph.D.
Department: Mathematics and Statistics

The mountain pine beetle (MPB, *Dendroctonus ponderosae* Hopkins) attacks living *Pinus* trees across a widespread area of western North America, causing significant ecological and economic damage. The ability to make accurate predictions of how MPB populations across this range will respond to changing temperatures, which directly but non-linearly affect MPB progress through life stages, is essential for optimal forest management. There is not currently a predictive phenology model for populations of southern MPB, despite concerns that those populations may be more susceptible to change from univoltinism to bivoltinism, which would have devastating impacts on pine forests. While there are models for northern MPB populations, northern and southern populations are genetically different in response to temperature, and consequentially southern populations require geographic-specific model parameters. In this thesis I develop a novel oviposition model for populations of southern MPB, which I incorporate in a phenological cohort model that allows estimation of previously unknown development rates for the southern MPB teneral adult stage, completing a southern MPB phenological model.

In Chapter 2 I develop a predictive oviposition model for a southern population of MPB using the oviposition rate curve developed by McManis et al. (2019), incorporating

variation in both oviposition rate and fecundity. I also introduce a method for determining the time delay before oviposition, t_0. The model can return the probability of oviposition for a season of MPB attacks using phloem temperature and adult MPB attack data collected from a single field site over two years. I also develop an asymptotic approximation of MPB oviposition that is less complex as well as less computationally taxing. The detailed oviposition model and its asymptotic approximation are compared with other previously used modeling methods. The predictive capacity of each model is evaluated against laboratory data collected on southern MPB oviposition.

McManis et al. (2018) parameterized development from eggs through pupation for a southern MPB population, but were unable to procure developmental data for the difficult-to-observe teneral adult stage. In Chapter 3 I determine developmental rates for the difficult to observe teneral adult stage using a cohort phenology model and the field data for a southern population of MPB. I first present the incorporated models as well as teneral adult rate curves tested while developing the model. Then I explain the method by which the teneral adult rate curves were parameterized and how the Brière curve was determined to be most suitable. The resulting model is then validated using an additional sample tree from the field data. The complete model is then used to examine the potential for bivoltinism in a southern population of MPB by increasing the mean temperature and testing for the successful emergence of a second generation. My model estimates that that southern MPB are unlikely to become bivoltine in warmer temperatures due to upper developmental thresholds of teneral adults.

(136 pages)

PUBLIC ABSTRACT

A PHENOLOGICAL MODEL FOR A SOUTHERN POPULATION OF MOUNTAIN
PINE BEETLE

Catherine E. Wangen

The mountain pine beetle (MPB, *Dendroctonus ponderosae* Hopkins) attacks living *Pinus* trees across a widespread area of western North America, causing significant ecological and economic damage. The ability to make accurate predictions of how MPB populations across this range will respond to temperatures, which affect MPB progress through life stages, is essential. Northern and southern populations of MPB are genetically different in response to temperature, requiring geographic-specific model parameters. There is not currently a predictive model for the southern MPB life cycle, despite concerns that those populations may be more susceptible to increased numbers of generations per year, which would have devastating impacts on pine forests. In this thesis I develop a novel oviposition model for populations of southern MPB, which I incorporate into a cohort model that allows estimation of previously unknown development rates for the southern MPB teneral adult stage, resulting in a complete southern MPB life cycle model.

In Chapter 2 I develop a predictive oviposition model for a southern population of mountain pine beetle using the oviposition (egg-laying) rate curve developed by McManis et al. (2019), incorporating variation in both oviposition rate and fecundity. I also introduce a method for determining the time delay before oviposition, t_0. The model can return the probability of oviposition for a season of MPB attacks using phloem (inner-bark) temperature and adult MPB attack data collected from the field. I also develop an asymptotic approximation of MPB oviposition that is less complex as well as less computationally taxing. The detailed oviposition model and its asymptotic approximation are compared

with other previously used modeling methods. The predictive capacity of each model is evaluated against laboratory data collected on southern MPB oviposition.

McManis et al. (2018) parameterized development from eggs through pupation for a southern MPB population, but were unable to procure developmental data for the difficult-to-observe teneral adult stage. In Chapter 3 I determine developmental rates for the teneral adult stage using a phenology model and the field data for a southern population of MPB. I first present the incorporated models as well as teneral adult rate curves tested while developing the model. Then I explain the method by which the teneral adult rate curves were parameterized and how the Brière curve was determined to be most suitable. The resulting model is validated using an additional tree from the field data. The complete model is then used to examine the potential for bivoltinism in a southern population of MPB by increasing the mean temperature and testing for the successful emergence of a second generation. My model estimates that that southern MPB are unlikely to become bivoltine in warmer temperatures due to upper developmental thresholds of teneral adults.

ACKNOWLEDGMENTS

I am truly thankful for the support and guidance of my advisor, Dr. James Powell. I am also appreciative for the very helpful feedback of my committee members, Dr. Barbara Bentz and Dr. John Stevens. Many thanks to Gary Tanner, for being an indispensable Graduate Program Coordinator.

CONTENTS

LIST OF TABLES

LIST OF FIGURES

CHAPTER 1

INTRODUCTION

The mountain pine beetle (MPB, *Dendroctonus ponderosae* Hopkins, Coleoptera: Scolytidae), attacks living *Pinus* trees across a large geographic area in western North America ranging from Baja California Norte, Mexico, to northern British Columbia and Alberta, Canada (Dowle et al. 2017). Adults must attack en masse to overwhelm host defenses in order to successfully kill a *Pinus* host and reproduce in the inner-bark (phloem), as a host will successfully repel a small number of attacking MPB. MPB progress through the stages of their life cycle according to varying temperature thresholds, and thus phloem temperatures directly but non-linearly affect development (Bentz et al. 1991; Powell and Logan 2005). These thresholds allow MPB to be successful in a thermal niche where they are univoltine, and synchronize emergence from dead *Pinus* hosts in order attack new living hosts simultaneously.

Changing temperatures have geographically increased that thermal niche and allowed the MPB range to expand, resulting in MPB-induced tree mortality of over 5.2 million hectares in western Canada (Meddens et al. 2012). The range of *Pinus* host species in western North America extends both northward and southward beyond the known historical distribution of MPB (Giroday et al. 2012; Sambaraju et al. 2019), indicating that this expansion could continue further. Increases in temperatures have allowed MPB migration northward in Canada due to decreased winter mortality, and it is projected billions of dollars in damage could be done in British Columbia by 2054 (Corbett et al. 2015). Factors delimiting the range of southern MPB populations are less known, and while MPB were once considered rare to absent south of the USA, MPB were recently found in dead *Pinus strobiformus* in Chihuahua, Mexico (Armendáriz-Toledano et al. 2017). Accurate predictive models are becoming more critical as research suggests all aspects of insect outbreak behavior, include voltinism (the number of generations per year), will increase due to climate

change (Logan et al. 2003).

Thermal input is the main driver of many exothermic life cycles, including insects in general and MPB in particular. The idea of integrating temperature through time to predict life history events dates back to the degree day model of de Reamur in 1735, in which development rate is assumed to be linear above a temperature threshold (Bonhomme 2000). In more recent times, empirical non-linear models, such as the logistic equation of Davidson (Davidson 1944), the matched asymptotic curves of Logan et al. (1976), and the Brière curve (Brière et al. 1999) improve upon degree day models by incorporating non-linearity at high and low temperature thresholds. While details of thermal response vary among rate curves, they all provide a way to sum developmental response to varying temperatures over time and predict timing of observable life history events.

While some models focus exclusively on the development of a typical (median) individual, this ignores the intrinsic variability of rates/fecundity in a population. The most frequently used models incorporating developmental variability are distributed delays (assuming development is a Poisson process), individual based (directly sampling from an assumed distribution of rates, usually normal or lognormal), and cohort-based (requiring a computational or analytic inversion of the rate distribution to ascertain a distribution of emergence times). These models can be used to understand the competing requisites of bet hedging (to avoid catastrophic events) and synchronization (to find/attack hosts and encounter mates).

Another important consideration is how temperature dependent rate models incorporate the natural variability in rates. Models that focus only on the development of a median individual ignores the intrinsic variability of rates/fecundity in a population, which skews predictions. Instead more frequently used models incorporating developmental variability by using distributed delays (which assume development is a Poisson process), individual based variability (by directly sampling from an assumed, usually normal or lognormal, distribution of rates), and cohort-based (which require a computational or analytic inversion of the rate distribution to ascertain a distribution of emergence times for each cohort). For

many insects, this genetic variability in developmental timing is crucial as it increases the chances that offspring distributed throughout the year will be able to obtain the resources necessary for survival and reproduction (Hopper 1999). In contrast to these overlapping generations that optimize resource attainment, many specialist poikilotherms such as MPB require synchronous emergence from a life stage in order to take advantage of ephemeral resources for successful mating and reproduction, or to successfully attack a host.

1.1 Southern MPB Oviposition

Similar to other developmental stages of insects, the oviposition process is often controlled by temperature. In contrast, however, behavioral aspects unique to oviposition create unique modelling challenges. Oviposition includes behavioral factors such as host selection and placement of eggs, as opposed to larval or pupal lifestages in which an organism is primarily focused on feeding and development with no or minimal movement. There are many factors of oviposition strategy that can be contradictory, for instance the challenge of finding a suitable host while there is still the possibility of continuing on to find an even better host (Janz 2002). The distribution and number of eggs is effectively an optimum foraging problem for insects that oviposit on discrete patches of larval resources (Ives 1989). When more than one female oviposits on a single resource, optimal clutch size is dependent on the competition between larvae of a single female, as well as the competition between larvae from other females. These pre-ovipositional behaviors can directly affect the timing of oviposition and are thus important to consider when developing a model. The required synchrony of MPB attacking a host leads to trade-offs during oviposition, as intraspecific competition is an inherent aspect of the process.

Additionally MPB, like many insects, exhibit variability in total number of eggs (fecundity) of an individual. To complicate matters, MPB oviposition is difficult to observe directly as it occurs in the phloem underneath the bark of a host tree, and accordingly McManis et al. (2019) performed non-invasive x-ray imaging on MPB infested boards. The authors parameterized an oviposition rate curve for a southern population of MPB accounting for variability in fecundity and rate, but suggested no predictive model. While previous

predictive *Dendroctonus* oviposition models incorporate one or the other of these sources of variability, no previous predictive model incorporates both (McManis et al. 2019).

Female MPB have a unique oviposition behavior, in which after mating within the tree there is a period of several days during which the female is boring further into the host (Amman 1972; McManis et al. 2019). This egg free distance allows MPB to circumvent the defensive response of the *Pinus* host by interrupting resin delivery, as well as conserve moisture and avoid desiccation. There is not currently a predictive model taking into account this time to excavate the egg-free gallery, t_0, which is important to include in order to determine when oviposition truly starts. Unlike many other insects in which females oviposit a single clutch relatively quickly (Ives 1989), MPB females lay individual eggs over the course of many days as an egg gallery is bored (Amman 1972), leading to great variability in times of oviposition.

In Chapter 2 I use the oviposition rate curve developed by McManis et al. (2019) to develop a predictive oviposition model for a southern population of mountain pine beetle, incorporating both varying oviposition rate and fecundity. I also assess two different methods for calculating the time delay before oviposition, t_0, during which the egg-free gallery is constructed, and establish that this process occurs at a rate unrelated to oviposition. The model can predict the probability of oviposition for a season of beetle attacks using phloem temperature and adult mountain pine beetle attack data collected from the field. I also derive an asymptotic approximation of MPB oviposition which is simpler and more computationally efficient. The oviposition model derived from the McManis rate curve and the asymptotic approximation are compared with other modeling approaches, including a median model and cohort model previously used to predict oviposition for a northern MPB population.

1.2   Southern MPB Teneral Adult Rates

The MPB has a univoltine (one-year) life cycle across most of its range, though in some regions semi-voltine (two-year) emergence is also present. A majority of the MPB life cycle is spent inside the phloem of a *Pinus* host, other than for a period of a few days in

late summer (late July to early September) during which newly developed parent adults emerge to search for a new living host. MPB females attract males with pheromones for reproduction, and initiate mass attacks on new host trees. After mating and oviposition, nearly all adult beetles perish within the tree, and their offspring complete the life cycle in the following summer.

While wild populations of MPB are most commonly univoltine and occasionally semi-voltine, there are concerns that warmer temperatures from range expansion or global warming could lead to wild bivoltine populations, which could have significant impacts on pine forests. MPB bivoltinism faces the significant barrier of the cold tolerance of certain lifestages. Though larger larvae have a level of cold tolerance, MPB eggs and pupae are considered to have the lowest cold tolerance among MPB lifestages and could experience significant mortality if correct seasonality was not maintained (Bleiker and Smith 2019; Reid and Gates 1970). Mortality occurs with exposure to 0℃ for both egg and pupal stages, (Bleiker and Smith 2019; Bleiker et al. 2017). A phenology model parameterized for northern US MPB populations suggests bivoltinism is possible in the southern MPB range under future warming scenarios (Bentz et al. 2016), though bivoltine MPB have not been observed in the field (Bentz and Powell 2014).

However, geographic-specific models are required as northern and southern MPB populations are genetically different in response to temperature, and southern MPB have been found to have longer generation times in northern MPB temperatures (Bentz and Powell 2014). McManis et al. (2018; 2019) successfully parameterized a phenology (life-cycle) model for a southern population of MPB from lab data, using infested phloem in 'sandwiches' between layers of glass. However they were unable to parameterize the teneral adult stage, which ends when the MPB leave the tree to find a new host, since adults could not leave the sandwich. Developmental parameters found by for the southern population varied from those found for northern MPB (Régnière et al. 2012), but not enough to account for longer observed developmental time of Arizona MPB populations, which suggests that teneral adult rates must be considerably lower in order to account for this time (McManis

et al. 2018). Soderberg et al. (2021) completed reciprocal translocation experiments with southern and northern populations of MPB, and observed seasonally appropriate univoltine emergence at all sites, suggesting that MPB have adapted to remain univoltine even in warmer environments. In the absence of a model of teneral adult development it is not possible to predict if the southern population, which is most likely to experience significant warming, could potentially become bivoltine.

In Chapter 3 I use a phenology model and field data for a southern population of mountain pine beetle in order to determine developmental rates for the cryptic teneral adult stage. I first introduce rate models for the earlier life stages using the parameters of McManis et al. (2018). I develop a model for deviance between the model predictions and field observations, which is used to connect candidate teneral models to emergence distributions. Teneral curves were parameterized using field data collected from two trees for a southern MPB population in Arizona, and the most suitable curve was selected by comparing nominal and bootstrapped AIC values. The complete model was then cross-validated using an additional tree from the field data. I then increase mean temperatures in the model and maintain reasonable constraints for appropriate seasonality to examine the possibility of bivoltinism in a southern population of MPB.

My results shed light on how the previously unmodeled southern MPB oviposition and teneral adult life stage differ from northern populations, and can inform future responses to forest management with a complete phenological model.

CHAPTER 2

OVIPOSITION MODEL FOR A SOUTHERN POPULATION OF MOUNTAIN PINE

BEETLE

2.1 Introduction

Poikilotherms, animals which are unable to self regulate body-temperature, comprise the vast majority of life on earth. Without the ability to regulate body temperature, these animals are dependent upon external temperatures for their life cycles, and correspondingly at risk to be affected by climate change. Thomas et al. (2004) predicted that 13-24% of the animals in their study area would become extinct due to global warming. Beyond imminent extinction, changes in temperature are critical for many developmental processes, including those of insects. The impact of changing temperatures on insect life cycles could increase both the range and emergence of pest insects (Logan et al. 2003). While the impacts of changing temperatures on these insects will be observable as they occur, a greater understanding is necessary predict these changes and prevent ecological and economic damage.

The idea of integrating temperature through time to predict life history events dates back to the degree day model of de Réaumur in 1735 (Bonhomme 2000), in which development rate is assumed to be directly proportional to temperature above threshold. In more recent times, empirical non-linear models, such as the logistic equation of Davidson (1944), the matched asymptotic curves of Logan et al. (1976), and the Brière curve (1999) improve upon degree day models by reflecting non-linearity at high and low temperature thresholds. Incorporating rate curves into deterministic models allows for predictions from one year to the next, such as the circle map model of Logan and Powell (2001). For many insects with a seasonal life cycle, these models can be used to predict possible changes in generation time due to warming temperatures. Changes in voltinism, the number of generations/broods an insect completes in a single year, could result in increased population growth of herbivorous

forest pests and lead to increased tree mortality (Bentz and Powell 2014). Accurate predictive models are becoming more critical as research suggests all aspects of insect outbreak behavior, include voltinism, will increase due to climate change (Logan et al. 2003).

In addition to the relationship between rate models and temperature, another consideration is how models incorporate the natural variability in rates. While some models focus exclusively on the development of a median individual, this ignores the intrinsic variability of rates/fecundity in a population. The most frequently used models incorporating developmental variability are distributed delays (assuming development is a Poisson process), individual based (directly sampling from an assumed distribution of rates, usually normal or lognormal), and cohort-based (requiring a computational or analytic inversion of the rate distribution to ascertain a distribution of emergence times). For many opportunistic poikilotherms this genetic variability in developmental timing is critical, as it increases the chances that offspring distributed throughout the year will have the resources necessary for survival (Hopper 1999). Many specialist poikilotherms require synchrony to take advantage of ephemeral resources and for successful mating and reproduction. This synchrony can lead to ovipositional trade-offs, as intraspecific competition is a necessary part of the process.

Oviposition strategies are dependent on many factors that are often contradictory, such as the difficulty of finding a suitable host and the possibility of continuing to find an even better host (Janz 2002). Many insects oviposit on discrete patches of larval resources (Ives 1989), and the distribution and number of eggs is effectively an optimum foraging problem. When more than one female oviposits on a resource, optimal clutch size depends not only on the competition between larvae of a single female, but the competition between groups of larvae from different females. As with the progress through developmental lifestages, the oviposition process is controlled by temperature. Unlike these lifestages however, oviposition is a behavioral life phase, which creates additional modeling challenges. As opposed to larval or pupal lifestages in which an organism is primarily focused on feeding and development with minimal movement, oviposition includes behavioral factors such as site or host selection and placement of eggs to avoid larval competition and protect offspring. These

pre-ovipositional behaviors can directly affect the timing of oviposition. Many of these themes are present in the case of the moutain pine beetle (MPB, *Dendroctonus ponderosae* Hopkins, Coleoptera: Scolytidae), a species of economic and environmental concern.

Temperatures directly but non-linearly affect progress through stages of the MPB life cycle which have varying temperature thresholds (Bentz et al. 1991; Powell and Logan 2005). Adults must attack a host simultaneously to overwhelm host defenses and successfully colonize a *Pinus* host, ovipositing in the inner-bark (phloem) and killing the host tree. MPB have variable rates of development across their life cycle but require synchrony in order to successfully reproduce and oviposit in hosts (McManis et al. 2019). Too many eggs can increase intraspecific competition among the developing larvae and result in reduced survival (Cole 1962). This increased intraspecific competition ultimately results in less than optimal reproductive success for food, in this case phloem of a certain thickness in the *Pinus* host tree (Amman 1972). Conversely, death of the host is necessary for successful MPB reproduction, and can only be achieved by the synchronous attack of many beetles (Logan and Powell 2001). The host tree will successfully expel the beetles via defensive resin if the number of beetles that attacks a tree is too low.

MPB attack living *Pinus* trees across an extensive area in Western North America ranging from Baja California Norte, Mexico, to northern British Columbia and Alberta, Canada (Dowle et al. 2017). Changing temperatures have broadened the MPB niche geographically, leading to tree mortality of over 5.2 Mha in the western US (Meddens et al. 2012). The distribution of *Pinus* host species in western North America extends both northward and southward beyond the known historical distribution of MPB (Giroday et al. 2012; Sambaraju et al. 2019). Increases in temperatures have allowed MPB migration northward and eastward in Canada, where it is projected billions of dollars in damage could be done in British Columbia by 2054 (Corbett et al. 2015), but the possible future effects on southern MPB populations are less known. Northern and southern MPB populations are genetically different in response to temperature, requiring geographic-specific model parameters. An accurate predictive model of southern MPB oviposition is critical to predict possible changes

in voltinism and range.

Oviposition data among *Dendroctonus* species is difficult to observe directly as it occurs in the phloem underneath the bark of a host tree. After mating within the tree there is a period of several days during which the female is boring further into the host (Sahota and Thomson 1979). This egg free distance allows MPB to avoid the potentially fatal induced resin response of the *Pinus* host as well as to avoid desiccation. Taking into account this time to excavate the egg-free gallery, t_0, is important for determining when oviposition truly starts, but there is not currently a predictive model. Females then lay individual eggs over the course of many days as an egg gallery is bored (Amman 1972), unlike many other insects in which females oviposit a single clutch relatively quickly (Ives 1989). MPB, like many insects, exhibit variability in both oviposition rate and total number of eggs (fecundity) of an individual. While previous predictive *Dendroctonus* oviposition models incorporate one of these sources of variability, no predictive model incorporates both (2019). McManis et al. (2019) performed non-invasive x-ray imaging on MPB infested boards and parameterized an oviposition rate curve for a southern population of MPB accounting for both sources of variability, but these authors suggested no predictive model.

The goal of this chapter is to develop the predictive oviposition model for a southern population of mountain pine beetle using the oviposition rate curve developed by McManis et al. (2019), incorporating both varying oviposition rate and fecundity. We also describe a method for calculating the time delay before oviposition, t_0, and establish that this process occurs at a rate unrelated to oviposition. Using phloem temperature and adult mountain pine beetle attack data collected from the field, the model can return the probability of oviposition for a season of beetle attacks. We also develop a simpler and less computationally taxing asymptotic approximation of MPB oviposition. The detailed oviposition model (MPBovi) and its asymptotic approximation are compared with other modeling approaches, including a median model and cohort model (Gilbert et al. 2004) which were previously used to predict oviposition for a northern (Utah/Idaho) MPB population. The predictive capacity of each model is tested against McManis' laboratory data on southern

MPB oviposition.

2.2 Models for MPB Oviposition

For insects and other organisms whose oviposition is completely or mostly determined by temperature, predictive models of the relationship between temperature and phenology (developmental timing) are based on the idea of relating the fraction of progress through a lifestage to rate functions of that lifestage (Cobbold and Powell 2011; Logan and Powell 2001). If $a(t)$ represents the fraction of development towards completion of oviposition j by time t, then

$$\frac{da}{dt} = r_0(T(t)), \quad a(t_0) = 0 \tag{2.1}$$

where $r_0 T(t)$ is the rate of oviposition, dependent on the temperature of the organism's environment, $T(t)$. The initial condition of $a(t_0) = 0$ indicates oviposition begins immediately after the egg-free gallery is completed. Equation (2.1) can be solved by integrating

$$1 = a(t) = \int_{t_0}^{t_1} r_0(T(\tau)) \, d\tau, \tag{2.2}$$

where oviposition is completed at at time t_1, and the next life stage (the development of eggs) begins. The simplest example of a developmental rate function is the degree day model,

$$r(T) = \psi \cdot \max(T - T_b, 0) \tag{2.3}$$

in which T_b is the lower temperature threshold, and ψ is 1/degree days required to complete oviposition.

Basedo on this, Logan and Bentz (1999) developed a model that determines the median day of oviposition, using where the rate is simply 1/time to the median oviposition state, and correspondingly to find the median day of oviposition the rate is summed to 1

$$1 = \sum_{\text{start day}}^{\text{median day}} D_i \tag{2.4}$$

where D is the proportion of the oviposition completed on day i summed over hours,

$$D_i = \sum_{n=1}^{24} r_0 T(t) \Delta t \qquad (2.5)$$

and t_n is the nth hour of day i with $\Delta t =$ hour. Though this allows for a predictive model with an output of a single day, it does not take into account variability in either fecundity or rate nor the fact that eggs are distributed continuously along the gallery after the egg-free length. To include some variability for eggs being laid over time, Gilbert et al. (2004) used the Extended von Foerester equation (EvF),

$$\frac{\delta}{\delta t} u(a,t) + r_0[T(t)] \frac{\delta}{\delta a} u(a,t) = \frac{1}{2} \sigma_0^2 \frac{\delta^2}{\delta a^2} u \qquad (2.6)$$

which expands upon Logan and Bentz's model by assuming rates are normally distributed with mean $r_0(T)$ and variance σ_0^2, and reflects the distribution in times at which different individual eggs are laid. Then $u(a,t)$ is the density of eggs at time t and fraction of egg gallery completed a (normalized such that $0 \leq a \leq 1$), $r_0[T(t)]$ is developmental rate at temperature $T(t)$, and $p_0(t) = u(a = 1, t)$ is the distribution of oviposition over time.

The Green's Function solution to the Extended von Foerster equation

$$p_0(t) = \int_0^\infty A(\tau) \frac{e^{\frac{-(1 - \int_{\tau+t0}^{t} r_0(T(s))ds)^2}{2\sigma_0^2(t-\tau+t0)}}}{\sqrt{2\pi\sigma_0^2(t - \tau + t0)^3}} d\tau \qquad (2.7)$$

results in a density of eggs based on a distribution of all attacks $A(\tau)$ over days τ (Powell and Bentz 2009). While this model successfully incorporates variability assuming normally distributed rates, it does not incorporate variability in fecundity.

Taking a different approach, Régnière et al. (2012) used an exponential oviposition rate constant across individuals, but accounted for variability in fecundity using a lognormal distribution. Assuming that each female has a fixed potential fecundity, Ω, and that a female oviposits her remaining potential fecundity, F, at a declining exponential rate dependent

upon temperature, T, the rate of potential oviposition expenditure is

$$\frac{dF}{dt} = -r_0(T)F, \quad F(t = t_0 + \tau) = \Omega \tag{2.8}$$

where oviposition begins at day of attack τ, plus the time required to construct the egg-free gallery t_0. Defining $O(t)$ as the cumulative oviposition at time t, $O(t) = \Omega - F(t)$, the potential fecundity minus the remaining fecundity at time t. Thus for $\tau < t$ the cumulative distribution function for oviposition for females attacking on day τ

$$p_0(t) = 1 - e^{-R(t,\tau+t_0)} \tag{2.9}$$

and $p_0(t) = 0$ when $t_0 + \tau$. Here

$$R(t, t_0 + \tau) = \int_{t_0+\tau}^{t} r_0(T(t'))dt' \tag{2.10}$$

is the cumulative oviposition index from beginning of oviposition to time t.

2.3   Lab Results for Southern MPB

McManis et al. (2019) quantified fecundity of individuals from a southern mountain pine beetle population via non-invasive X-ray imaging of infested boards. Unmated adult southern MPB were obtained from the Kaibab National Forest, near Flagstaff, AZ. Experimental boards were obtained by cutting sections from a southwestern white pine harvested in the same region. Each board was infested with one randomly selected female-male mountain pine beetle pair. Forty infested boards were placed in incubators with constant temperatures of 10, 20, 27, and 29°C. Temperatures were selected to give broad coverage of the oviposition rate curve, emphasizing the upper threshold. During the incubation each board was X-rayed 3 times per week, and oviposition gallery length for successive days was measured using the X-ray images. After 30 days boards were stored at 0°C to stop oviposition and egg development. The phloem and outer bark were peeled from each board and the location of eggs and first instars were marked and photographed. Three boards did not

result in successful galleries and were not included, resulting in 37 boards. Estimated times of oviposition for each egg were calculated assuming a linear relation between observation days, then daily counts were used to create a distribution from the observed lab data.

McManis et al. (2019) observed that oviposition rate and fecundity vary independently. They developed a novel approach to estimating exponential oviposition rates using the X-ray data. The total fecundity for individual m, Ω_m, was found to be related to the fecundity of the median individual, Ω_0, by

$$\Omega_m = \Omega_0 \delta_m, \tag{2.11}$$

where δ_m is lognormally distributed with mean 1 and variance parameter σ_{egg}^2, following (Régnière et al. 2012). Their model also included a normal distribution for individual rates, thus the rate for any individual female m can be written as

$$r_m(T) = r_0(T) + \epsilon_m, \quad \epsilon_m \sim N(0, \sigma_0^2), \tag{2.12}$$

where $r_0(T)$ is the exponential rate function of the median individual which Régnière et al. (Régnière et al. 2012) and McManis et al. (McManis et al. 2019) took to be

$$r_0(T) = \psi \left[e^{\omega(T - T_b)} - \left(\frac{T_m - T}{T_m - T_b} \right) e^{-\frac{\omega(T - T_b)}{\Delta_b}} - (\frac{T - T_b}{T_m - T_b}) e^{\omega(T_m - T_b) - \frac{T_m - T}{\Delta_m}} \right] \tag{2.13}$$

and 0 for $T \notin [T_b, T_m]$. Here T_m and T_b correspond to the upper and lower temperature transitions from normal to negligible development at the upper and lower thresholds, ω describes the expected exponential acceleration of rate with temperature, ψ is proportional to the maximum development rate, and Δ_m and Δ_b are the width of the thermal transitions for the upper and lower thresholds. While McManis successfully described both varying rate and fecundity, it was not clear how to incorporate both into a predictive model.

In addition to incorporating varying rates and fecundity, there is a period of time after MPB mate in the phloem during which the female creates a characteristic "J" shaped initial gallery to avoid host defenses and before beginning oviposition, which we defined as t_0. This period has been shown to temperature dependent in lab experiments, varying 2-13 days at

various constant temperatures for *Dendroctonus* species (McManis et al. 2019; Sahota and Thomson 1979).

Sahota and Thomson (1979) observed variability in both fecundity and oviposition rate via non-invasive X-ray imaging of spruce beetle (*D. rufipennis*) oviposition. Spruce beetle are behaviorally similar to MPB, and relevant as the egg-free distance of *Dendroctonus* species has been minimally studied. Yet their observations were not suitable for a predictive model, as their calculation of rates depended on cumulative gallery length for constant temperatures. The rates correspondingly could not be used for varying temperatures, since mathematically beetles could be required to create negative gallery to achieve shorter galleries at lower temps. Amman (1972) measured the number of MPB eggs laid at constant temperatures, by infesting boards and peeling the bark off after 13 days. Due to this method of data collection the sources of the variability in rate and fecundity were confounded. Without more frequent measurements it is impossible to distinguish if variability in the the number of eggs laid during the sampling period is due to ovipositon rate or fecundity. Thus Amman's data allowed for a model with constant fecundity (Logan et al. 1995) or oviposition rate (Régnière et al. 2012) but not both.

McManis et al. (2019) X-rayed infested MPB boards incubated at constant temperatures of of 10, 20, 27, or 29°C over a thirty day period. After 30 days the bark was peeled off, and the egg free distance of each board, l, was measured directly. Though only female MPB were visible in the X-ray images, the time delay t_0 was calculated using the length of gallery recorded in X-ray images, and interpolating the time at which the egg-free gallery was completed assuming a constant speed of movement. Thus for each board and temperature there is an observed value of t_0. Although the length of gallery constructed before oviposition did not vary among temperatures, t_0 was found to be up to a week longer for the 10°C (the lowest temperature). This difference in t_0 required to build the same length of gallery indicates that gallery construction is a temperature-dependent phase similar to oviposition. As a temperature dependent process construction of the egg-free gallery could possibly affect synchronous and seasonally appropriate emergence.

2.4 Modeling the Time Required to Excavate Egg-Free Distance

We discuss two methods for predicting egg free distance and the hypothesis that the egg free gallery is constructed at a rate proportional to the oviposition rate. We assume that there is a linear relationship between the oviposition rate and the velocity of gallery construction. Integrating the velocity to the average egg free length l_0 gives an estimate of t_0. In contrast, the independent method assumes that the $\frac{1}{t_0}$ value for each board is a direct observation of the rate of gallery construction. We fit these observations to a rate curve (2.3) and use bootstrapping to assess whether or not gallery construction and oviposition occur at related rates.

2.4.1 Egg Free Length Constructed Proportionally to Oviposition

If the velocity of gallery is proportional to the oviposition rate, there exists a constant d such that

$$V(T) = d \cdot r_0(T). \tag{2.14}$$

where the velocity is the time to create the egg free distance divided by observed t_0,

$$V(T) = \frac{l_0}{t_0}, \tag{2.15}$$

with $l_0 = 6.7356$ cm calculated from the data of McManis et al. (McManis et al. 2019). We estimated for the coefficient d using using a linear regression regression, minimizing

$$\sum_{i,j}(V_j(T_i) - d \cdot r_0(T_i))^2 \tag{2.16}$$

where V_j is the jth observation of velocity at T_i=10, 20, 27, 29°C.

2.4.2 Egg Free Length Constructed Independently of Oviposition Rate

We also pursued an independent approach that assumed the egg free distance is independent of oviposition. The parameters for the independent rate of completion of the egg

free distance, $r_{\text{indep}}(T)$, were fit by assuming observed t_{0_j}

$$t_{0_j}(T_i) = \frac{1}{r_{\text{indep}}(T_i)} + \epsilon_j \tag{2.17}$$

where ϵ_j is normal and $r_{\text{indep}}(T_i)$ is given by (2.3). Nonlinear regression parameters appear in Table 2.1.

Life stage	Ω	Ψ	T_b	T_m	Δ_b	Δ_m
Oviposition	0.0913	0.0309	6.6000	30.9000	1.3613	1.9889
Independent	0.0632	0.1773	5.8992	29.6069	2.5514	2.7269

Table 2.1: This table contains the parameter values for the creation of egg free distance found in this paper, as well as the ovipositional parameter values found by McManis et al. (2019).

Determination that Independent Method is Most Appropriate

Assuming that the velocity of gallery construction is proportional to oviposition rate would have been both mechanistic and minimized the number of new parameters needed, as the related rate would be,

$$r_{\text{related}}(t) = \frac{1}{t_0} = \frac{d}{l_{obs}} r_0(T(t)) \tag{2.18}$$

with r_{related} being proportional to the parameters of r_0 by $\frac{d}{l_0}$. However comparing our predicted values of t_0 from the related method to those found by McManis et al. (2019) indicated that the predicted values were particularly error prone at extreme temperatures (Figure 2.4) and that the independent method was more consistent with observations, and the independent rate curve appears more suitable.

The related method results in a poor fit to t_{obs} (Figure 2.4), because variability in observed t_0 and l_0. The assumption that the rate is related to the velocity introduces this compounding factor that may have reduced the fit. In addition, the related method

is inherently restricted by the oviposition curve. The derivation of the related rate curve ultimately results in a rate that is the oviposition rate multiplied by the constant $\frac{d}{l_0}$. Thus the parameters of T_b, T_m, and the temperature where max rate occurs, T_{opt}, cannot differ from the initial oviposition rate curve. As seen in Figure 2.5, the more suitable independent rate curve has significantly different values for these parameters.

To computationally verify that the parameters of the independent method are distinct from the parameters of the oviposition and related method, the related method rate curve was fit to 1000 bootstraps of the infested board data by minimizing (2.16). All of the independent curve parameters differed from the oviposition curve parameters significantly. The temperature thresholds T_b and T_m were smaller in 87.3% and 100% of bootstrapped cases (Figures 3.26 and 3.27). The temperature at which maximum rate is achieved, T_{opt}, was calculated for each of the bootstrapped independent curves. The nominal T_{opt} value of 24.59°C, and 100% of the bootstrapped T_{opt} values were less than the oviposition curve of 27.01°C.

While the independent method was ultimately much more suitable for predicting the time required to excavate the egg free distance, this highlights the fact that that excavating egg free distance has differing temperature thresholds, and is a biologically distinct process.
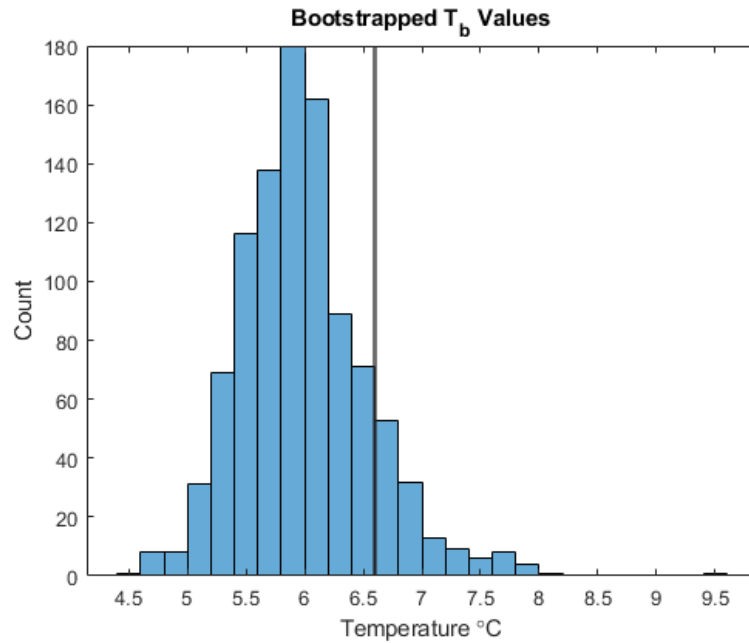
Fig. 2.1: Histogram of minimum temperature thresholds (T_b) generated for 1000 bootstrapped fits of the independent rate curve. In 87.3% of cases T_b was smaller than the related T_b of 6.6°C, which is noted by the vertical line.
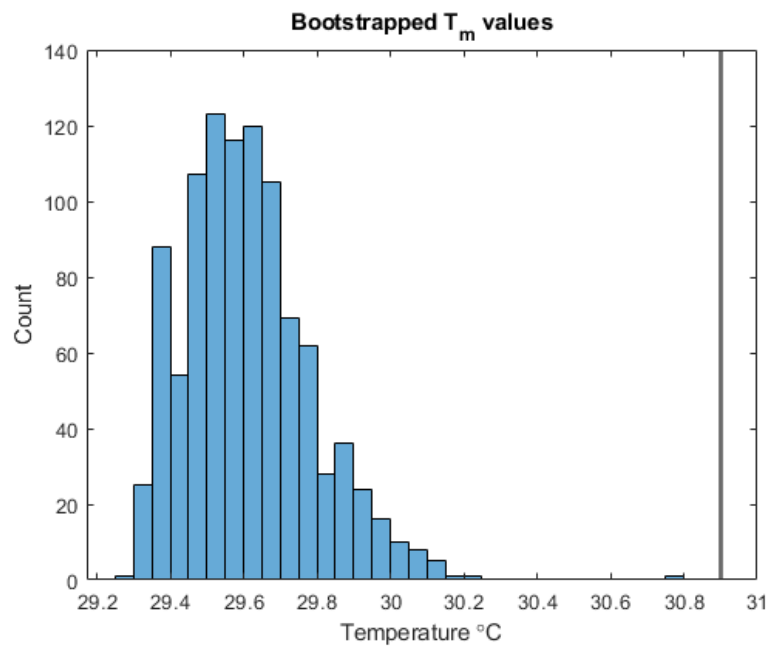
Fig. 2.2: Histogram of maximum temperature (T_m) thresholds generated for 1000 bootstrapped fits of the independent rate curve. In 100% percent of cases T_m was smaller than the related method T_m of 30.9°C, which is noted by the vertical line.
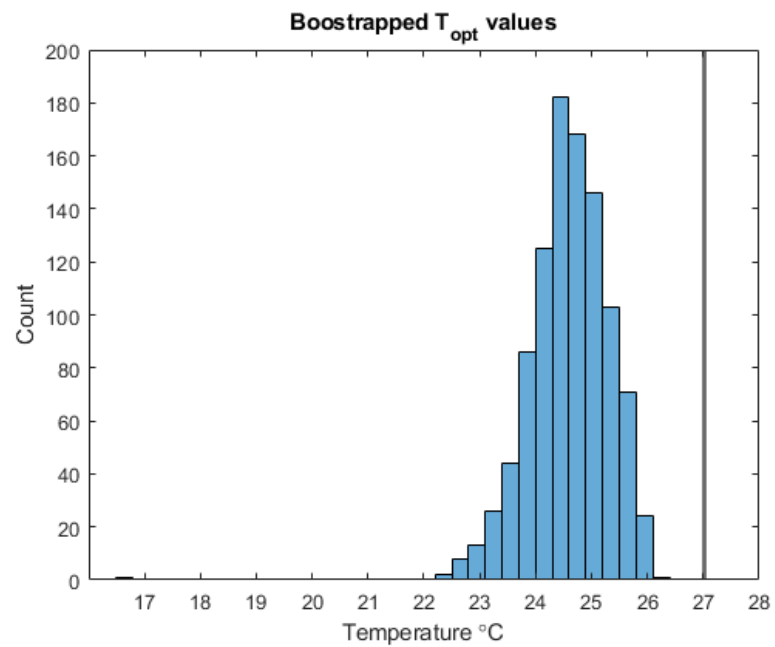
Fig. 2.3: Histogram of optimum temperature thresholds (T_{opt}) generated for 1000 bootstraps of the related method rate curve. In 100% of cases the temperature at which the maximum rate occurred, T_{opt} was greater than the related value of 27.0067, which is noted by the vertical line.

2.4.3   Variability in Time for Egg-Free Gallery Construction

We wanted to be certain that the variability of predicted t_0 values would remain reasonably low, as high variability could poorly estimate t_0 at varying field temperatures, and necessitate using a more computationally taxing cohort model. This was done by calculating the variance between the predicted and observed rates, and using the the Extended von Foerester model (2.7) to project the overall variability in predicted time to complete the egg-free length at constant and varying field temperatures.

We estimated $\sigma^2 = 0.031$, and using EvF found the impact of variability was small at 15, 20, and 25°C (2.6), and more significant at 10°C, with a variance in median completion time of ± 2 days. This variance in time is relatively minor, particularly considering that field temperatures are close to 10°C only a small percentage of the time during the excavation of the egg-free distance. When calculating the distribution with the field phloem temperature data (Figure 2.7) the variability was much smaller for an increase of 5°C, which is more likely to occur than a decrease with current temperature warming predictions. Since the impact of variability was so small, we chose to neglect variability in order to reduce computational complexity. Thus, to calculate the time to begin oviposition, cumulative daily rates were used in equation (2.3), and t_0 was calculated by integrating to 1.
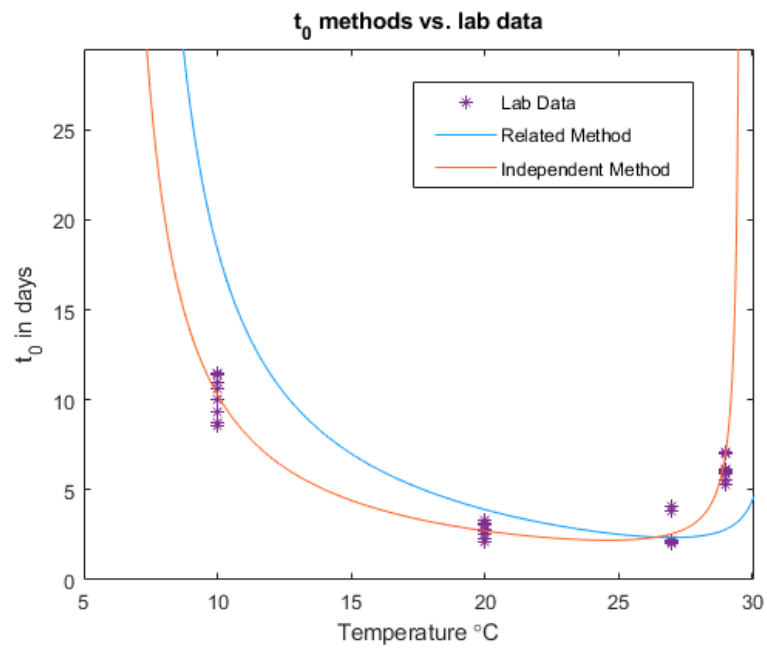
Fig. 2.4: Observed t_0 values in the laboratory for constant temperature with predicted values of both the related (blue) and independent (orange) methods. Values of t_0 were recorded for infested boards incubated at constant temperatures of at 10, 15, 25, and 29°C. The temperature thresholds of the related method result in a poorer fit at the extremes as well as overall, while the new thresholds of the independent method allow for a more suitable fit to the data.
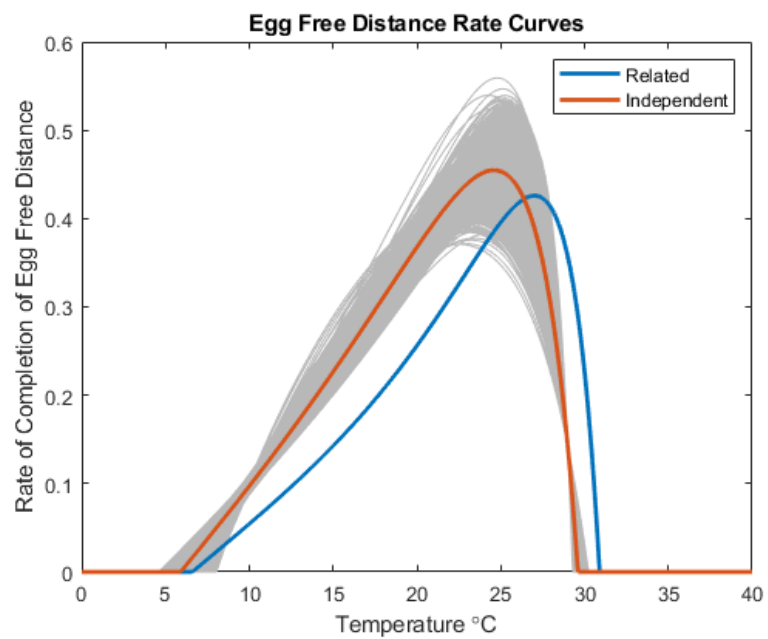
Fig. 2.5: A comparison rate curve for the related method (blue) and independent method (orange), as well as the related method rate curves resulting from fitting to 1000 bootstraps of the infested board data (gray). Though the bootstrapped curves do vary with different fits, the related curve thresholds are significantly different than the oviposition rate curve.
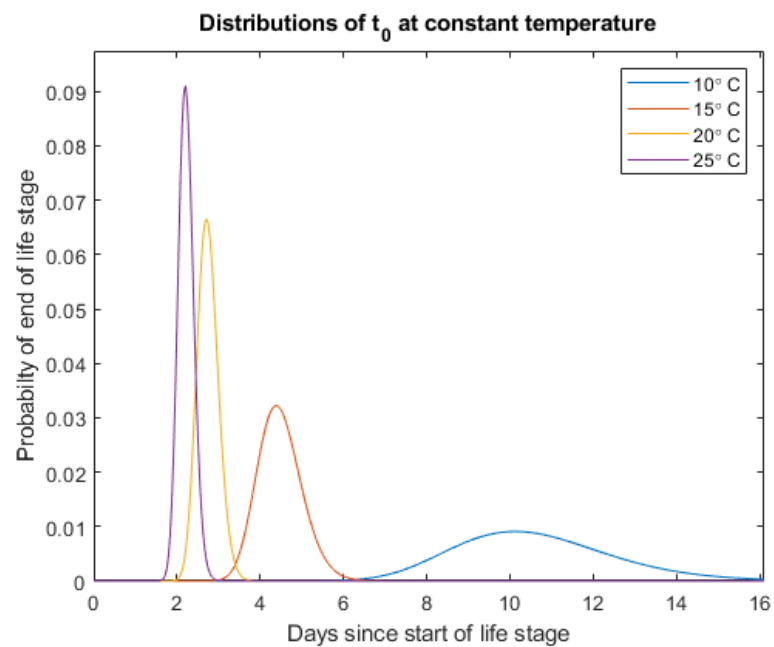
Fig. 2.6: Probability distributions of t_0 for the independent method projected using the EvF equation using constant phloem temperature data. Variability in t_0 decreases as temperature increases, with a noticeably wider distribution for 10°C. Even at that temperature most egg-free gallery is predicted within two days of median emergence, indicating that the complexity of the cohort model is not necessary.
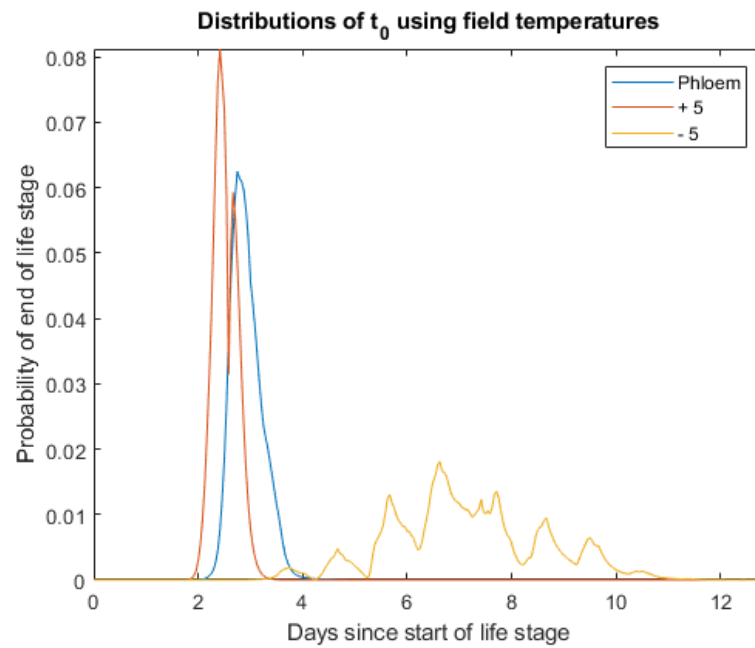
Fig. 2.7: Probability distributions of t_0 for the independent method projected using the EvF equation using field phloem temperature data. Though the variance noticeably increases with a decrease in the mean phloem temperature, for an increase in phloem temperature that is more likely to occur under current global warming regimes, the variance is much less pronounced. (Field phloem temperatures were collected at hourly intervals in 2015 at Lockett Meadows, Cococino National Forest, AZ.)

2.5 Calculating the Distribution of Oviposition

In this section we derive the detailed ovipositional model, MPBovi. First we determine the distribution of oviposition, p_{ovi}, conditioned on egg quantiles of remaining fractional fecundity, f. We then determine the distribution of f, in order to weight each quantile of remaining fecundity. After determining the distribution of f, we sum over quantiles to calculate the density of eggs, p_{egg} conditioned on an attack date τ. The procedure is illustrated using hourly phloem temperature data, $T(t)$, and attack data , $A(\tau)$, collected in 2015 at Lockett Meadows, Cococino National Forest, AZ.

2.5.1 Distribution of Oviposition Quantiles

After a gallery is initiated at a time τ, there is a delay period, t_0, before oviposition begins, calculated using the method in section 2.2. Thus when $t \leq t_0 + \tau$, the maximum potential fecundity is Ω. Using this condition and solving (2.8) for F produces the following equation for remaining potential fecundity for a time t :,

$$
F = \begin{cases} \Omega \left[e^{-\int_{t_0+\tau}^{t} r_0(T(t')-\epsilon)dt'} \right], & t > t_0 + \tau \\ \Omega, & t \leq t_0 + \tau \end{cases}.
\tag{2.19}
$$

Here $r_0(T(t'))$ is the rate of oviposition and ϵ is the normal variability in rates. Since the data collected by McManis et al. (2019) is eggs over time, the oviposition model is in terms of the cumulative oviposition at time t, $O(t) = \Omega_m - F$, resulting in the following model:

$$
O(t) = \begin{cases} \Omega \left(1 - e^{-\int_{t_0+\tau}^{t} r_0(T(t'))dt'} \right) + \epsilon, & t > t_0 + \tau \\ 0, & t \leq t_0 + \tau \end{cases}
\tag{2.20}
$$

where $(1 - e^{-\int_{t_0+\tau}^{t} r(T(t'))dt'})$ is the fraction of remaining oviposition at time t.

The time at which the nth egg is laid satisfies following equation:

$$
n = \Omega \left(1 - e^{-\int_{t_0+\tau}^{t} (r_0(T(t'))-\epsilon)dt'} \right).
\tag{2.21}
$$

Let f be the remaining fraction of potential fecundity, that is $f = 1 - \frac{n}{\Omega}$. Solving (2.21),

$$f = e^{-\int_{t_0+\tau}^{t}(r_0(T)-\epsilon)d\tau} = e^{(\epsilon(t-t_0-\tau)-R(t,t_0+\tau))}, \tag{2.22}$$

where $R(t, t_0 + \tau)$ is the cumulative oviposition index between $t_0 + \tau$ in equation (2.10). We then invert equation (2.22) for ϵ,

$$\epsilon = \frac{\ln(f) + R(t, t_0 + \tau)}{t - t_0 - \tau}. \tag{2.23}$$

Since $\epsilon \sim N(0, \sigma^2)$ is truncated on the right, we know that for any positive ϵ the cumulative distribution function is

$$P(t' > t \text{ for egg n }) = \int_{-\infty}^{\epsilon} \frac{1}{\sqrt{2\pi\sigma^2}} e^{-s^2/2\sigma^2} ds \tag{2.24}$$

Taking the derivative of this CDF results in the PDF of oviposition over time conditional upon remaining fraction fecundity and attack date:

$$\begin{aligned} p(t|\tau, f) &= \frac{d}{dt}\left(\int_{-\infty}^{\epsilon} \frac{1}{\sqrt{2\pi\sigma^2}} e^{-s^2/2\sigma^2} ds\right) \\ &= \frac{1}{\sqrt{2\pi\sigma^2}} e^{-\epsilon^2/2\sigma^2} \left|\frac{d}{dt}\epsilon\right| \end{aligned} \tag{2.25}$$

We can conclude that, for any particular f,

$$p_{ovi}(t|t_0 + \tau, f) = \frac{C_f}{\sqrt{2\pi\sigma^2}} e^{-\left(\frac{\ln(f)+R(t,t_0+\tau)}{t-t_0-\tau}\right)^2/2\sigma^2} \left|\frac{-(\ln(f) + R(t, t_0 + \tau))}{(t - t_0 - \tau)^2} + \frac{r_0(T(t))}{t - t_0 - \tau}\right| \tag{2.26}$$

where C_f is a normalization constant related to the truncation. Note that while
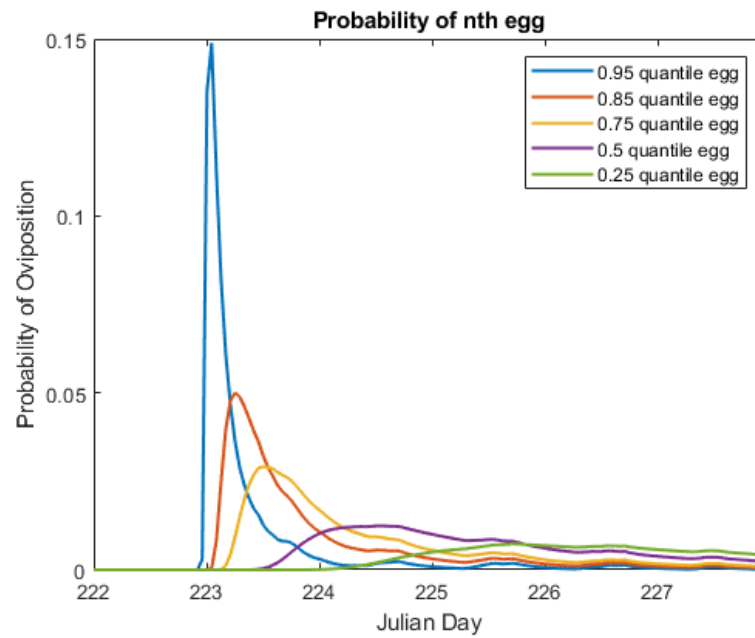
Fig. 2.8: The probability distribution function p_{ovi} created when using field phloem temperature data as input for different values of f. The earlier an egg is laid, the less it is affected by the variability in rates as all MPB begin oviposition simultaneously in the model, hence the steep peak for the 0.05 percentile eggs. As oviposition continues and the MPB continue on with varying rates, the probability distribution of any particular egg spreads across a longer period of time.

$\epsilon \sim N(0, \sigma^2)$, (2.24) is truncated such that $0 \leq r_0(T) + \epsilon$, in order to avoid inplausible negative rates. Correspondingly, all distributions required normalization. The remaining fractional fecundity f has a noticeable effect on the probability of oviposition, as the variation in rates results in longer distributions for later eggs (Figure 2.8).

2.5.2 Distribution of Egg Quantiles is Approximately Uniform

In order to use (3.2) in a predictive model, it was necessary to determine the distribution of the f, $\pi(f)$, and we determine π in this section. While computational tests suggested f was uniformly distributed, it is not initially clear why this should be so. For females $1, ...m, ...M$, the individual fecundity of the nth individual female can be represented by:

$$\Omega_m = \Omega_0 \delta_m \tag{2.27}$$

with $\delta_m = e^{\gamma_m}$, and $\gamma_m \sim N(-\frac{1}{2}\sigma_{egg}^2, \sigma_{egg}^2)$ (Régnière et al. 2012). The average fecundity of the Arizona mountain pine beetle in McManis et al (2019) was estimated at $\Omega_0 = 89.8$, and we can calculate σ_{egg} directly from the histogram of observed female fecundity in McManis et al (2019), who hypothesized that $\pi(f)$ was uniform. Taking the log of the observed values in the histogram and calculating the standard deviation results in $\sigma_{egg} = 0.6316$. Using equation (2.22), the nth egg of the mth individual female is in quantile

$$f_{m,n} = 1 - \frac{n}{\Omega_m}. \tag{2.28}$$

We used the lognormal function in MATLAB to create 200 lognormally distributed δ_m (Figure 2.9). The corresponding f values were calculated by taking the fractional fecundity for each egg (integer) until Ω_m. Note that as ovipositing females lay at least one egg, we did not sample $n = 0$. Since $n \neq 0$, there are less observations between 0.9 and 1.0 (2.10), but if n were continuous the distribution would be perfectly uniform.
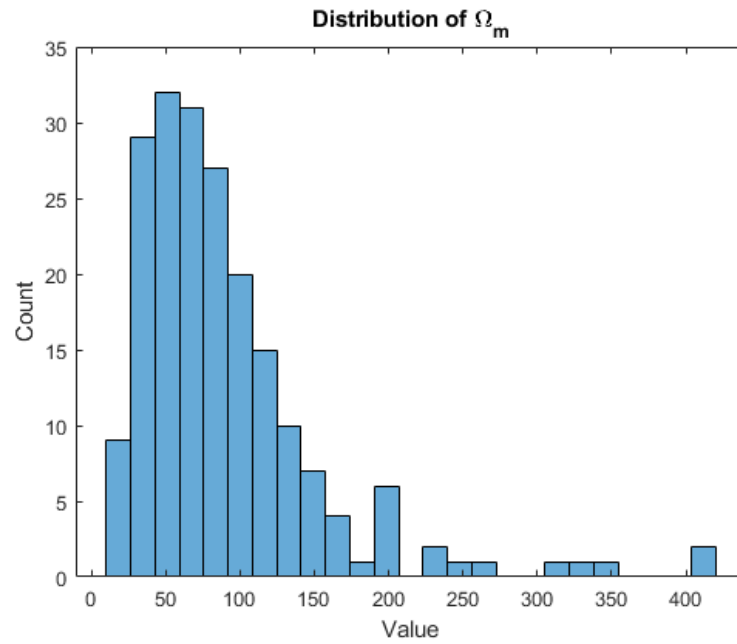
Fig. 2.9: The distribution of potential maximum fecundity, Ω_m, used to create Figure 2.10. The average potential fecundity of a southern MPB population was assumed to be $\Omega_0 = 89.8$ as seen in McManis et al. (2019).
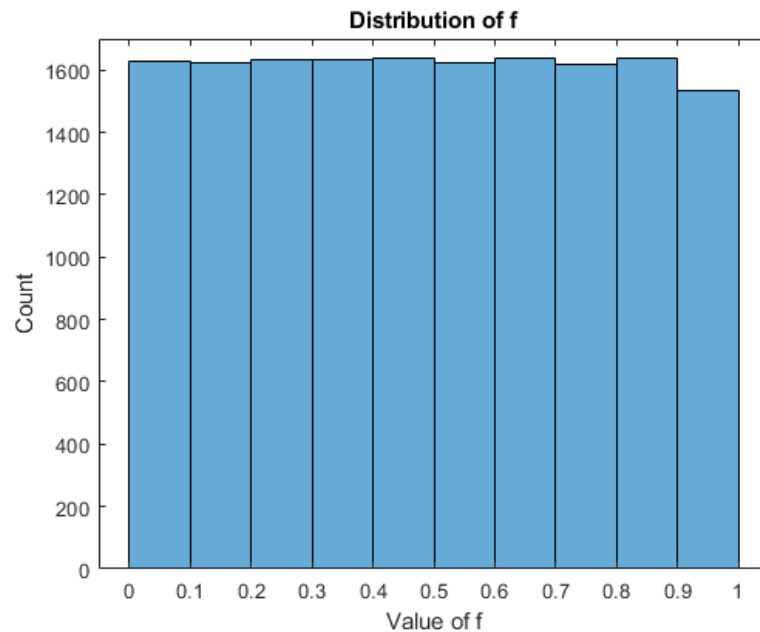
Fig. 2.10: The histogram of remaining potential fecundity, f, values created for 200 individuals using the lognormal potential fecundity, Ω_m (Figure 2.9). Since all MPB reach maximum fecundity in egg (integer) increments the distribution is uniform despite differences in maximum fecundity, except for the uppermost bin. Since all ovipositing females lay at least one egg, there are fewer values in the uppermost bin.

To see why this should be so analytically, consider (2.5.2). Despite the varying value of Ω_m, the number of eggs n increases uniformly for each Ω_m resulting in uniformly increasing fractional values for $\frac{n}{\Omega_m}$ as the value of n approaches Ω_m. More explicitly, Ω_m are is large, we can approximate $x = \frac{n}{\Omega_m}$ as a continuous variable. Then taking the derivative of x results in

$$\frac{df}{dx} = \frac{d}{dx}(1 - x) = 1, \tag{2.29}$$

indicating that the change in f is constant and therefore the continuous distribution would be uniform. In addition, f is effectively an empirical CDF, and correspondingly the CDF has a uniform distribution, as seen in Example 3.1 of Embrechts and Hofert (2013).

2.5.3 Distribution of Eggs

We can calculate the probability of oviposition for any given t and τ by integrating,

$$p_{ovi}(t|t_0 + \tau) = \int_0^1 p(t|t_0 + \tau, f)\pi(f)df \tag{2.30}$$

where we assume $\pi(f) \approx \mathcal{U}(0, 1)$. This was performed computationally by first calculating the value of t_0 as described in Section 2.4. Then $p_{ovi}(t|t_0 + \tau)$ was calculated for uniformly distributed values of f using cumulative trapezoidal integration of the temperature dependent oviposition rates (2.3), and computationally normalized (Figure 2.11). Finally, (2.30) was approximated using trapezoidal quadrature in f and evenly spaced increments of with $\Delta f = 0.05$.

For any individual tree, there are multiple attack dates τ, each with a corresponding numbers of attacks that day. The probability density of eggs on any particular day can therefore be represented by

$$p_{egg}(t) = \int_{\tau_{min}}^{\tau_{max}} A(\tau)p_{ovi}(t|t_0 + \tau)d\tau \tag{2.31}$$

where $A(\tau)$ is the number of attacks on the tree on day τ. This was calculated by weighting the p_{ovi} (2.30) calculated for each day of attack by the number of attacking beetles that

day, then summing the densities and normalizing them.

The procedure is illustrated for field conditions in Figure 2.12. Phloem temperatures and number of attacks observed on sample days for a baited tree were used to initialize the model. The output of the model reflects the fluctuations in both number of attacking beetles and phloem temperature.
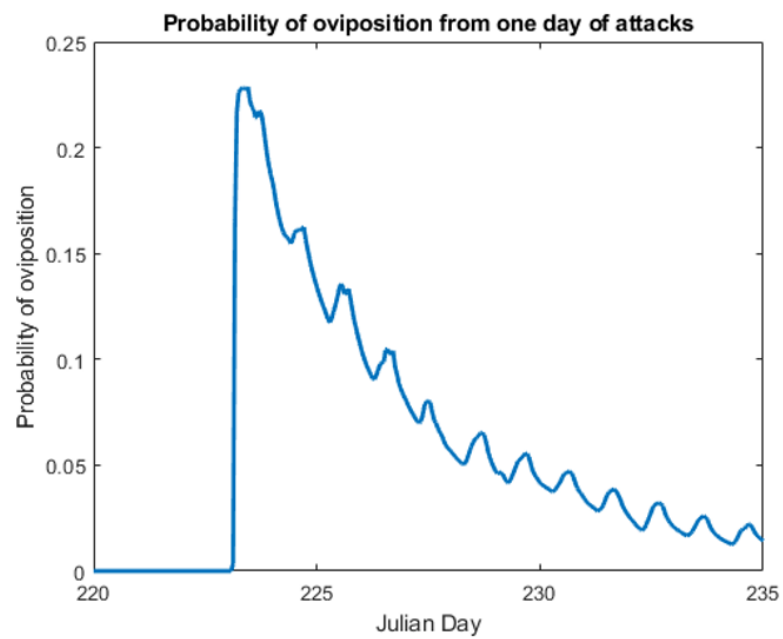
Fig. 2.11: The probability distribution function p_{ovi} created when using field phloem temperature data. The probability of oviposition decreases rapidly from an initial peak as the variability in rates and fecundity begins to take effect. Oscillations in the curve reflect diurnal temperature swings.

(a) Weighted oviposition PDFs for each day of attack

(b) Oviposition PDF for a single tree
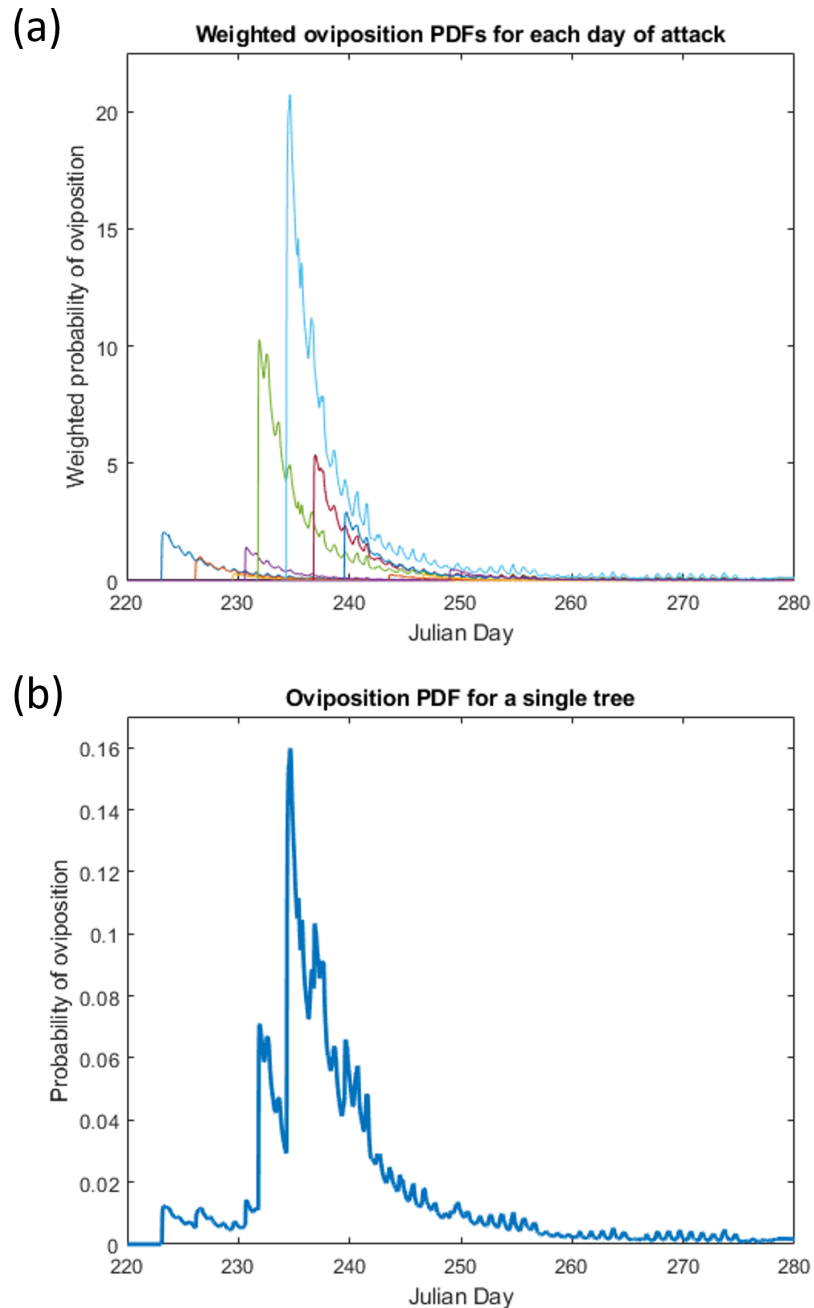
Fig. 2.12: The weighted probabilities of oviposition are combined and normalized in order to create the probability of oviposition for a single tree over a season. a) The probability distributions of p_{ovi} created when using field phloem temperature data and attack data as input and weighted individual dates of attack. Each distribution represents a single date of attack weighted by the number of attacking beetles. Weighted distributions were summed and normalized in order to calculate p_{egg}. b) The probability distribution function p_{egg} created when using field phloem temperature data and attack data as input. The shape of the curve is reflective of multiple attack dates, varying number of beetle attacks, and changing phloem temperatures seen in a).

2.6   Asymptotic Approximation for Distribution of Oviposition

In practice the oviposition model is computationally taxing and the variance in rates is relatively small, so we explored Laplace's method to find an asymptotic approximation for p_{ovi} (2.30). Laplace's method approximates integrals of the form

$$I = \int_a^b e^{-\lambda \phi(u)} F(u) du. \tag{2.32}$$

For $\lambda >> 1$, the integral at may be written

$$I = \frac{\sqrt{2\pi}}{\sqrt{\lambda \phi_{uu}^*}} e^{-\lambda \phi(u^*)} (F(u^*) + O(\lambda^{-1})), \tag{2.33}$$

where $u* \in (a, b)$ satisfies $\frac{\delta \phi}{\delta u}(u^*) = 0$ and $\phi_{uu}^* = \frac{\delta^2 \phi}{\delta u^2}(u^*) > 0$ (Logan 2013).

We must first use substitution to get (2.33) in the form of (2.26). Let $u = \ln(f)$, then $du = \frac{df}{f} = e^{-u} df \Rightarrow df = e^u du$. Substituting into equation (2.30) and adjusting the limits of integration gives

$$p_a(t|t_0 + \tau) = \int_{-\infty}^0 \exp\left[-\frac{(u + R(t, t_0 + \tau))^2}{2\sigma^2(t - t_0 - \tau)^2}\right] \frac{|r(T(t))(t - t_0 - \tau) - u - R(t, t_0 + \tau)|}{(t - t_0 - \tau)^2 \sqrt{2\pi\sigma^2}} e^u du. \tag{2.34}$$

For equation (2.34) to have the form of equation (2.32), let

$$\lambda = \frac{1}{\sigma^2}, \tag{2.35}$$

$$\phi = \frac{(u + R(t, t_0 + \tau))^2}{2(t - t_0 + \tau)^2}, \tag{2.36}$$

and

$$F(u) = \frac{|r(T(t))(t - t_0 + \tau) - u - R(t, t_0 + \tau)|}{(t - t_0 + \tau)^2 \sqrt{2\pi\sigma^2}} e^u. \tag{2.37}$$

Taking the derivative to find the critical point, u^*,

$$\frac{\partial \phi}{\partial u} = \frac{u + R(t, t_0 + \tau)}{(t - t_0 + \tau)^2} \stackrel{\text{set}}{=} 0. \tag{2.38}$$

This gives

$$u^* = -R(t, t_0 + \tau) \tag{2.39}$$

and

$$\phi_{uu}^* = \frac{1}{(t - t_0 + \tau)^2}. \tag{2.40}$$

Then

$$F(u^*) = e^{u^*} \frac{|r(T(t))(t - t_0 + \tau)|}{\sqrt{2\pi\sigma^2}(t - t_0 + \tau)^2} = e^{-R(t,t_0+\tau)} \frac{r(T(t))}{\sqrt{2\pi\sigma^2} |t - t_0 + \tau|}, \tag{2.41}$$

and substituting into (2.33), we find

$$I \approx \frac{\sqrt{2\pi}}{\sqrt{\frac{1}{\sigma^2(t-t_0+\tau)^2}}} \frac{1}{|t - t_0 + \tau| \sqrt{2\pi\sigma^2}} e^{-R(t,t_0+\tau)} r(T(t)). \tag{2.42}$$

The oviposition distribution may therefore be approximated

$$p_a(t|t_0 + \tau) = e^{-R(t,t_0+\tau)} r(T(t)) + O(\sigma^2). \tag{2.43}$$

Notably, this approximation is equivalent to the closed form of the distribution found by Régnière et al. (2012). Taking the derivative of Régnière's cumulative fractional oviposition (2.9) results in the oviposition density,

$$p_{Reg}(t|t_0 + \tau) = r(T(t)) e^{-R(t,t_0+\tau)} \tag{2.44}$$

although the authors did not comment on this. It is also worth noting that

$$\int_{\tau+t_0}^{\infty} e^{-R(t,t_0+\tau)} r(T(t)) dt = \int_0^{\infty} e^s ds = 1 \tag{2.45}$$

if $s = R(t, t_0 + \tau)$ and $ds = r(T(t)) dt$; thus the approximation is already normalized.

2.7   Model Behavior and Comparison with Data

The models derived in this paper, MPBovi and the asymptotic model, as well as the EvF cohort model and the median model, are compared to lab data obtained from MPB infested boards by McManis et al. (2019). Observed values of t_0 were used (instead of model t_0 to exclusively compare oviposition distributions to the lab data. The oviposition rate and variance found by McManis et al. (2019) were used in each model, though the rate was divided by $\ln 2$ for the EvF model to reflect the timing of the median event. Model output was weighted using the total realized fecundity for each infested board, then normalized to create a distribution. The lab data distributions were created using daily increments, and integrals approximated using trapezoidal quadrature and hourly time steps.

Values of R^2 were calculated for the EvF, asymptotic, and derived oviposition models over the range of the laboratory data (0-30 days), using bins of 24-hour width to match the laboratory data. McManis incubated MPB infested boards at four constant temperatures, but only total eggs counted were available for 29°C before day 7. Thus probability distributions are not present for 29°C, but cumulative distributions were created with the remaining data.

The probability distributions reflect the differences in model assumptions (Figure 2.13). MPBovi and the asymptotic model both peak in the beginning and decrease rapidly, MPBovi has a greater maximum probability due to incorporating variability in fecundity and rate. While fecundity and rates begin to vary over time, the model assumes that all beetles begin at the same time. The EvF model instead derives from variation around the median, and correspondingly the EvF model predicts peak oviposition later, with spread on both sides from the median. While the EvF model is somewhat more successful at the higher temperatures than at 10°C, both the asymptotic and derived model are closer to the timing of the laboratory data (Figure 2.13). The EvF model has the poorest R^2 values in all cases, though is somewhat more successful for cumulative oviposition at 20°and 27°C (Table 2.2). The asymptotic model has higher R^2 values than the derived model in each case, and is much higher for the 10°C probability distribution function.

	EvF	Asymptotic	MPBovi
10°C	0.0001	0.5706	0.0199
20°C	0.2436	0.7761	0.6829
27°C	0.2102	0.6329	0.5176

Table 2.2: Table of the calculated R^2 values for the probability distribution functions of discussed models. All models performed most poorly with the laboratory data at 10°C, and the asymptotic model performed best at all temperatures.

For all of the models except MPBovi, a majority of the oviposition at 10°C is predicted to occur past the observation window of the lab data (Figure 2.13). Both the asymptotic and MPBovi exponentially decrease in proportion to the rate, and 10°C is near the lower temperature threshold, thus oviposition is predicted to take much longer. The nature of the EvF model is that predictions are based upon the median, and correspondingly it is also affected by the low changes in rates, as the median individual takes much longer to complete oviposition. MPB oviposition takes place in late summer, thus 10°C is the least reflective of field oviposition temperatures, and less likely to affect a predictive model. It is also uncertain how much MPB oviposition at a constant temperature of 10°C is directly comparable to MPB in the field experiencing fluctuating temperatures.

The cumulative distributions provide additional context of model success (Figure 2.14) over time. The EvF model had the lowest R^2 values at all temperatures, and the asymptotic model had the highest R^2 values for all except 27°C, where MPBovi had a slightly higher value (Table 2.3). MPBovi is best at predicting the first half of cumulative oviposition at 10°C due to the predicted initial peak in emergence, while the asymptotic model and
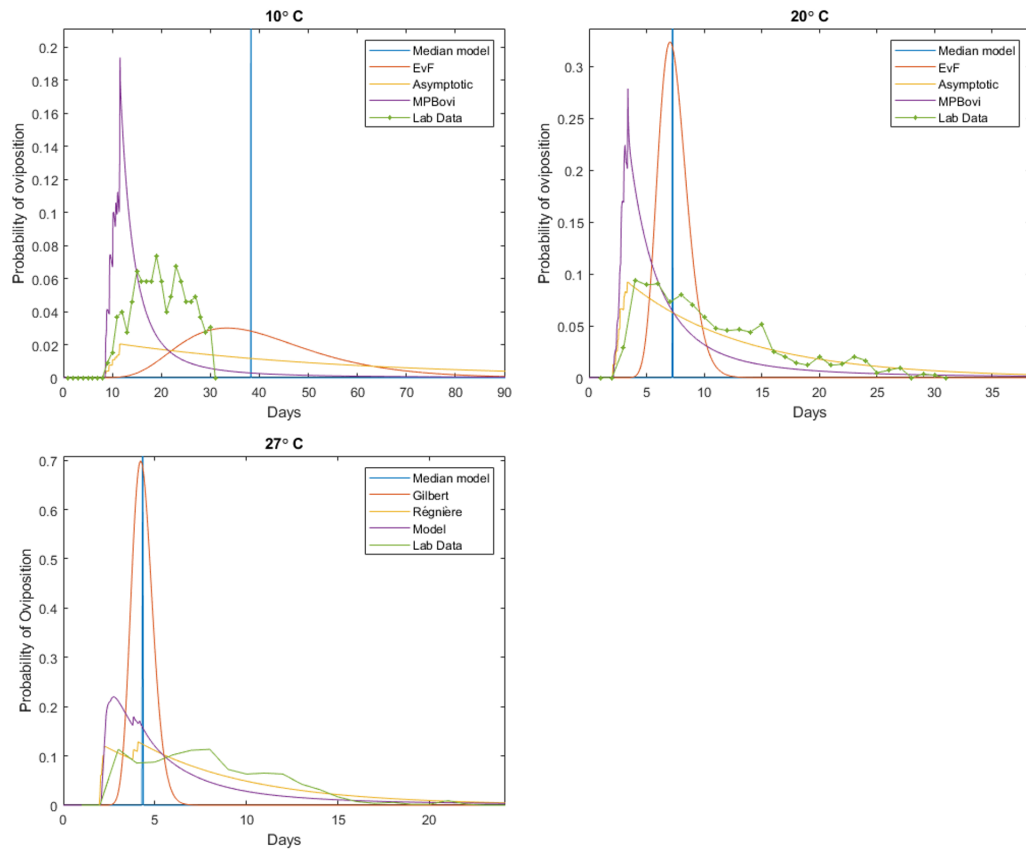
Fig. 2.13: The probability distribution functions of the lab data and the discussed models for 10°C, 20°C, and 27°C. Due to the relationship between the computational models and the lower oviposition rate at 10°C, all but MPBovi predicted a sizable proportion of oviposition to occur past the observation period. MPB oviposition is unlikely to occur during an extended period of 10°C in the field, as MPB oviposit in the late summer. Note that though the median model may initially appear to be different than the EvF model, the long tail of the EvF distribution results in the delayed median as is plotted.
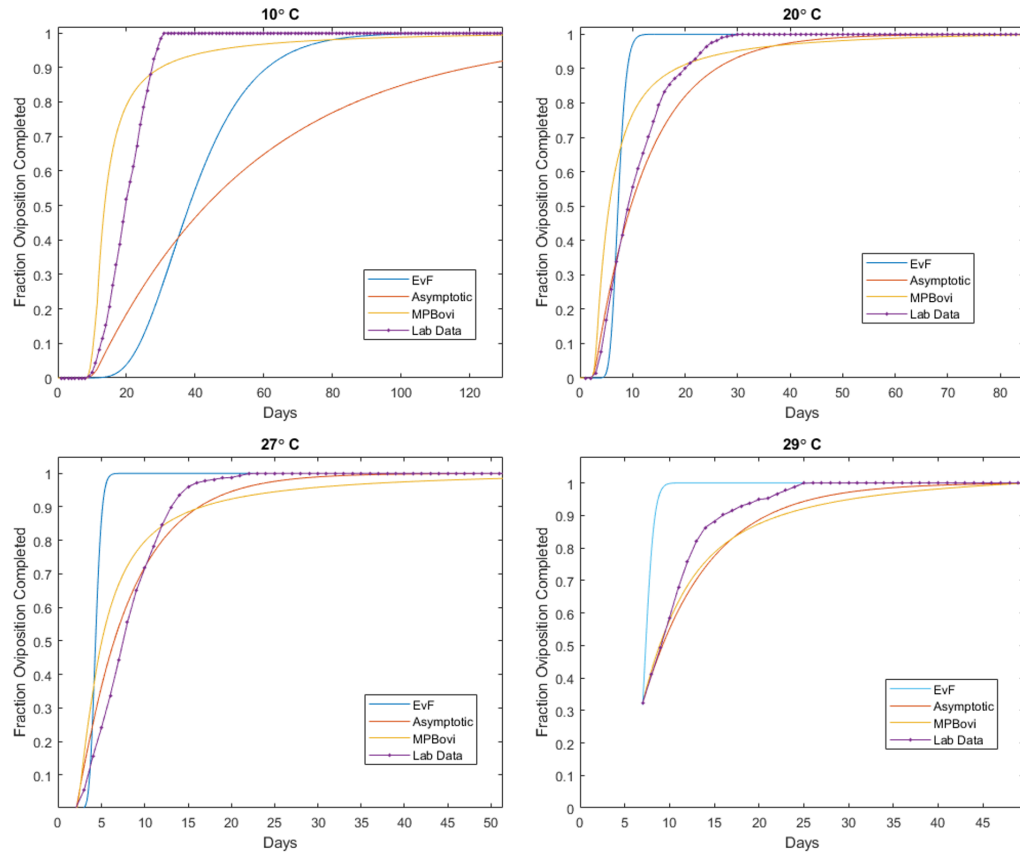
Fig. 2.14: The cumulative oviposition functions of the lab data and the discussed models for 10°C, 20°C, 27°C, and 29°C. While the asymptotic model had the highest R^2 value for all temperatures except 27°C, MPBovi also fits the data well, particularly at 10°C. The EvF model was least successful in all cases. Due to missing lab data, the 29°C plots were manually adjusted to begin at the fraction of fecundity remaining at day 7 in the lab data, as lab data was unavailable before day 7.

	EvF	Asymptotic	MPBovi
10°C	0.7932	0.9984	0.8625
20°C	0.5322	0.9922	0.9860
27°C	0.4213	0.9250	0.9363
29°C	0.3368	0.9710	0.9583

Table 2.3: Table of the calculated R^2 values for the cumulative distribution functions of discussed models. The EvF model was the least suitable at all temperatures, with lower R^2 values near the temperature thresholds. The asymptotic and MPBovi were both suitable with similar R^2 values, though the derived model has a higher R^2 value for 10°C.

EvF lag significantly behind. The asymptotic model is very successful at 20°C, nearly matching the lab data for the first half of oviposition, after which it begins to under predict.

2.8   Conclusion

In this paper we developed models to address challenges in predicting ovipositional phenology for a southern population of MPB. Models were parameterized with and compared to oviposition data collected by McManis et al. (2019). We introduce a method for determining the time delay before oviposition, t_0, which was found to be independent of oviposition rate. A novel oviposition model with lognormal variability in fecundity and normal variability in oviposition rate, MPBovi, was derived, as well as a simpler and more computationally efficient asymptotic approximation. When comparing MPBovi and the asymptotic approximation, as well as the previously used EvF model, to the lab data, both of the new models were more successful at reflecting the observed distribution of eggs.

We found that the time required to complete the egg-free gallery was not well described in by the oviposition rate, and instead better predicted using an independent rate curve. Assuming that the rate of completion of the egg free distance is proportional to the oviposition rate, resulted in greater error near the temperature thresholds, and estimated optimum temperature differing significantly from the oviposition model. An independent model with new parameters, with bootstrapped parameters that differed significantly from the oviposition rate curve parameters, more accurately described the time required to excavate the egg free distance.

We compared two novel oviposition models, the derived model MPBovi which incorporates varying fecundity and rate, as well as an asymptotic approximation, with other models that have been used to describe MPB oviposition. Both models have their positive and negatives, and compare more favorably to lab data than previously used median and cohort (EvF) models. Since oviposition occurs in the phloem under the bark, we were unable to directly compare the model output with field observations. We were able to compare the output of the models to the laboratory data of McManis et al. (2019). This was not ideal as the oviposition rate curve used in each model was calibrated via this data, but it does allow for some degree of validation. The asymptotic model is the best fit for the laboratory data in terms of R^2, but it is not clear if that would be the case with a larger sample size, which would better express the variability of fecundity and rate. It would be worth investigating further if the predictive power of the derived model is more useful on a larger scale, as both sources of variability have been found to exist in previous research (McManis et al. 2019). Regardless, the asymptotic model also has the benefits of simplicity and computational efficiency.

Quantifying temperature dependent lifestage events, particularly those that vary along latitudinal climes, is an important step to predicting life cycles in a changing climate, and preventing ecological and economic damage. Our methodologies for predicting southern MPB oviposition provide a basis for analysis not only of MPB populations, but also other *Dendroctonus* species and other insects with temperature dependent thresholds and variable fecundity/rate. The southern MPB oviposition model is also suitable to be used in a phenology model for the entire life cycle, which is the subject of the following chapter.

CHAPTER 3

A TENERAL ADULT RATE MODEL FOR A SOUTHERN MOUNTAIN PINE

BEETLE POPULATION

3.1 Introduction

The mountain pine beetle (MPB, *Dendroctonus ponderosae* Hopkins Coleoptera: Scolytidae) attacks living *Pinus* trees across a widespread area in Western North America ranging from Baja California Norte, Mexico, to northern British Columbia and Alberta, Canada (Dowle et al. 2017). Adults must attack a host simultaneously to overwhelm host defenses and successfully colonize, reproducing in the inner-bark (phloem) and killing the host tree. Phloem temperatures directly but non-linearly affect MPB progress through the stages of their life cycle which have varying temperature thresholds (Bentz et al. 1991; Powell and Logan 2005). These thresholds allow MPB to be successful in a thermal niche where they are univoltine and synchronize emergence.

Changing temperatures have broadened that niche geographically, leading to tree mortality of over 5.2 Mha in the western US (Meddens et al. 2012). The distribution of *Pinus* host species in western North America extends both northward and southward beyond the known historical distribution of MPB (Giroday et al. 2012; Sambaraju et al. 2019). Increases in temperatures have allowed MPB migration northward in Canada, where it is projected billions of dollars in damage could be done in British Columbia by 2054 (Corbett et al. 2015). MPB induced *Pinus* mortality also has notable ecological effects, including changing forests from carbon sinks to carbon sources until trees regrow (Arora et al. 2016). Factors delimiting the southern edge of the MPB distribution in the US are less known, and while MPB are considered rare to absent south of the USA/Arizona border, MPB were recently found in dead *Pinus strobiformus* in Chihuahua, Mexico (Armendáriz-Toledano et al. 2017).

The MPB has a one-year (univoltine) life cycle in most of its range, though in some regions semi-voltine (two-year) emergence occurs. A majority of the MPB life cycle is spent inside a host tree, except for a period of a few days in late summer (late July to early September) during which newly developed parent adults emerge from the previous *Pinus* host in search for a new one. MPB females initiate attacks on new hosts, attracting males with pheromones, allowing for an attack en masse to overcome host defenses. After mating and oviposition, most adult beetles perish within the tree, and their offspring begin the process again in the following year.

While wild populations of MPB are univoltine or semi-voltine, there are concerns that warmer temperatures from global warming or range expansion could lead to bivoltine populations. Bivoltinism could have devastating impacts on pine forests, but a key barrier for MPB bivoltinism is the cold tolerance of certain lifestages. MPB eggs and pupae are considered to have the lowest cold tolerance among lifestages (Bleiker and Smith 2019; Reid and Gates 1970), while larger larvae are the most cold tolerant. While supercooling points are indicative of immediate mortality, mortality also occurs with extended exposure to 0℃ for both egg and pupal stages (Bleiker and Smith 2019; Reid and Gates 1970). Successful bivoltine MPB have not been observed in the field (Bentz and Powell 2014), although a phenology model parameterized for northern US MPB populations suggests bivoltinism is possible in the southern MPB range under future warming scenarios (Bentz et al. 2016).

However, northern and southern MPB populations are genetically different in response to temperature, requiring geographic-specific model parameters (Bentz and Powell 2014). McManis et al. (2018; 2019) successfully parameterized a phenology (life-cycle) model for a southern population of MPB from lab data, except for the teneral adult stage, which ends when MPB leave the tree. Since MPB lab experiments often involve infested phloem in enclosed containers, leaving the container is not possible. Developmental parameters were found to vary from those found for northern MPB (Régnière et al. 2012), but not sufficiently to account for longer observed developmental time of Arizona MPB populations, which suggests that teneral adult rates must be substantially lower (McManis et al. 2018).

Soderberg et al. (2021) performed reciprocal translocation experiments with northern and southern populations of MPB, and observed seasonally appropriate univoltine emergence at all sites, indicating southern MPB have adapted to maintain univoltism even in warmer environments. How these differences between northern and southern populations would affect the possibility of bivoltinism is unknown, but possibly critical, as one would expect southern populations to be more susceptible to increased temperatures as they occupy the warmer regions of the MPB range.

The goal of this chapter is to determine developmental rates for the cyptic teneral adult stage using a phenology model and field data for a southern population of mountain pine beetle. We first introduce rate models for earlier life stages and teneral adult rate curves tested as we developed the model. Teneral curves were parameterized using two trees and the best curve was selected by comparing nominal and bootstrapped AIC values. The resulting model is then validated using an additional tree from the field data. We then examine the possibility of bivoltinism in a southern population of mountain pine beetle by increasing mean temperatures and reasonable constraints for appropriate seasonality.

3.2 Field Data for a Southern MPB Population

Field data from a southern population of MPB was collected at Lockett Meadows, in the Cococino National Forest near Flagstaff Arizona, from 2015-2017. Populations in this area are currently univoltine, and two full MPB life cycles were observed (2015/2016, 2016/2017). Data from Tree 2 (2015/2016) and Tree 1 (2016/2017) were used to calibrate the model, and Tree 3 (2015/2016) was used only for validation because emergence was sparse. Phloem temperatures, number of beetle attacks, and number and timing of emerging beetles were collected.

Phloem temperature was measured at hourly intervals for north and south sides of each tree using battery operated temperature recorders. North and south sides were chosen as previous field data indicates that the southern side of a tree often has an increased mean temperature due to ensolation, which may cause significant differences in developmental timing for beetles collected on different tree sides. Phloem temperatures were recorded

from 6/4/2015 to 6/27/2017 for trees observed in the 2015/16 season, and from 8/9/2016 to 9/19/2017 for trees observed in the 2016/17 season. Phloem temperatures varied not only seasonally (Figure 3.1) but also during time of day (Figure 3.2). The phloem temperature of particular tree and side i is referred to as T_i.

Attacks were observed in late summer of 2015 and 2016. When MPB flight was occurring in the tree stand, a MPB pheromone bait was attached to each tree on the north bole aspect at 4.5 ft. from the ground. Tree baits were removed approximately 1 week later when about 10-15 attacks were observed on the tree. Once attacks were initiated, attacks were monitored every other day around the entire circumference of each tree bole from 1 ft to 5 ft above the ground. On each observation day, the entire sample space was surveyed, counting attacks that were indicated by either frass or resin exuding from small holes. A permanent marker was used to place a mark near each attack so that it would not be counted in following days. Attacks were monitored until no attacks were observed for 2 consecutive observation days. Observations occurred at intervals of 2-4 days, without differentiation between sides. Thus all attacking beetles from the end of the previous observation to the current observation are included in a day of attack. The number of attacks on side i on attack date τ_n is denoted $A_i(\tau_n)$.

At the end of the attack season, emergence cages were fixed to the north/south aspects of the bole, and the number of emerging beetles was counted the following year. Emergence was counted separately for the north and south sides of trees as southern sides have earlier emergence due to higher temperatures (Figure 3.4). Emerging beetles were counted at 2-6 day intervals. Similarly to the attack data, all emerging beetles from the end of the previous observation to the current observation are included on observed day of emergence.

While three trees were observed each field season, due to a lack of observed attacks and/or emergence only three trees were suitable for inclusion. Data from Tree 2 (2015-16) (Figures (3.1), (3.3), (3.4)) and Tree 1 (2016-17) were used for parameterization and cross-validaing the model. Emergence data for Tree 3 (2015-2016) was very sparse (3.24), and thus it was used only for model validation instead of parameterization. Numerical data for
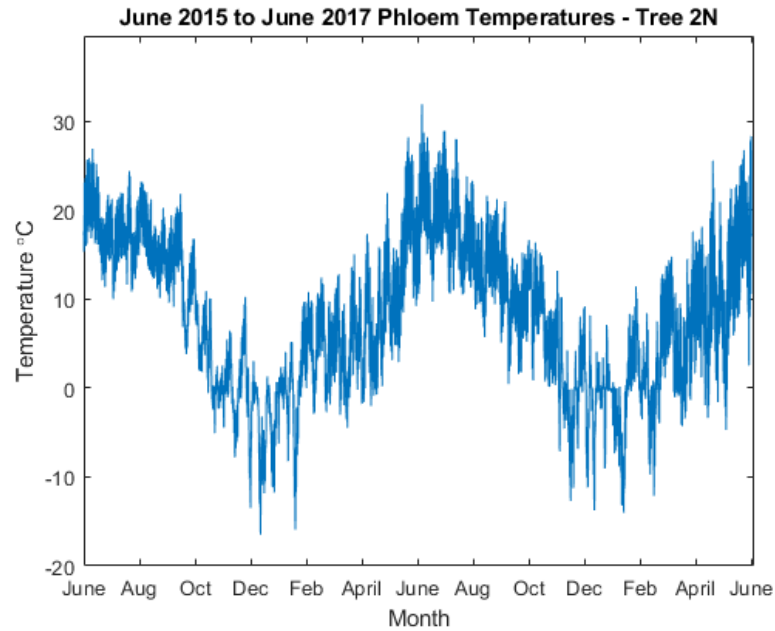
Fig. 3.1: Phloem temperatures from north side of Tree 2 from June 18th, 2015 to June 18, 2016. There is a strong seasonality to the temperatures, with an over 30°C change between summer and winter. Temperatures below freezing can be fatal to life stages that do not develop cold tolerance. Temperatures near the 20°C are considered optimal for most life stages.
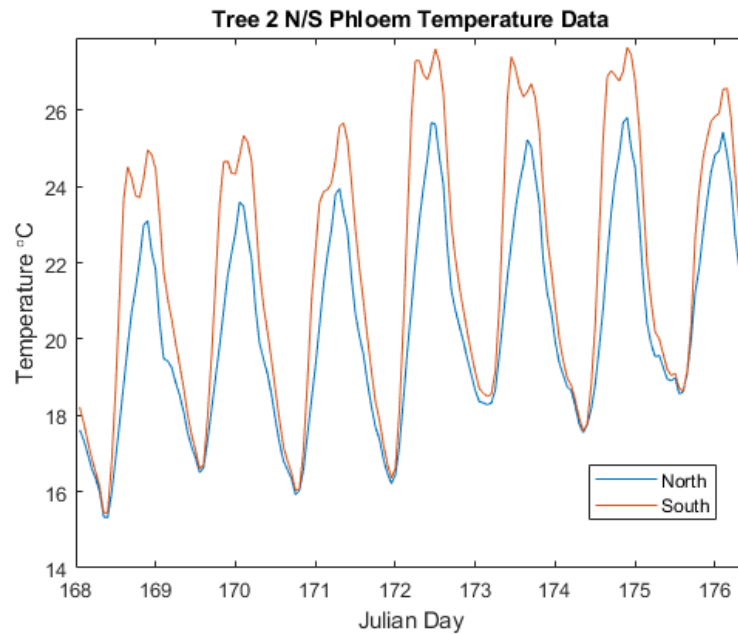
Fig. 3.2: Phloem temperatures from the north and south sides of tree 2 from June 18th, 2015 to June 26, 2015. The south side of the tree is noticeably warmer during the day, with higher peak temperatures which could result in increased cumulative development and affect emergence.
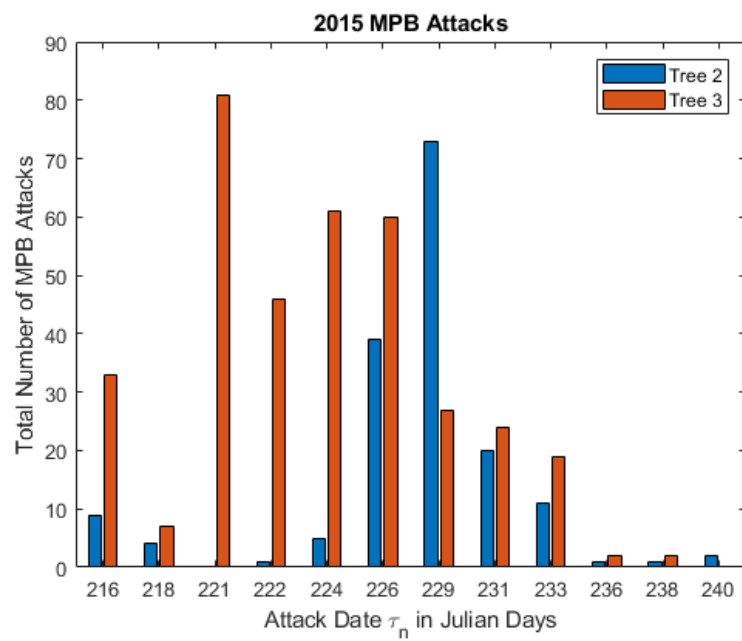
Fig. 3.3: Number of MPB gallery entrances ("attacks") observed on the two trees in 2015. The number of MPB attacks is accumulated from the previous date of observation. Attack dates are in Juilan day format, where January 1st is 1. Attacks were counted without discerning between the north and south sides of a tree.
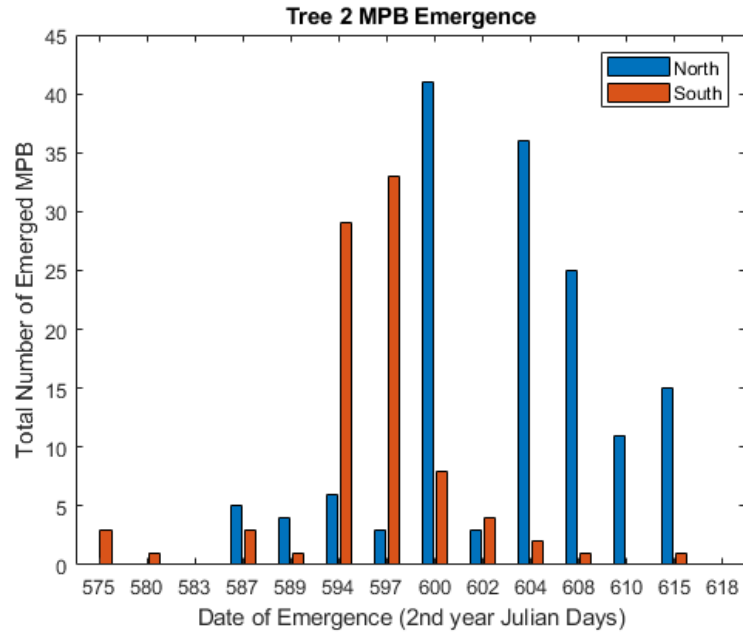
Fig. 3.4: Number of emerged MPB from both sides of Tree 2 in 2016. Emergence on the southern side of the tree was earlier than the northern side, due to warmer temperatures which increase the rate of development.
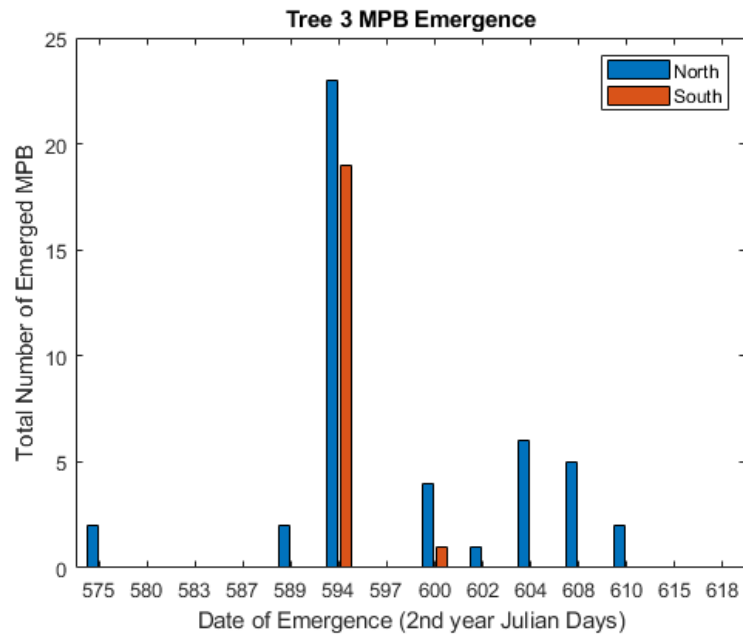
Fig. 3.5: Number of emerged MPB from the north and south sides of Tree 3 in 2016. While emergence for the northern side of the tree was less irregular, emergence was only observed on two days for the southern side. Due to this spare emergence Tree 3 was used only for model validation.

all three trees discussed can be found in Appendix A.

3.3   Model Development

In order to determine a developmental rate curve for the cryptic teneral adult stage, we incorporated a novel oviposition model (Chapter 2), southern MPB rate curves developed by McManis et al. (2018), a previously developed MPB cohort model (Gilbert et al. 2004), and previously developed as well as novel forms for teneral adult rate curves. An important aspect of oviposition is that variability occurs not only in oviposition rate, but also in fecundity. We also developed a method of calculating the time delay before oviposition, t_0, and incorporated that into our predictive oviposition model. This oviposition model was used as input to the cohort model incorporating stage-specific rate and known variability.

3.3.1   Review of Models Describing Southern MPB Phenology

Oviposition and Gallery Construction

There is a time period after MPB mating during which the female is boring deeper into the phloem but has yet to begin oviposition, which we defined as t_0. This egg-free gallery length allows MPB to avoid the induced resin response of the *Pinus* host, as well as reduce dessication. We parameterized a rate curve for the pre-oviposition stage my minimizing sum squared error with Matlab 's fmincon function for laboratory data of MPB development at constant temperatures. The rate curve used by McManis et al. (2019) is written

$$r_0(T) = \psi \left[e^{\omega(T-T_b)} - \left(\frac{T_m - T}{T_m - T_b} \right) e^{-\frac{\omega(T-T_b)}{\Delta_b}} - (\frac{T - T_b}{T_m - T_b}) e^{\omega(T_m - T_b) - \frac{T_m - T}{\Delta_m}} \right], \qquad (3.1)$$

and 0 for $T \notin [T_b, T_m]$. Here T_m and T_b correspond to the upper and lower temperature transitions from normal to negligible development at the upper and lower thresholds, ω describes the expected exponential acceleration of rate with temperature, ψ is proportional to the maximum development rate, and Δ_m and Δ_b are the width of the thermal transitions for the upper and lower thresholds. Parameters for the time required to produce the egg-free

gallery appear in Table 3.1.

Using the relationship between the maximum fecundity and the normal variability in oviposition rates, the probability of oviposition of the fth quantile given an attack date τ is

$$p_{ovi}(t|\tau, f) = \frac{1}{\sqrt{2\pi\sigma^2}} e^{-\left(\frac{\ln(f)+R(t,t_0+\tau)}{t-t_0}\right)^2/2\sigma^2} \left| \frac{-(\ln(f)+R(t,t_0+\tau))}{(t-t_0)^2} + \frac{r_0(T(t))}{t-t_0} \right| \quad (3.2)$$

where t_0 is the time delay before oviposition, and $R_0(t, t_0 + \tau)$ is the integral of the rates (3.1) from $t_0 + \tau$ to t. Integrating across quantiles, where $\pi(f)$ is approximately uniform (described in detail in Chapter 2).

$$p_{ovi}(t|\tau) = \int_0^1 p(t|\tau)\pi(f)df. \quad (3.3)$$

Finally, for any individual tree, there are multiple attack dates τ, each with a corresponding numbers of attacks that day. The resulting density of eggs for any particular day can therefore be represented by

$$p_{egg}(t) = \int_{\tau_{min}}^{\tau_{max}} A(\tau)p_{ovi}(t|\tau)d\tau. \quad (3.4)$$

Individual distributions are determined computationally for an attack date τ by the following method. The value of t_0 is calculated by using hourly time and phloem temperature vectors as input to the rate equation (3.1) with the egg free rate parameters (Table 3.1). Hourly rates are summed into daily rates using the trapezoidal rule. The trapezoidal rule is again used to obtain a cumulative approximation to the integral, and these are integrated from start date τ until the rate summation is 1, which is the time at which the egg free distance is completed.

Then distributions for specific values of f beginning at $\tau + t_0$ are then calculated using equation (3.2). Cumulative rates are computed by using the trapezoidal rule on the rates equation (3.1) using the oviposition parameters for a southern population of MPB (3.1), and each PDF is then normalized. The process is repeated for $f = 0.05, 0.10, ..., 0.095$ resulting

in oviposition density (3.3) approximated using trapezoidal quadrature.

Parameterized southern MPB rate curves

McManis et al. (2018) obtained rate curve parameters for southern MPB lifestages using experimental observations. MPB eggs were placed inside a "phloem sandwich" of phloem between sterilized glass and plexiglass plates. After inserting MPB eggs, the sandwiches were held at constant temperatures, which were chosen to asymmetrically sample the range of developmental temperatures across the previously developed rate curve for the northern population. Development of each individual was monitored on a daily basis to observe developmental milestones. However, the final, teneral adult stage, which ends upon leaving the tree, was not parameterized because completion of the teneral adult stage could not be observed, as MPB were unable to leave the sandwich. The process of parameterizing this unobservable lifestage is a novel development of this paper. In contrast to northern MPB populations, McManis observed normal variability in rates and fit the rate curve (3.1) accordingly (Table 3.1).

Lifestage	ψ	ω	T_b	T_m	Δ_b	Δ_m	σ
Egg-free gallery	0.1813	0.0622	5.9394	5.9394	29.6756	2.5471	2.7909
Oviposition	0.0913	0.0309	6.6000	30.9000	1.3613	1.9889	0.32
Eggs	0.0326	0.2045	6.0251	31.9309	0.5410	5.5031	0.038
First instar	0.0521	0.1517	4.6029	31.7661	0.0117	5.4256	0.2181
Second instar	0.0431	0.1374	5.9791	31.8337	0.0413	4.4534	0.1524
Third instar	0.017	0.1856	6.0115	31.2656	0.0	4.3079	0.1650
Fourth instar	0.0545	0.1694	14.9999	31.4364	0.0	5.2947	0.1354
Pupae	0.0166	0.1658	6.3504	30.8041	0.0	3.5426	0.0673

Table 3.1: Egg-free gallery parameters found in Chapter 2 and life stage parameters for a southern population of MPB found by McManis et al. (2018; 2019)

.

Extended von Foerster Cohort Model

The output of our oviposition model was used as input for the egg to pupae cohort model utilizing the parameters from McManis et al. (2019). While some models focus exclusively on the development of a median individual, this ignores the intrinsic variability of rates in a population. A cohort model provides an efficient way in order to incorporate the variability in rates over time for individuals in the cohort. McManis et al. (2019) determined rates had normal variance, which allows us to use the Extended von Foerster (EvF) equation developed by Gilbert at al. (2004),

$$\frac{\partial}{\partial t}u_j(a,t) + r_j[T(t)]\frac{\partial}{\partial a}u_j(a,t) = \frac{1}{2}\sigma_j^2\frac{\partial^2}{\partial a^2}u_j. \tag{3.5}$$

Here j is the developmental lifestage index, $u_j(a,t)$ is the population density at time t and age a (normalized such that $0 \leq a \leq 1$), $r_j[T(t)]$ is developmental rate at temperature $T(t)$, and σ_j^2 is the variance in development for life stage j. The density, $u_j(a,t)$, and emergence distribution, $p_j(t)$, are related by $p_j(t) = u_j(a = 1, t)$. The EvF equation reflects that since individuals are aging slower and faster than the mean, there is a flux forward and backward in age relative to the median individual, which is effectively diffusion among ages. The Green's Function solution to the Extended von Foerster equation,

$$p_j(t) = \int_0^\infty p_{j-1}(\tau)\frac{e^{\frac{-(1-\int_\tau^t r_j(T(s))ds)^2}{2\sigma_j^2(t-\tau)}}}{\sqrt{2\pi\sigma_j^2(t-\tau)^3}}d\tau, \tag{3.6}$$

was used with oviposition providing the initial distribution, that is $p_{egg}(t) = p_0(t)$ (Powell and Bentz 2009). Parameters for southern MPB populations estimated by McManis et al. (2018) were used for the egg, L1-L4 and pupal stage rate curves (Table 3.1).

The EvF equation allows us to project each emergence cohort on day τ into a subsequent distribution of emergence, including the effects of normal variability. Equation (3.6) was evaluated numerically by obtaining hourly rates using the phloem temperature data, then using trapezoidal integration to sum the rates over each day. Thus the rates are in daily

increments, but incorporate hourly variability. To avoid excess integration, the cumulative integral of the rates was calculated in advance; integrals between $\tau + t_0$ and t could then be rapidly approximated as a difference in cumulants between daily indices.

3.3.2 Potential Teneral Adult Rate Curves

For the unknown rate of teneral development we used five different rate curves of varying complexity. Adult emergence predicted using competing rate curves could then be compared with field observation to determine which candidate curves were most descriptive.

Logistic

The first teneral adult curve we considered used the logistic equation of Davidson (1944),

$$r_{logistic}(T) = \frac{r_{max} \cdot e^{(T-T_C)/\Delta_b}}{1 + e^{(T-T_C)/\Delta_b}} \tag{3.7}$$

which plateaus at a peak developmental rate of r_{max}, T_C specifies the developmental threshold, and Δ_b determines the sensitivity to that threshold. In order to reflect the upper thresholds seen in MPB development, we adjusted (3.7),

$$r_{logmax}(T) = \frac{r_{max} \cdot e^{(T-T_b)/\Delta_b}}{1 + e^{(T-T_b)/\Delta_b}} - \frac{r_{max} \cdot e^{(T-T_m)/\Delta_m}}{1 + e^{(T-T_m)/\Delta_m}}. \tag{3.8}$$

Here T_b and T_m are the lower and upper temperature thresholds, while Δ_b and Δ_m determine the sensitivity to those thresholds (Figure 3.6).

Logan

The rate curve used by Logan et al. (1976) as well as Hansen et al. (2011),

$$r_{Logan}(T) = \psi \left([e^{\omega(T-T_b)} - 1] - [e^{\omega(T_m-T_b)} - 1]e^{-(T_m-T)/\Delta_m} \right) \tag{3.9}$$

for $T_b < T < T_m$, and 0 otherwise. Here T_m is the upper temperature threshold, T_b is the

lower temperature threshold, ψ controls the peak rate, ω controls the rate acceleration at lower temperatures, and Δ_m controls the thickness of the upper threshold boundary (Figure 3.7).

Brière

The rate curve developed by Brière et al. (1999)

$$r_{Brière}(T) = \psi \frac{T}{T_m}(\frac{T}{T_b} - 1)\sqrt{1 - \frac{T}{T_m}} \tag{3.10}$$

for $T_b < T < T_m$, and 0 elsewhere. Here T_m is the upper temperature threshold, T_b is the lower temperature threshold, and ψ controls the peak rate.

We applied a normalizing factor computationally, allowing us to directly use r_{max} as a parameter (3.8). The temperature where r_{max} occurs, T_{opt}, was calculated using equation (3.8), and thus the normalizing constant

$$N = T_{opt}(T_{opt} - T_b)\sqrt{|1 - \frac{T_{opt}}{T_m}|} \tag{3.11}$$

can be used in equation 3.10 such that

$$r_{BrièreMax}(T) = r_{max} \cdot \frac{T}{N}(T - T_b)\sqrt{|1 - \frac{T}{T_m}|}. \tag{3.12}$$

Non-parametric rate curves

We also developed two non-parametric rate curves using piece-wise linear functions. The simpler, triangular curve, referred to as non-parametric curve 1 (NP1), has a minimum temperature threshold T_b, a maximum temperature threshold T_m, a maximum rate r_{max}, and an optimal temperature T_{opt} at which r_{max} occurs (Figure 3.9). The second curve (NP2) includes an additional temperature break point, T_1, where the rate is equal to r_1, with $r_1 < r_{max}$ (Figure 3.10).
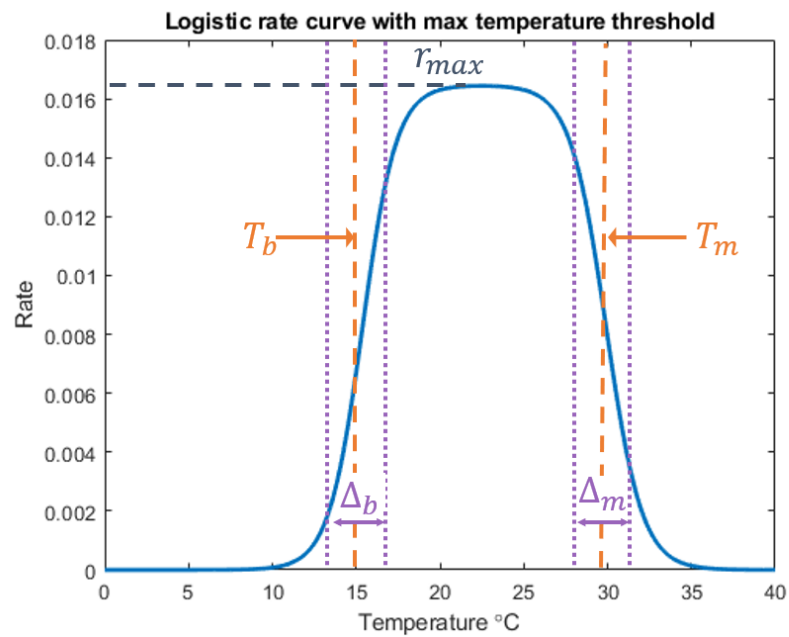
Fig. 3.6: The logistic rate curve with an upper threshold peaks at a developmental rate of r_{max}. The lower and upper temperature temperature thresholds, T_b and T_m, indicate the temperatures at which the steepness of the curve begins to decrease or increase, respectively. The sensitivity (slope of curve) at those thresholds is determined by Δ_b and Δ_m.
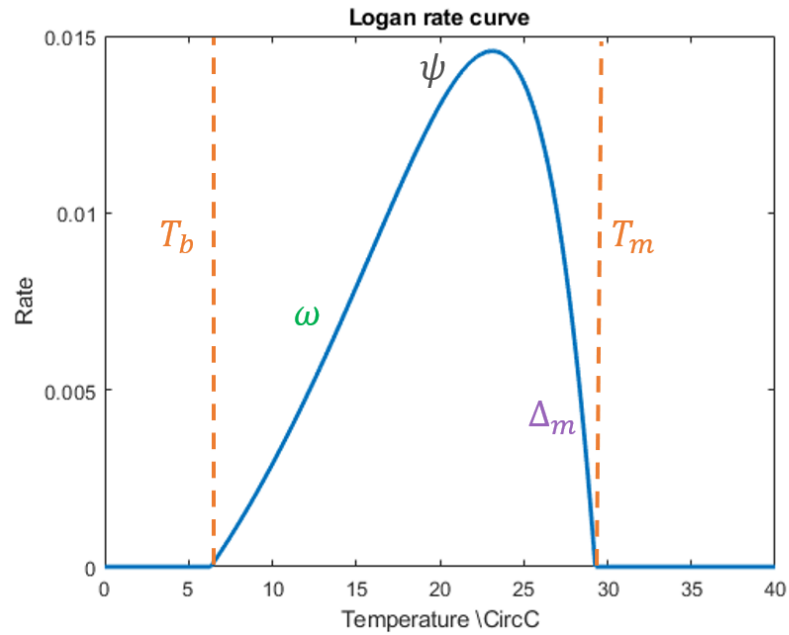
Fig. 3.7: While it is obvious that the Logan rate curve is greater than zero between the upper and lower thresholds, T_b and T_m, the other parameters affect the rate less directly. The maximum rate is linearly increased due to multiplication with *psi*, with larger values increasing the maximum rate. The steepness of the lower threshold is affected by ω, while the steepness of the upper threshold is affected by Δ_m.
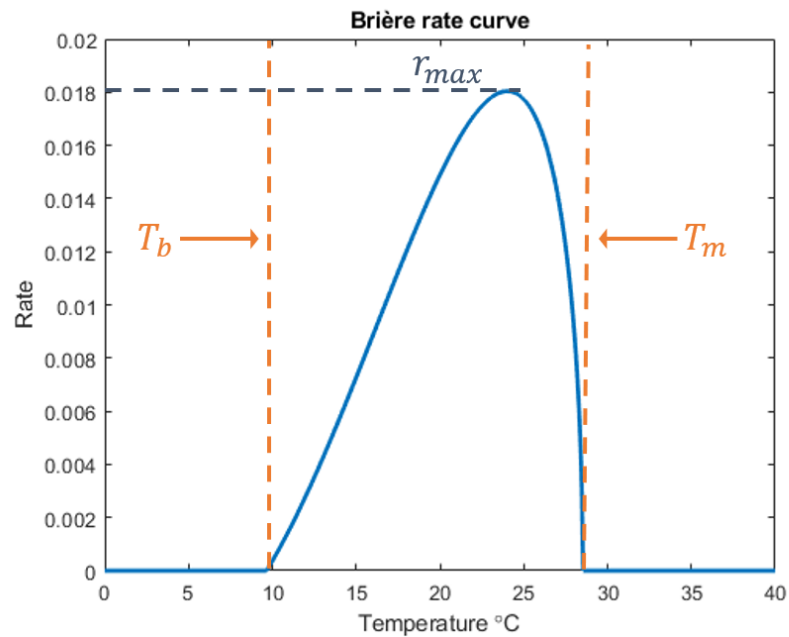
Fig. 3.8: The Brire rate curve begins to increase at the lower threshold, T_b, peaks at a rate proportional to ψ, then decreases until the rate is zero at the upper threshold, T_m.
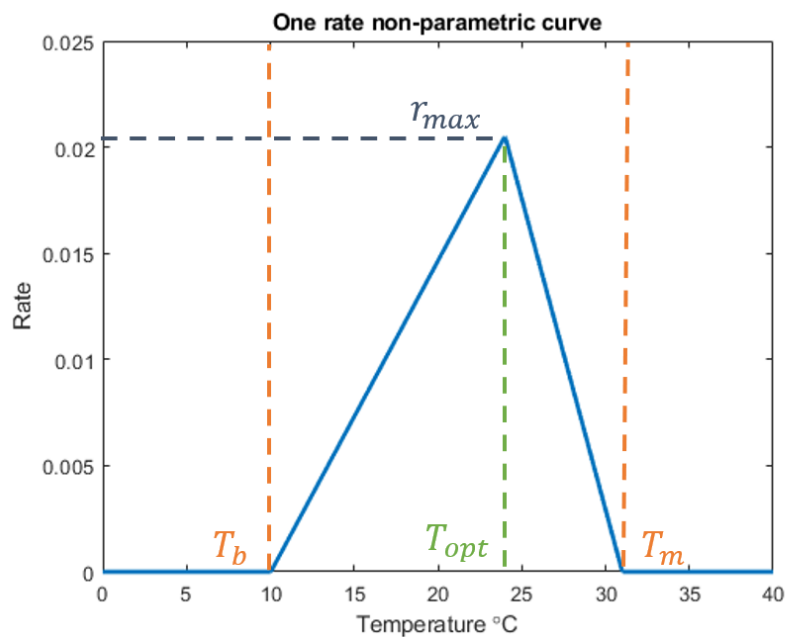
Fig. 3.9: The NP1 curve begins to linearly increase beginning at the lower threshold, T_m until a maximum rate of r_{max} is reached at optimal temperature T_{opt}, then linearly decreases from r_{max} to until the rate is zero at the upper threshold, T_m.
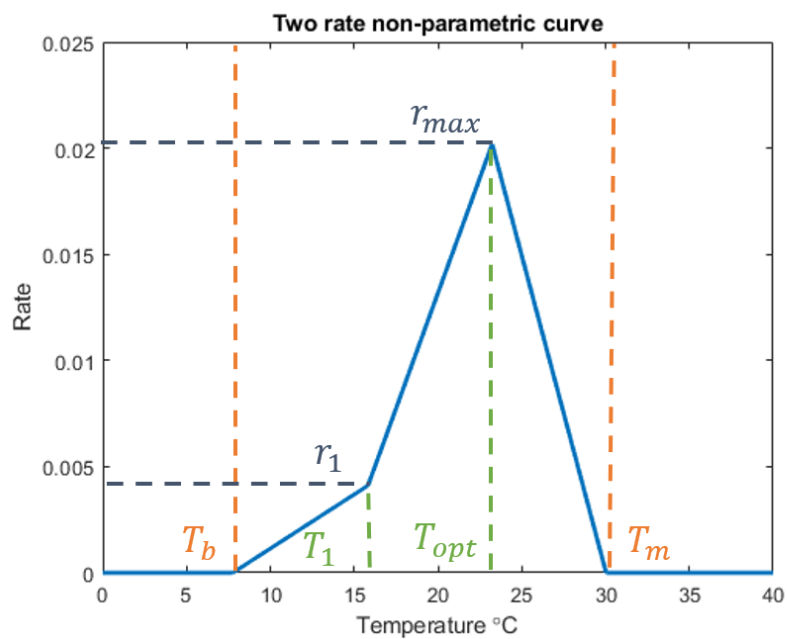
Fig. 3.10: The NP2 curve begins to linearly increase beginning at the lower threshold, T_m until a rate of r_1 is reached at T_1, then linearly increases fto r_{max} at T_{opt}, the mid-temperature threshold. The curve then decreases until the rate is zero at the upper threshold, T_m.

3.4 Inferring Teneral Adult Rates

In this section we describe the likelihood framework relating predicting emergence to observations, by which we determined a suitable teneral adult rate curve. The MPB field emergence data is described and linked to emergence; the distribution of deviance is also discussed. The process of bootstrapping emergence data is described, allowing us to draw inference regarding possible teneral adult rate curves.

3.4.1 MPB Emergence Data

Teneral adult rate curves are parameterized using emergence data from the Arizona MPB population in Lockett Meadows, Cococino National Forest, AZ. Attack data from the previous year was used as input for the oviposition model, the output of which was used as input for the EvF cohort model as described in (3.3.2). The complete data set can be found in Appendix A.

Field observations of MPB emergence were recorded every 4-6 days. The total number of observed beetles for a tree on side i is the sum of beetles emerged on that side, N_i. The predicted emergence for a tree side i between observation days was weighted by the total number of beetles that emerged from the tree in order to be directly compared to the field data,

$$\text{pred}_{i,k} = N_i \int_{t_{k-1}}^{t_k} p_8(t)dt. \tag{3.13}$$

3.4.2 Determining Appropriate Distributions for Deviance

In order to determine the best error model for the deviance between predicted and observed adult emergence, we calculated the negative log likelihood (NLL) using normal, Laplace, and Poisson distributions. For given data and a candidate rate curve, parameters for rate curves and error distributions were determined by minimizing NLL computationally. The Akaike Information criterion (AIC) (Burnham 2002),

$$\text{AIC} = 2\,\text{NLL} + 2(\text{number of parameters}), \tag{3.14}$$

was used to allow deviance models to compete on an equal footing.

Laplace Deviance Distribution

If the errors have a Laplace distribution, for a single observation on side i on day k, $\mathrm{obs}_{i,k}$,

$$\mathrm{Prob}(\mathrm{obs}_{i,k}|\mathrm{pred}_{i,k}) = \frac{1}{2\alpha_i} \exp\left[-\frac{\left|\mathrm{obs}_{i,k} - \mathrm{pred}_{i,k}\right|}{\alpha_i}\right] \tag{3.15}$$

for a particular tree, where α_i is an additional parameter specifying the variance. Correspondingly the NLL function for a single tree is

$$\mathrm{NLL} = \sum_i \sum_k \log\left(2\alpha_i\right) + \frac{1}{\alpha_i}\left|\mathrm{obs}_{i,k} - \mathrm{pred}_{i,k}\right|. \tag{3.16}$$

Normal Deviance Distribution

If the errors have a normal distribution, for a single observation on a tree,

$$\mathrm{Prob}(\mathrm{obs}_{i,k}|\mathrm{pred}_{i,k}) = \frac{1}{\sqrt{2\pi\sigma_i^2}} \exp\left[\frac{-\left(\mathrm{obs}_{i,k} - \mathrm{pred}_{i,k}\right)^2}{2\sigma_i^2}\right], \tag{3.17}$$

where σ_i^2 is the variance. Correspondingly, the NLL function for a single tree is

$$\mathrm{NLL} = \sum_i \sum_k \left[\frac{1}{2}\log(2\pi\sigma_i^2) + \frac{1}{2\sigma_i^2}\left(\mathrm{obs}_{i,k} - \mathrm{pred}_{i,k}\right)^2\right]. \tag{3.18}$$

Poisson Deviance Distribution

If the errors have a Poisson distribution, for a single observation on a tree,

$$\mathrm{Prob}(\mathrm{obs}_{i,k}|\mathrm{pred}_{i,k}) = \frac{e^{-\mathrm{pred}_{i,k}}(\mathrm{pred}_{i,k})^{\mathrm{obs}_{i,k}}}{\mathrm{obs}_{i,k}!} \tag{3.19}$$

for the kth observation on tree side i. Correspondingly the NLL function for a single tree is

$$\mathrm{NLL} = \sum_i \sum_k \left[\mathrm{pred}_{i,k} - \mathrm{obs}_{i,k}\log(\mathrm{pred}_{i,k}) + \log(\mathrm{obs}_{i,k}!)\right]. \tag{3.20}$$

3.4.3 Computation and Bootstrapping

Errors and AIC were calculated by using the MATLAB fmincon function to minimize NLL on bootstrapped emergence data. Bootstrapping was performed by randomly selecting with replacement from the emergence data of all days for the number of total observations for all days. Each individual beetle was considered an observation for a day, as was any day where no emergence was recorded. As an interesting consequence, this resulted in selections where days with no emergence were picked more than a single time. Correspondingly, bootstraps were weighted to take into account multiple selections of days where there was zero emergence.

The Briére rate curve for teneral adults had the smallest nominal, or best-fit to non-bootstrapped data, AIC value across trees and error models, and was correspondingly used to determine the most suitable deviance distribution with the field data from Tree 2. After the appropriate distribution was determined, the process was repeated using all of the potential teneral adult curves. Bootstrapping was then performed on both trees. If parameter estimates did not converge across error distributions for a particular set of bootstrapped data, it was removed from the data set.

3.4.4 Deviances have Laplace Distribution

The nominal AIC values (values for unbootstrapped data and the Briére rate curve) were $\text{AIC}_{\text{Laplace}} = 179.7149$, $\text{AIC}_{\text{Normal}} = 193.6050$, and $\text{AIC}_{\text{Poisson}} = 231.2407$. Calculating the ΔAIC between the distributions (with $\Delta\text{AIC} > 5$ as the difference considered to be significant improvement), the Laplace distribution ΔAIC values are 13.8901 for the Normal distribution and and 51.5258 for Poisson distribution, indicating that the Laplace distribution better describes the deviances in the context of the data, which was confirmed by the bootstrapped data. All of the bootstrapped Laplace AIC values were less than the nominal Poisson AIC, and 99.4% of the normal AIC values were smaller (3.11). Thus even considering realistic redistributions of the data, the Poisson distribution was the least descriptive.
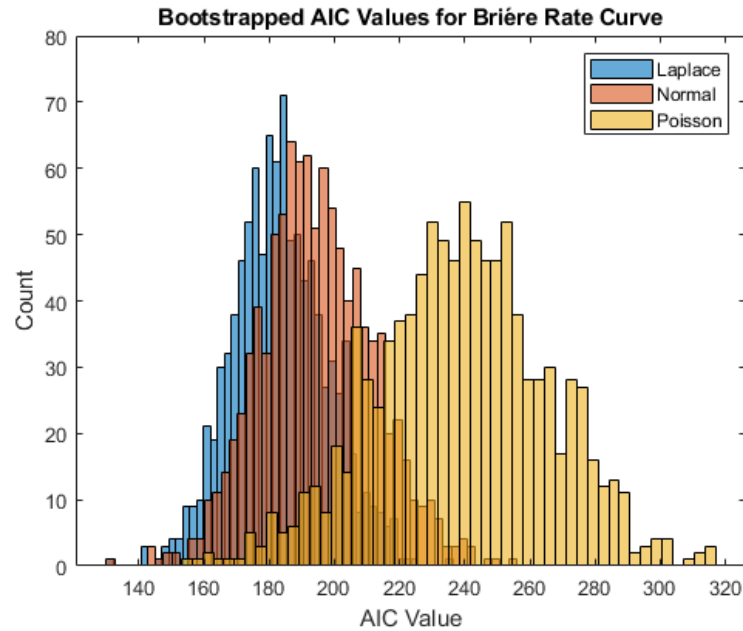
Fig. 3.11: Histograms for the three distributions considered for 1000 bootstrapped sets of data using the Briére rate curve. While it was clear that the Poisson distribution was least suitable, the Laplace and normal distributions were investigated further.
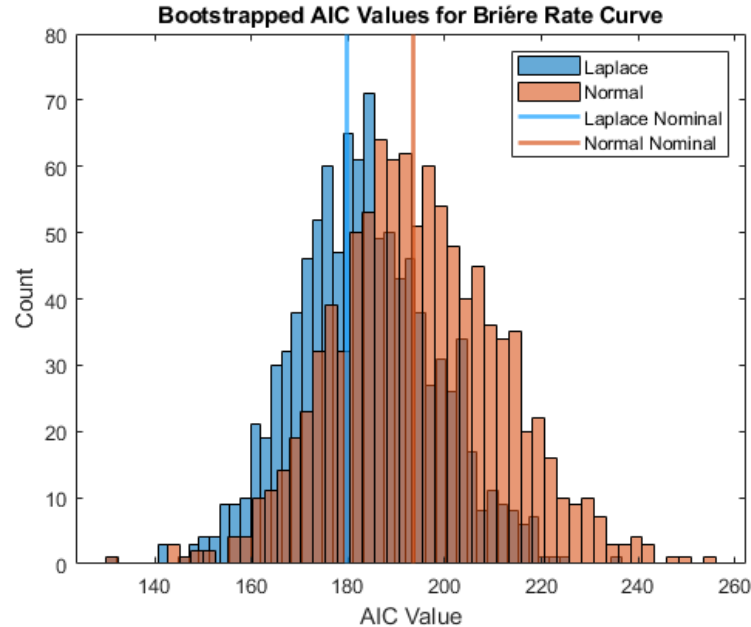
Fig. 3.12: Histograms for the two distributions considered for 1000 bootstrapped sets of data using the Briére rate curve including the nominal (non-bootstrapped) AIC values. The Laplace nominal AIC is 179.7149, normal is 193.6050. A ΔAIC of 13.8901 indicates the Laplace distribution is a significantly better fit. We found 99.6% of Laplace AIC values were smaller than the corresponding normal AIC value in pairwise comparison of bootstraps, giving us high confidence the Laplace distribution was found to be more suitable than a normal distribution.

The Laplace and normal bootstrapped AIC values were much closer, as can be seen in Figure 3.12. Considering bootstrapped resampling of the data, only 41.1% of the bootstrapped normal AIC values were smaller than the nominal Laplace AIC, as opposed to 91.3% of the bootstrapped Laplace AIC values being smaller than the nominal normal AIC. Comparing individual bootstraps pairwise, 99.6% of Laplace AIC values were smaller than the corresponding normal AIC value. The significant ΔAIC value as well as the better performing bootstraps highly suggested that the Laplace distribution was most suitable for the data, and thus was used for teneral adult rate curve selection.

3.5   Results and Validation

In this section we present the parameters and AIC values for the bootstrapped emergence for Tree 1 and 2, using the Laplace deviance model. We then investigate which rate curve and set of parameters is most suitable for the teneral adult model, using bootstrapped distributions and cross-validation to assess the suitability of parameters. With the chosen teneral adult rate curve we validate using the field data for Tree 3, and compare with observed emergence in the field.

3.5.1   Teneral Adult Rates and Rate Curve Selection

Teneral adult rate curve parameters were fit by minimizing Laplace NLL as shown (3.16), testing all five candidate rate models. As seen in Figures 3.13 and 3.14, temperature thresholds and maximum rates vary among the rate curves, but the curves are somewhat similar, notably at inflection points. Nominal parameters for the various teneral adult rate curves can be seen in Table 3.2 (Tree 2) and Table 3.3 (Tree 1). For both trees the Briére rate curve had the smallest nominal AIC value, indicating it could be the best fit. Note that since emergence data is different for each tree, NLL/AIC values cannot be compared across trees, but calculating the ΔAIC between curves for an individual tree allows comparison among the competing teneral adult rate curves.

For Tree 2, the ΔAIC between the Briére curve the curve with the next lowest nominal AIC value, the Logistic curve, was not significant at 3.3802, but the Briére curve was a

significantly better fit than all other curves. The ΔAIC for the Tree 1 Briére curve is not significant for the NP1 and Logistic curves, which all had nearly the same value (Table 3.3). The Tree 1 Briére, NP1, and Logistic curves all have ΔAIC> 5 for the Logan and NP2 curves. We were confident in removing the NP2 and Logan curves from consideration based on the ΔAIC values, and further analyzed the bootstrapped AIC values of the Briére curve to the Logistic and NP1 curves using the nominal values and pairwise bootstraps.

The Tree 2 NP1 bootstrapped AIC values were lower than the Briére nominal AIC value in 88.93% of cases, while 59.40% of the Briére AIC values were lower than the NP1 nominal. The Logistic AIC values were lower than the Briére nominal AIC value in 57.67% of cases, and the Briére AIC values were lower than the Logistic nominal in 73.53% of cases.

The Tree 1 NP1 bootstrapped AIC values were lower than the Briére nominal AIC value in 28.13% of cases, and 37.47% of the Briére AIC values were lower than the NP1 nominal. The Logistic AIC values were lower than the Briére nominal AIC value in 28.80% of cases, and in comparison the Briére AIC values were lower than the Logistic nominal in 38.53% of cases.

p	Briére	NP1	Logistic	Logan	NP2
1	$T_m = 27.2079$	$T_m = 31.0004$	$T_m = 27.0832$	$T_m = 29.3404$	$T_m = 30.0218$
2	$T_b = 11.3539$	$T_b = 10.0305$	$T_b = 15.0430$	$T_b = 4.6950$	$T_b = 6.1280$
3	$r_{max} = 0.0197$	$T_1 = 24.0002$	$\Delta_m = 1.0500$	$\Delta_m = 5.5022$	$T_1 = 14.5194$
4		$r_{max} = 0.0205$	$\Delta_b = 0.9336$	$\omega = 0.1036$	$T_2 = 23.3252$
5			$r_{max} = 0.0161$	$\psi = 0.0076$	$r_1 = 0.0058$
6					$r_{max} = 0.0191$
σ	0.0009	0.0020	0.009	0.0009	0.0010
AIC	179.7149	191.3895	183.0231	198.4058	196.2578
p	4	5	6	6	7

Table 3.2: The parameters for the teneral adult curves discussed in for Tree 2 found by minimizing Laplace AIC as discussed in 3.16. The r_{max} value is not one of parameters of the Logan curve, but was calculated via the parameters above to be 0.0146.

p	Briére	NP1	Logistic	Logan	NP2
1	$T_m = 26.0813$	$T_m = 27.9051$	$T_m = 24.7417$	$T_m = 25.8880$	$T_m = 28.5829$
2	$T_b = 12.6750$	$T_b = 12.9662$	$T_b = 16.057$	$T_b = 6.5494$	$T_b = 9.3783$
3	$r_{max} = 0.0216$	$T_1 = 21.0696$	$\Delta_m = 0.9000$	$\Delta_m = 5.0124$	$T_1 = 13.7564$
4		$r_{max} = 0.0240$	$\Delta_b = 0.9000$	$\omega = 0.1405$	$T_2 = 21.0873$
5			$r_{max} = 0.0200$	$\psi = 0.0135$	$r_1 = 0.0060$
6					$r_{max} = 0.0192$
σ	0.0013	0.0012	0.0013	0.0025	0.0025
AIC	146.5389	146.4500	146.9061	161.6491	160.9793
p	4	5	6	6	7

Table 3.3: The parameters for the teneral adult curves discussed in for Tree 1 found by minimizing Laplace AIC as discussed in 3.16. The r_{max} value is not one of parameters of the Logan curve, but was calculated via the parameters above to be 0.0173.

While for a simple pairwise comparison of the Briére AIC values to the NP1 and Logistic values was overwhelmingly in favor of the Briére curve (Table 3.4), the percentage for which the ΔAIC was greater than 5 was much smaller. For Tree 2, the ΔAIC was at least 5 for 14.00% of the NP1 bootstrap AIC values, and 6.47% of the Logistic AIC values. For Tree 1, the ΔAIC was at least 5 for 32.93% of the NP1 bootstrap AIC values, and 27.47% of the Logistic AIC values.

The Briére curve was determined to be the best rate curve fit due to lower nominal fits for both trees, nominal ΔAIC values indicating it is the best fit for Tree 2, and overall better performance when bootstrapped.

	Pairwise		Significant	
Model	Tree 2	Tree1	Tree 2	Tree 1
Logistic	98.27	78.40	6.47	27.47
NP1	96.27	78.60	14.00	32.93
Logan	100.00	95.87	99.93	75.60
NP2	99.8	87.00	97.40	84.13

Table 3.4: The percentage of pairwise bootstraps (for 1500 bootstraps) for which the AIC value was at greater as well as significant (ΔAIC> 5) than the corresponding Briére bootstrap for the considered teneral adult rate curves, for each tree.
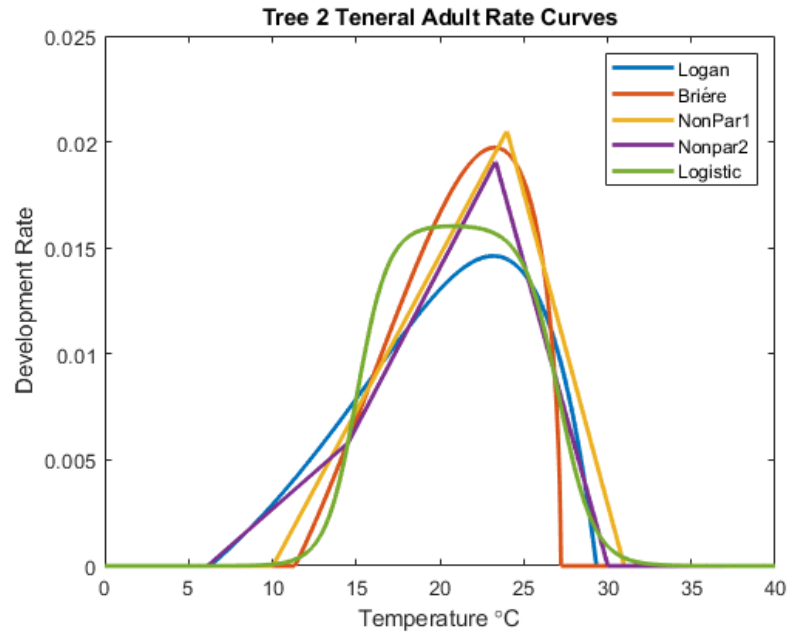
Fig. 3.13: The parameterized teneral adult rate curves for Tree 2 found by minimizing Laplace NLL as discussed in 3.16. The overlap of the curves at approximately 15 and 27°C suggests an underlying mechanism of MPB teneral development. The Briére curve had the lowest nominal AIC value suggesting it is most suitable for Tree 2.
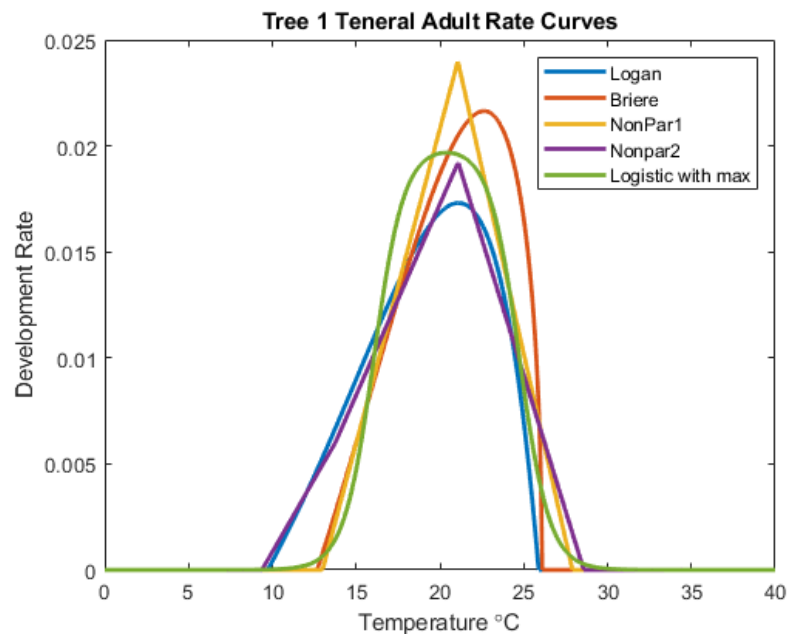
Fig. 3.14: Parameterized teneral adult rate curves for tree 1 found by minimizing Laplace NLL as discussed in 3.16. Overlaps in rate curves at inflection points near 15 and 27°C are present as seen in Tree 2. The Briére curve is again the most suitable curve nominal curve, with the lowest nominal AIC value.
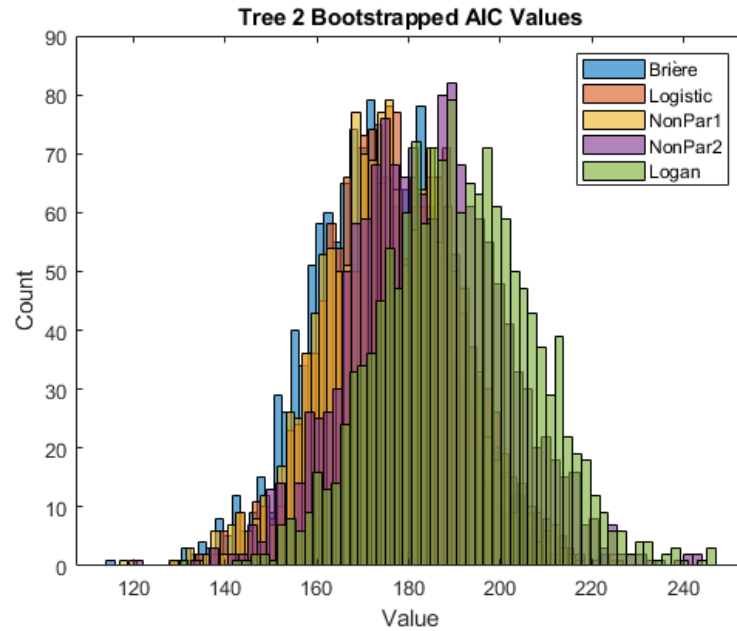
Fig. 3.15: Histograms of the AIC values found by minimizing Laplace NLL for Tree 2 for 1500 bootstrap samples of the field emergence data. We found 73.53% of Briére AIC values lower than the Logistic nominal value, the next lowest AIC value, while the Logistic bootstrap AIC values were lower than the Briére nominal value in 57.67% of cases.
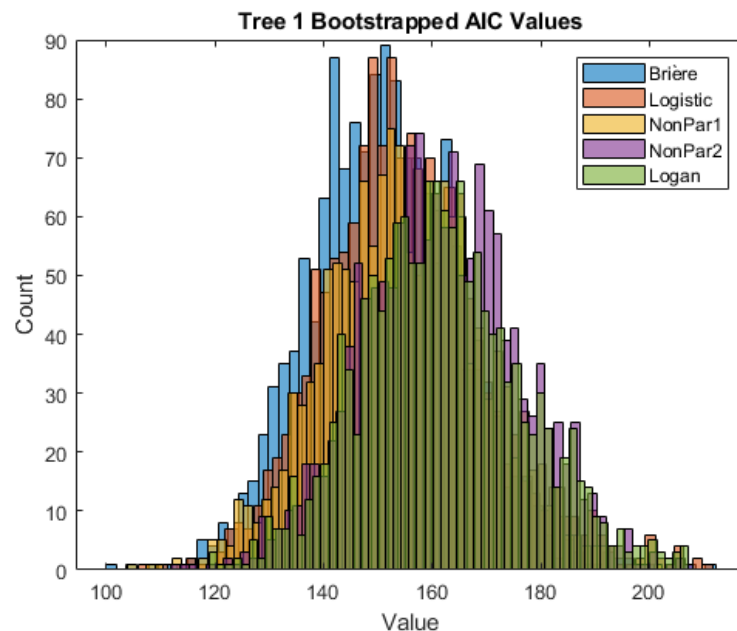
Fig. 3.16: Histograms of the AIC values found by minimizing Laplace NLL for Tree 1 for 1500 bootstrap samples of the field emergence data. We found 38.53% of Briére AIC values lower than the NP1 nominal value, the next lowest AIC value, while the NP1 bootstrap AIC values were lower than the Briére nominal value in 28.80% of cases.
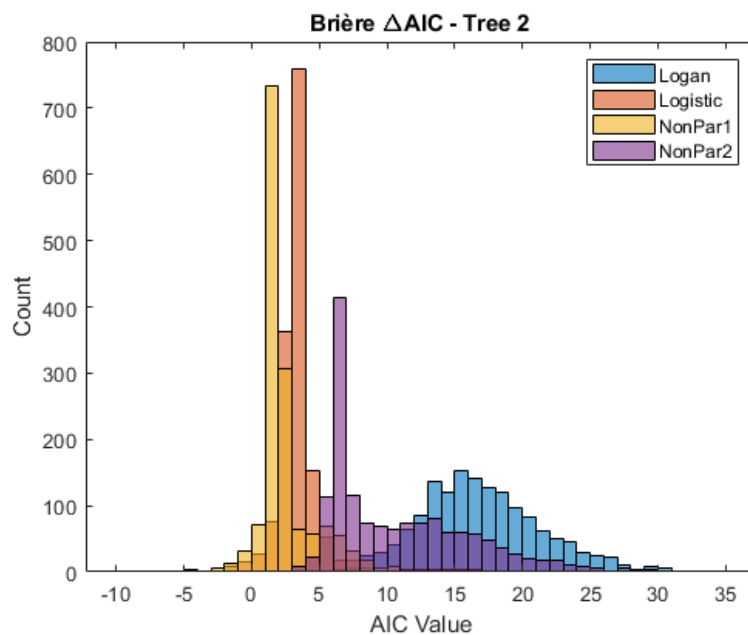
Fig. 3.17: Histograms of the AIC values found by minimizing Laplace NLL for Tree 2 for 1500 bootstrap samples of the field emergence data. For the Tree 2 bootstraps, 6.47% of Briére AIC values were at least 5 lower than the corresponding Logistic AIC values, the next lowest nominal NLL value.
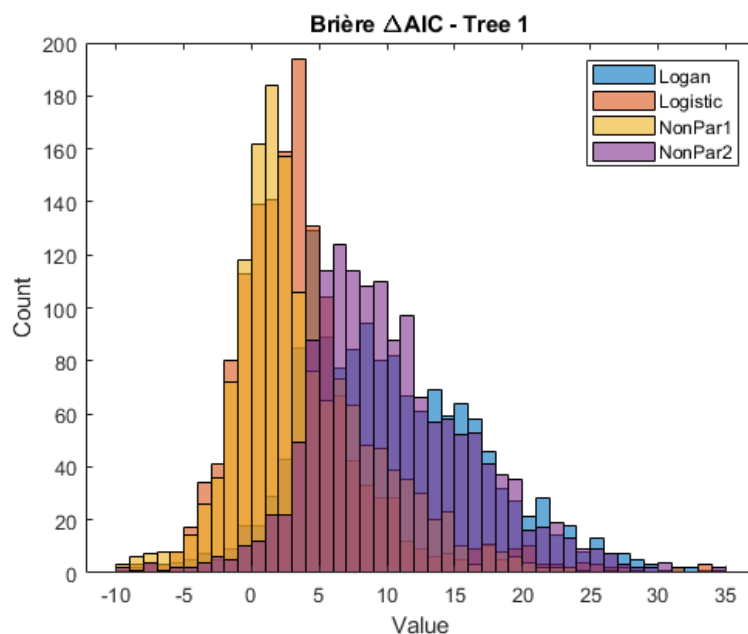
Fig. 3.18: Histograms of the AIC values found by minimizing Laplace NLL for Tree 1 for 1500 bootstrap samples of the field emergence data. For the Tree 1 boostraps 32.94% of Briére AIC values were at least 5 lower than the corresponding NP1 AIC values, the next lowest nominal NLL value.

3.5.2   Parameter Value Selection for Briére Rate Curve

After determining that the Briére curve was the most suitable rate curve to predict southern MPB teneral adult development, we wished to determine whether or not the set of parameters obtained for Tree 2 or Tree 1 would result in more accurate predictions. In order to determine this we cross-validated the data by calculating the NLL for each tree using the parameters of the other tree (Table 3.5).

Field Data Used	Tree 1	Tree 2
NLL with Tree 1 Curve	136.5389	296.0648
NLL with Tree 2 Curve	161.2320	169.7149

Table 3.5: A table of the NLL values for each tree using the fitted parameters, as well as those calculated via cross validation. Tree 1 was the least suitable in cross validation, with a higher NLL value due to incorrectly predicting emergence later than observed in the field.

While the Tree 2 parameters had larger NLL than the Tree 1 parameters using the Tree 1 field data as input, the Tree 1 parameters performed notably poorly with the Tree 2 field data. Though the parameterized curves appear to be quite similar (Figure 3.19), the differences in parameters resulted in a notable change in the cumulative distributions (Figure 3.20). The Tree 1 parameters were consequentially different enough for the change in the timing/density of emergence to greatly increase the NLL value. This is particularly evident when the distributions are used to calculate predicted field emergence for the days of field observation for the southern side of Tree 2 (Figure 3.21). The Tree 2 parameters correctly predict the peak of MPB emergence, while the Tree 1 parameters predict emergence too late, but also across a longer time period. This results in a much greater difference in predicted emergence, particularly on days 594 and 597 (Figure 3.21) and thus a much larger NLL value.

Additionally, we investigated the distributions of parameters fitted to the 1500 bootstraps of the emergence data. The parameter distributions are broader and less defined for the Tree 1 parameters, indicating that the fits are less suitable (Figure 3.22). We created 90% confidence intervals for each parameter and each tree, and the confidence intervals were
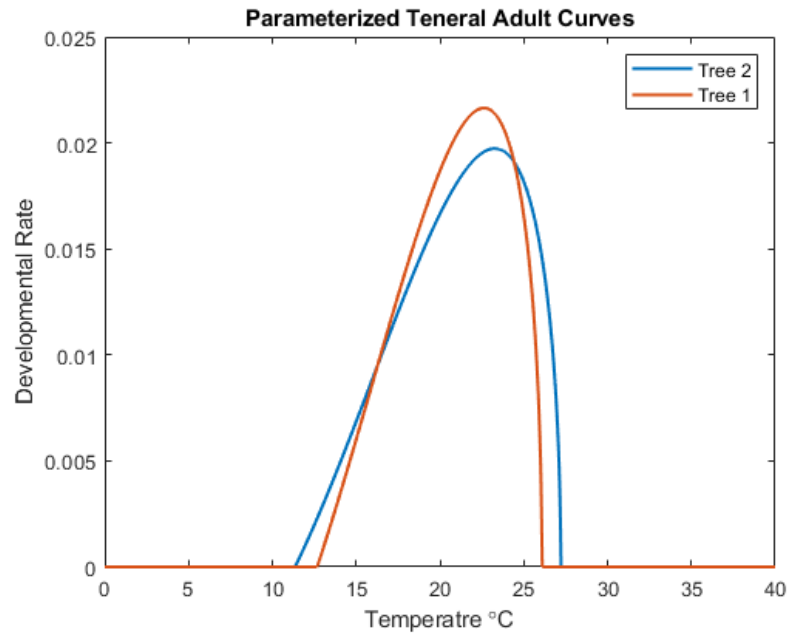
Fig. 3.19: The teneral adult curves found by minimizing Laplace AIC for Tree 1 and Tree 2. Though the curves appear to be quite similar, but the differences in parameters are enough for Tree 2 to outperform Tree 1 in cross-validation.
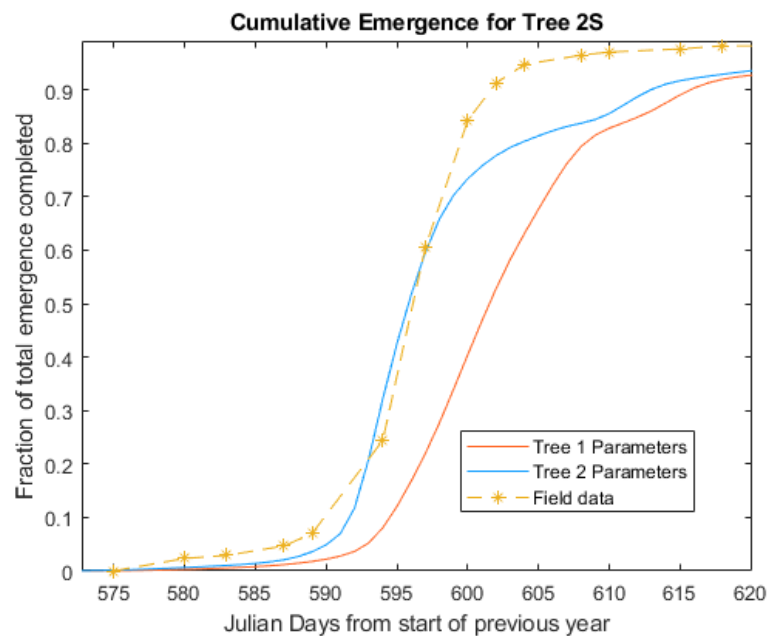
Fig. 3.20: The teneral adult cumulative predicted using field phloem and MPB attack data as input. Though there are similarities between the curves, the Tree 1 parameters result in a delayed and extended prediction of emergence and thus a much higher NLL value, missing the peak of observed adult emergence.
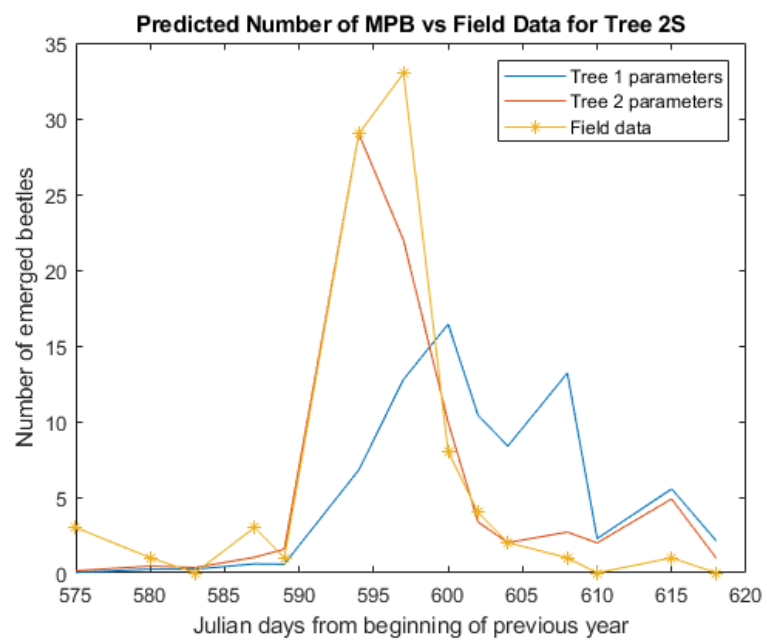
Fig. 3.21: Using the number of emerged beetles as weights in the emergence distribution more accurately reflects the sweeping emergence used for parameterization. The plots of predicted beetles for each day of field observation indicate not only that the Tree 2 parameters are a more suitable fit, as expected as this tree was used to create those parameters, but also indicate why the NLL for Tree 1 parameters was much higher.
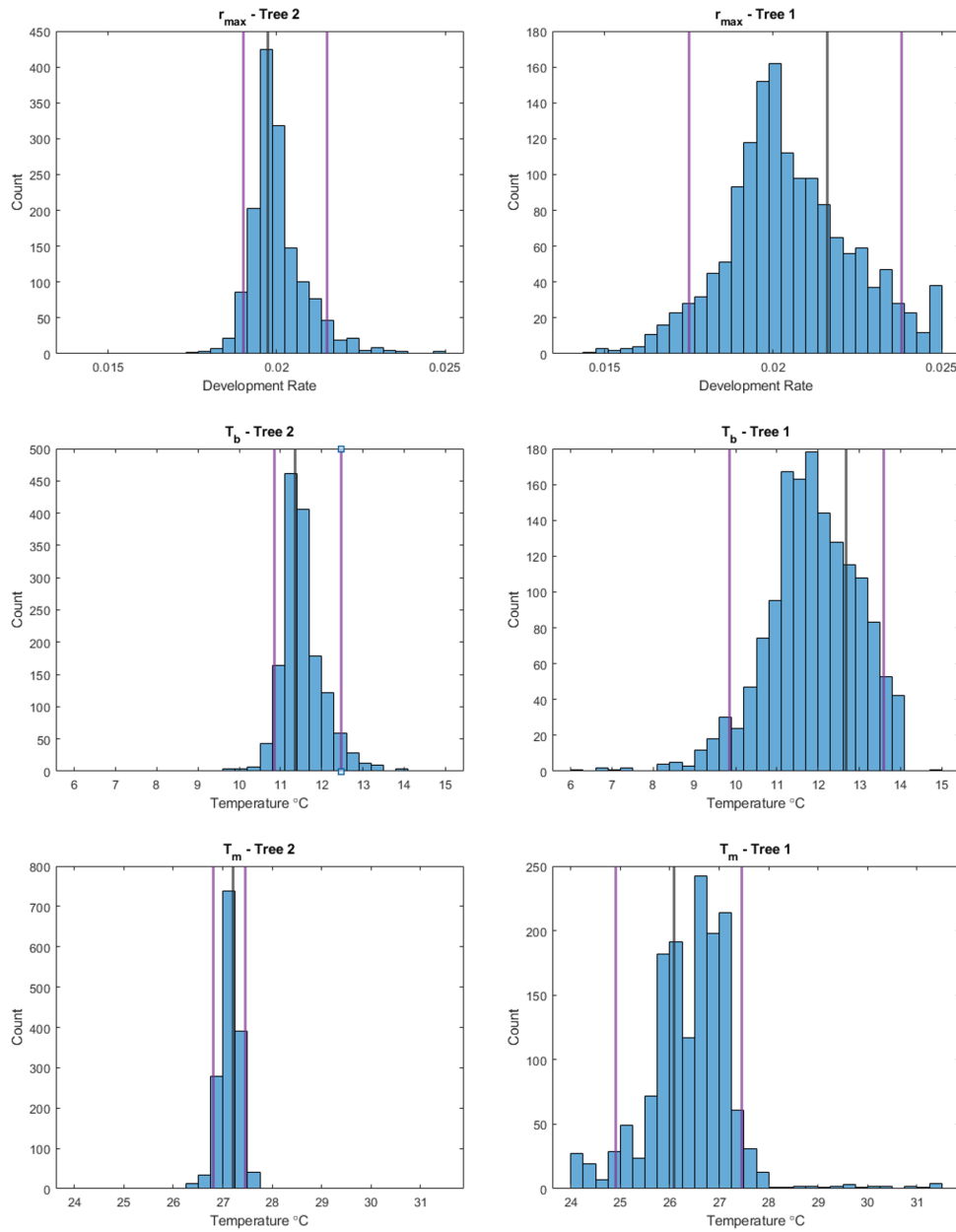
Fig. 3.22: Distributions of T_m, T_b, and r_{max} obtained from fitting parameters to 1500 bootstraps of field emergence data for each tree, with nominal parameter lines in black and 90% confidence interval bounds in purple. The Tree 2 distributions more close matched the nominal fits, had smaller confidence intervals, and were more appropriately distributed.

wider for Tree 1 in all cases. (Figure 3.22). Confidence intervals for Tree 2 were 39.68% the width for r_{max}, 43.41% for T_b, and 25.63% for T_b than the respective Tree 1 confidence intervals. Due to the more successful cross validation and smaller confidence intervals, the parameters from Tree 2 were determined to be more suitable for predicting southern MPB teneral adult development.

3.5.3 Validation with Field Data

Predictions using the Briére curve, parameterized with Tree 2, data, were compared with observations of emergence from Tree 3 from from the 2015-2016 season . Despite having a comparable number of attacks in the previous year, an abnormally small amount of MPB emergence was observed for Tree 3 (Figure 3.24). This caused difficulty when attempting to fit parameters for this tree, as non-emergence of MPB was a minimum NLL for teneral rate curve fitting, which is why Tree 3 was reserved for validation. The Briére rate curve from Tree 2 was still relatively successful for predicting MPB emergence on Tree 3. The peak predicted emergence for the north side of the tree was at day 597, which was only three days off from the observed peak of 594. The predicted date of median cumulative emergence was approximately three days behind the observed, and the timing was also close from 60-90% of total emergence completed. (Figure 3.23). The time frame of predicted emergence was correct, except for a lack of of emergence on days 575 and 589. The model correctly predicted minimal emergence from the south side of Tree 3, though the peak date of emergence was predicted at 587 instead of 594. Still, a majority of cumulative emergence was predicted in the same time frame was the observed (Figure 3.24).
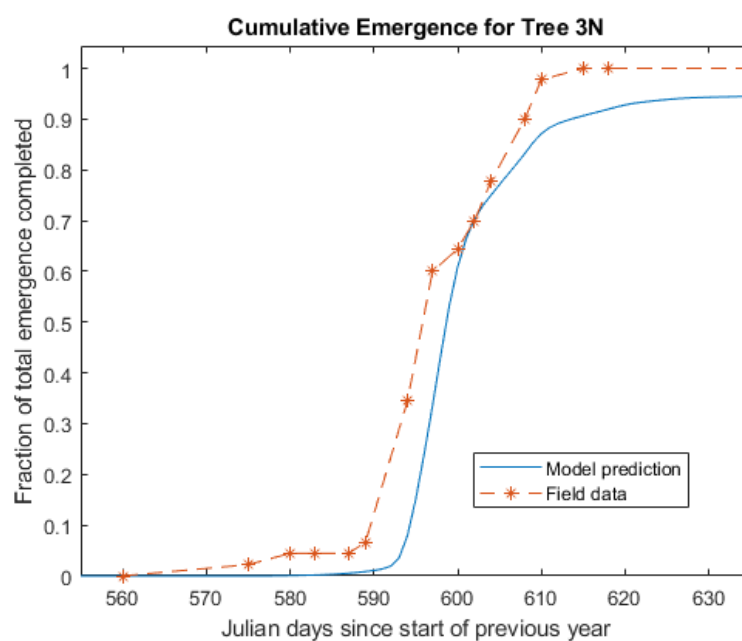
Fig. 3.23: The cumulative fraction of oviposition observed in the field and predicted by the model for the north side of Tree 3. The predicted date of median cumulative emergence was only approximately three days behind the observed day of emergence, and very close from 60-90% of total emergence completed.
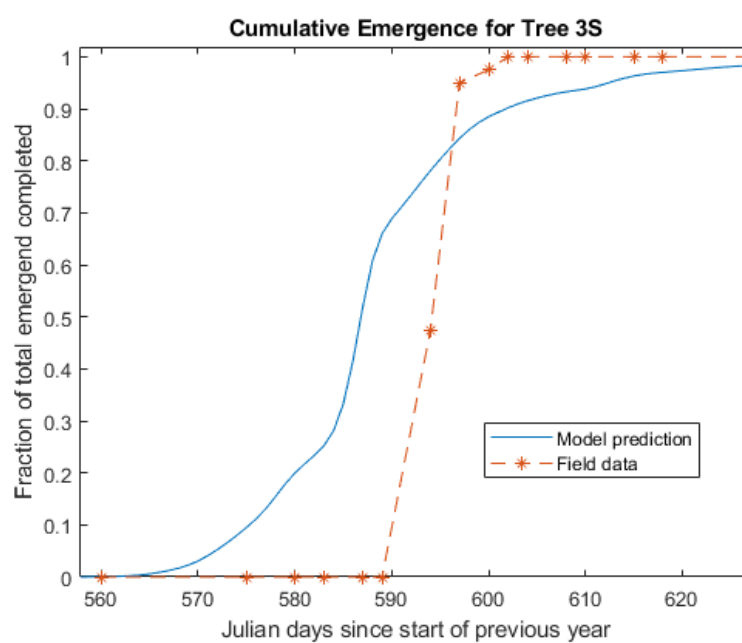
Fig. 3.24: The cumulative fraction of oviposition observed in the field and predicted by the model for the south side of Tree 3. The difference in the predicted median emergence was approximately 7.5 days. Unusually low emergence was observed in the field, and while the model correspondingly overestimated emergence, the majority of oviposition was predicted to be completed on day 600 as seen in the field.

3.6 Adaptive Phenology and Possibility of Changes in Voltinism

In addition to determining and parameterizing a suitable teneral adult rate curve for a southern population of MPB, additional goals of this paper were to assess the adaptive phenology of southern MPB and the possibility of bivoltinism. In order to determine the comparative adaptive phenology of southern and northern MPB populations, we compared the southern MPB teneral adult rate curve calibrated here to the rate curve parameterized to the northern population by Régnière et al (2012). We also compared generation time and emergence using each teneral rate curve in our phenology model for the southern population, with the 2015-2016 field attack and phloem temperature data as input.

3.6.1 Comparison of Parameters and Emergence

The teneral adult rate curve for a southern population of MPB found in this paper differs significantly from the one used for a northern population by Régnière et al. (2012), which was fit using equation (3.1). Though not all of the parameters of the two rate curves are directly comparable, we are able to compare the maximum rate and temperatures thresholds. All of the bootstrapped r_{max} for the southern population values were smaller than 0.0255, far below the northern r_{max} of 0.0752 (Figure 3.25). Taking into account the lognormal variance of the northern population by multiplying r_{max} by $\exp(\pm\sigma_{\text{North}})$, where $\sigma_{\text{North}} = 0.190$ (Régnière et al. 2012), the lower value of r_{max} for the northern population is still 0.0622, which is much higher than the southern population. (Figure 3.28)

All of the values of T_m were below the northern T_m of 35°C, with a maximum value of 31.60 (Figure 3.27). While the values of T_b are closer to the northern MPB threshold of $T_b = 4.2$ for the NP2 and Logan rate curves, these curves also have the higher nominal and bootstrapped AIC values and are less credible fits for southern MPB teneral adult development. The distribution of the lower temperature threshold of Brière, Logistic, and NP1 curves do not have values lower than 6.5°C.

The nominal values, as well as the distribution of parameters, indicate that teneral adult development in southern populations of MPB occur at lower maximum rate and within a narrower range of temperature, which makes evolutionary sense for a population

adapted to maintain univoltism in a warmer southern range. None of the Brière curves
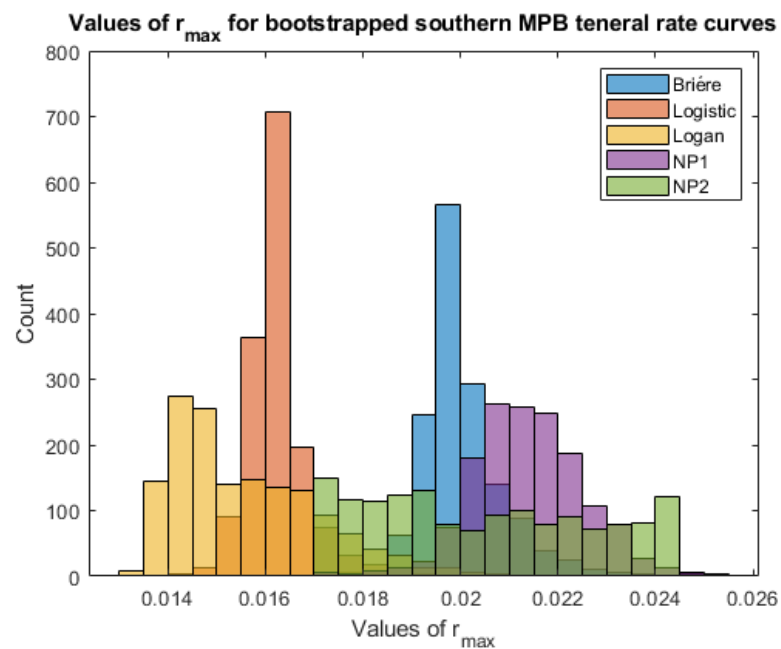
Fig. 3.25: Histograms of the values of r_{max} obtained from 1500 bootstraps of teneral adult rate curves for Tree 2. All values of r_{max} were lower than the curve previously parametrized northern MPB teneral adult rate curve r_{max} of 0.0198 (Régnière et al. 2012). The Logan r_{max} parameter was calculated computationally by finding the maximum point of each fitted curve.
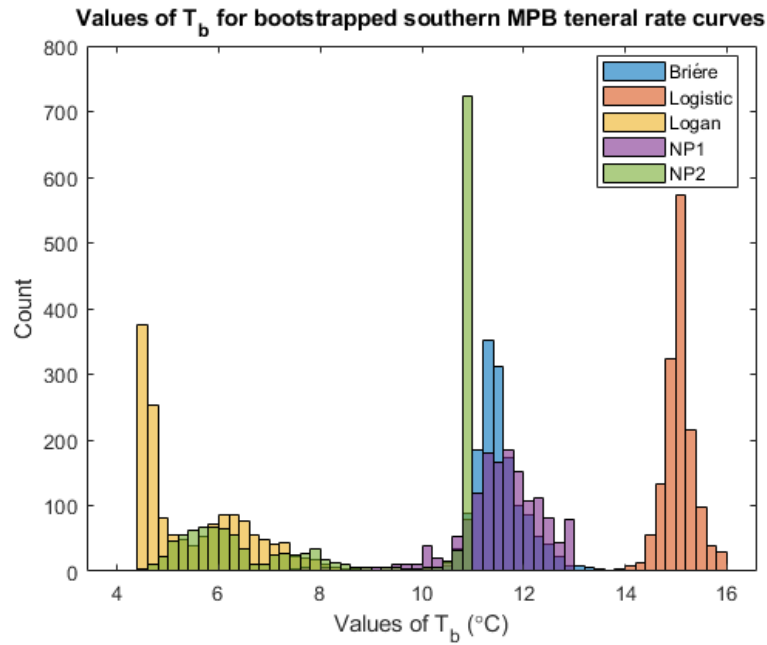
Fig. 3.26: Histograms of the values of T_b obtained from 1500 bootstraps of teneral adult rate curves for Tree 2. Though the Logan and NP2 curve have lower and unevenly distributed parameter thresholds, the three curves with the lower nominal and bootstrapped AIC values have distributions of T_b much greater than the northern MPB lower threshold of 4.5°C.
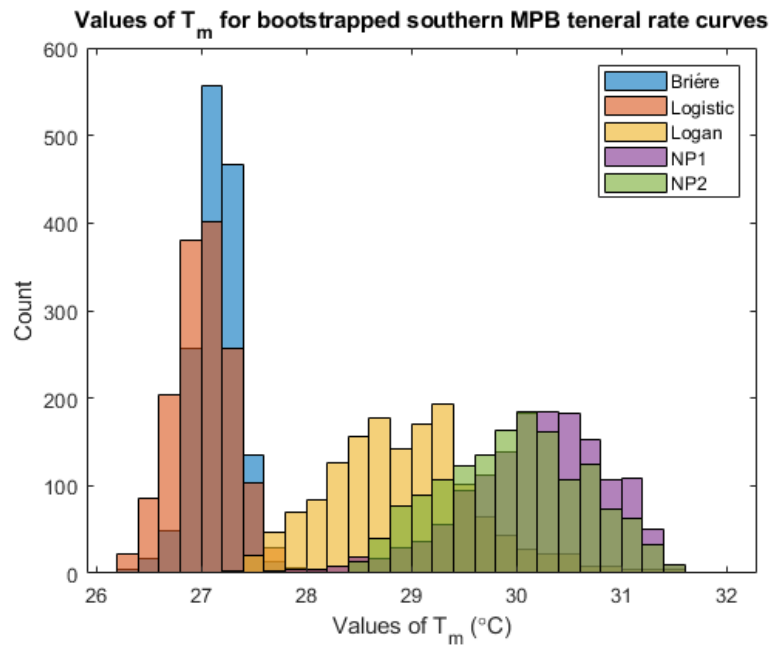
Fig. 3.27: Histograms of the values of T_m obtained from 1500 bootstraps of teneral adult rate curves for Tree 2. All values are much lower than the northern MPB T_m of 35°C.
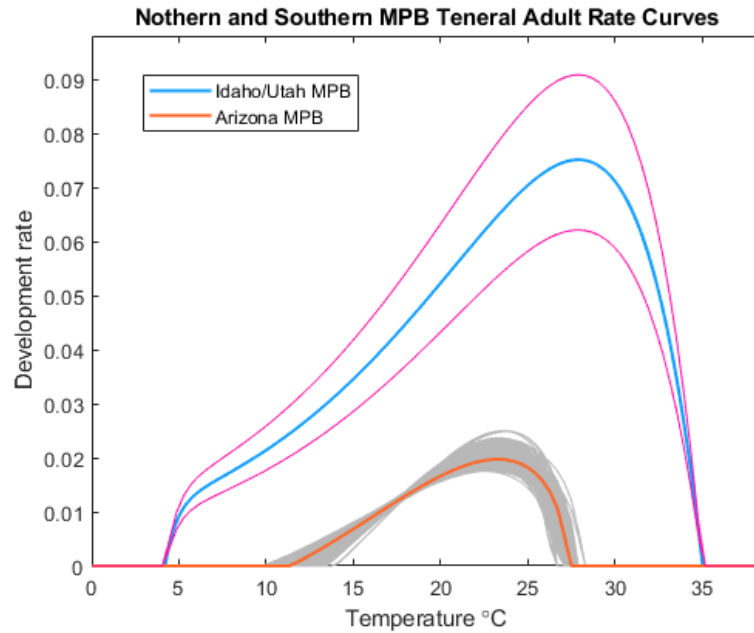
Fig. 3.28: The rate curve parameterized for a northern MPB population, using 3.1 and the northern MPB parameters (Régnière et al. 2012), as well as the teneral adult curve for a southern population of MPB determined by this paper. The gray cloud of curves is a plot of rate curves created using the 1500 bootstrapped parameters of Tree 2, indicating a substantially different rate curve for the southern vs. northern MPB population. The lines above and below the northern MPB curve indicate the maximum and minimal variability expected, which is still far different than the southern MPB rate curve.
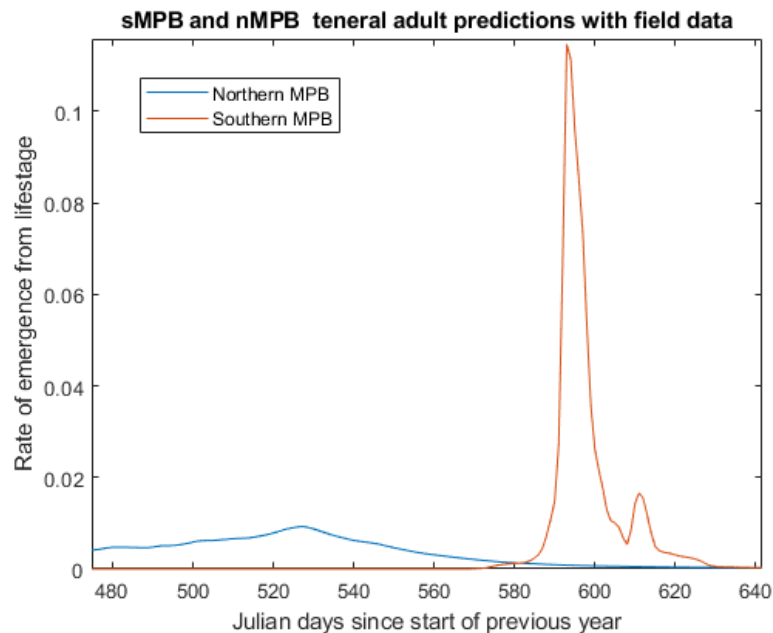
Fig. 3.29: Emergence distributions, calculated using the cohort model with the northern MPB teneral adult rate curve of Régnière et al. (2012) and the southern MPB teneral adult rate curve developed in this paper. The northern MPB rate curve results in emergence that is unseasonably early and noticeably unsynchronized due to a lower T_m and r_{max}.

from the bootstrapped data, or the final parameterized curve, overlap with the northern MPB rate curve within the temperature thresholds (Figure 3.28).

We also wanted to compare the predicted emergence between the southern and northern MPB using the corresponding teneral rate curve in the southern population cohort model with the same MPB attack and phloem temperature data. Due to the lower temperature thresholds and higher rate, northern MPB began to emerge much earlier than southern MPB, and nearly all emergence occurred before the actual timing of emergence (Figure 3.29). Much of this early emergence also occurs during the winter, which would result in pupal mortality and poorly timed adult emergence.

3.6.2   Possibility of Bivoltinism

One of the goals for our model was to determine the potential of bivoltinism as temperatures warm. Due to the ecological and economic effects of MPB *Pinus* mortality, bivoltinism could have devestating effects. Not only would there be two generations of MPB, but the second generation would be unaffected by winter mortality. The timing of MPB generations is a key part of possible bivoltinism, as cold tolerance is developed at during larval lifestages. Since the physiology of developing cold tolerance is complex and mortality occurs at different temperatures for different populations, we focused on the inability of eggs and pupae to survive at freezing temperatures.

Using the 2015 field data as input we increased the mean phloem temperatures and, using the output of one generation as input for the second generation, calculated the median date of the second generation emergence (Figure 3.30). Initially, as temperatures increased, the median day of second emergence decreased. However, the median day begins to increase at 5.0 degrees as temperatures above the upper temperature threshold result in decreased teneral rates. The earliest date of median emergence was October 30th for 5.0-5.5 °C added. Not only are MPB unable to fly at cooler temperatures, eggs must be laid early enough in the season for the MPB to be in the proper life stage (larvae or brood adult) to avoid mortality at freezing temperatures, with previous research suggesting eggs laid after August 30th would not survive (Powell and Bentz 2009). October 30th is seasonally inappropriate,
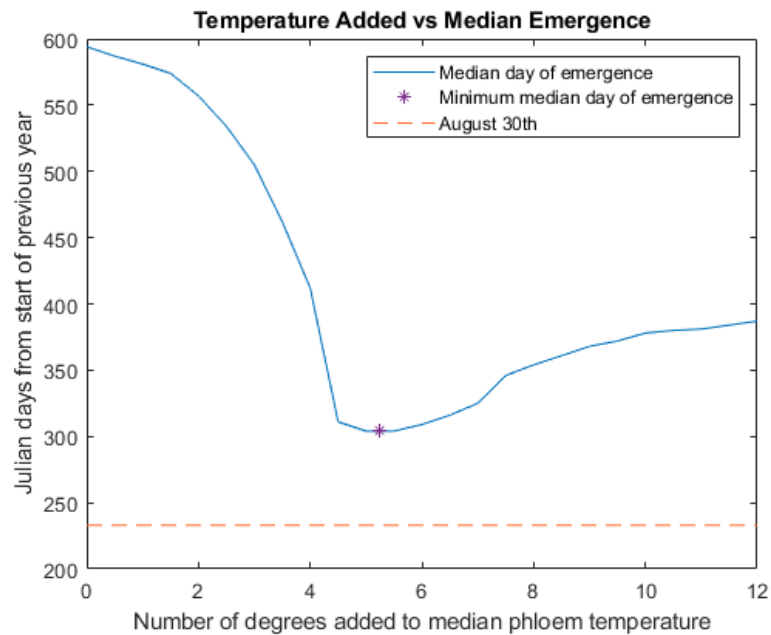
Fig. 3.30: The plot of median date of a second (bivoltine) southern MPB population using the parameterized teneral adult rate curve, and increasing the mean of the field phloem temperature data. While generation time initially decreases with increasing temperature, it reaches a minimum median day of emergence at 304 (October 30th), when 5°are added.. This date is far too late for successful MPB emergence. The model also indicates that further increasing temperatures could slow MPB teneral adult development as temperatures exceed the maximum temperature threshold.

suggesting that bivoltinism in southern MPB populations will not occur due to increased temperatures.

The details of MPB cold tolerance amongst life stages are more complex than simply measuring the median day of second emergence. Climate change is not directly comparable to across-the-board increases in mean temperature. We did not assess whether future generations could survive projected winter temperatures during more vulnerable MPB life stages. However, low developmental rates and the southern MPB phenology model indicates that the upper thermal threshold of teneral MPB development limits teneral adult emergence much later than required for successful bivoltinism, even without the possible limitations of development of other life stages.

3.7   Conclusion

In this paper we calibrate a suitable teneral adult rate curve for a southern population of MPB using field phloem temperatures, attack, and emergence data. We determined the most appropriate distribution of deviance between predicted and observed emergence via bootstrapping of emergence data. Model competition via AIC as indicated that the Brière rate curve was the best rate curve for available data. Cross-validation between the two trees, as well as parameter distributions, allowed us to choose the most suitable set of parameters. Validation was performed with an additional tree, indicating that, despite limited data, the model was able to predict southern MPB emergence.

Using bootstrapping, we were able to compare a spectrum of possible teneral adult rate curves to a previously developed curve for a northern popualtion of MPB, as well as model the differences in emergence between the parameterized Brière curve and the northern curve. This analysis indicated that southern MPB have clearly different maximum rates and thresholds, which allows them to maintain synchronous emergence under warmer temperatures. Modeling the possibility of bivoltinism using the southern MPB teneral adult rate curve in the EvF cohort model suggests that southern MPB are unlikely to become bivoltine with warmer temperatures. However, a more refined approach which takes into account temperatures at specific life stages could be helpful, since MPB life stages experience

cold mortality at variable cold temperatures.

Climate change has the potential to affect insect seasonality differently across latitudes. While previous research showed that southern and northern MPB populations must have differing teneral adult rates, a teneral adult rate curve for a southern population of MPB had not been developed in order to determine possible changes in MPB voltinism. This paper determined a suitable teneral adult rate curve with significantly narrower temperature thresholds and lower maximum rates, with the consequences that bivoltinism is unlikely to occur in a southern population of MPB under warmer temperatures.

CHAPTER 4

CONCLUSION

The mountain pine beetle (MPB, *Dendroctonus ponderosae* Hopkins Coleoptera: Scolytidae) attacks *Pinus* trees across a large area in western North America (Dowle et al. 2017), succeeding in a thermal niche that synchronizes development, allowing for mass attacks that overwhelm host defenses, and avoids winter mortality. The ability to predict temperature dependent lifestage events, particularly those that vary across a thermal-geographic niche, is critical to understanding MPB responses and preventing ecological and economic damage. McManis et al. (2018) parameterized developmental models for the egg through pupal stage of a southern population, and while those differed from parameters found for northern populations (Régnière et al. 2012), they did not fully describe the observed difference in generation time for southern MPB developing in northern temperatures (Bentz et al. 2001). Southern MPB are more likely to experience significant warming and possible changes in voltinism, but prior to this thesis there was not a complete phenological model.

In this thesis I developed a phenological model for a southern MPB population, introducing a novel oviposition model that incorporates varying rates and fecundity, as well as parameterized development of the teneral adult stage in southern MPB for the first time. The southern MPB oviposition models provided in Chapter 2 provide a basis not only for those populations, but other insects with temperature dependent thresholds that have variable rate and fecundity. The MPB ovipositon model can be used in a phenological model for the entire life cycle, and the phenological model allows for determination of a suitable teneral adult rate curve for a southern population of MPB in Chapter 3.

In Chapter 2 I introduced a method for determining the time delay before oviposition, t_0, incorporating previous data in order to create the first predictive model for this life phase. I also developed a novel oviposition model that uses lognormal variability in fecundity and normal variability in oviposition rate, and derived a simpler asymptotic approximation of the

oviposition model. These models address the unique challenges of predicting phenology for a southern population of MPB, and were parameterized with and compared to oviposition data collected in the lab by McManis et al. (2018) as well as other previously used models.

The time required to complete the egg-free gallery, t_0, was best predicted assuming independence from the oviposition rate. Temperature thresholds of oviposition were found to be significantly different than the thresholds for the rate to egg-free distance. Correspondingly, using oviposition rates created large predictive errors near the temperature thresholds. The independent model more accurately described the egg-free distance, and differences in rate parameters was affirmed via bootstrapping of the t_0 data.

I compared the new oviposition models, MPBovi, its asymptotic approximation, as well as the previously used median and cohort (EvF) models, to McManis's lab data at constant temperatures of 10, 20, 27, or 29°C over a thirty day period. Though both models have their positives and negatives, they compared more favorably to the lab data than the previously used median and EvF models. This was not an independent comparison, as the rate parameters of the oviposition rate curve used in each model were determined via this data, but it allowed for validation of the other aspects of the models. Oviposition is difficult if not impossible to observe in the field as it occurs in the phloem underneath the bark, and consequentially it was not possible to compare the output of the models directly to data from the field. Overall the asymptotic model was the best fit for the laboratory data with the highest R^2 values, but this might change with a larger sample size. The derived MPBovi model included the variability of both fecundity and rates, and this variability would be less captured by a smaller sample size. Further investigation would be worthwhile to determine if the predictive power of MPBovi is more useful in larger-scale real world settings, as both sources of variability have been clearly observed (McManis et al. 2019). Even so, the asymptotic model is much simpler and computationally efficient, and may be more practically useful if the difference in predictive accuracy remains small.

In Chapter 3 I used field phloem temperatures, attack, and emergence data from a southern population of MPB to determine and parameterize teneral adult rate curves. A

Laplace distribution was determined to most appropriately reflect the deviance between predicted and observed emergence via bootstrapping of emergence data. Nominal fits and model competition via AIC found that the Brière rate curve was the best fitting rate curve for the data from the two trees used. The distributions of the parameters for the two trees used, as well as cross-validation between the trees, allowed for confident selection of a single set of parameters. Validation was successfully performed with an additional tree, confirming that even with the limited data that the model is able to accurately predict southern MPB teneral adult emergence.

I was able to compare the bootstrapping results of the parameterized Brière curve, as well as the other teneral adult rate curves that were considered, to a previously parameterized rate curve for a northern population of MPB. The distributions of parameters indicate that the southern MPB have significantly different temperature thresholds and maximum rates than northern MPB, with lower rates that allow them to maintain synchonous emergence under warmer temperatures. I also modeled the possibility of bivoltinism by increasing the mean temperature of the field phloem data using the EvF cohort model with the southern MPB teneral adult rate curve. This assessment indicated that bivoltinism is unlikely in a southern MPB population, as the upper thresholds of development create a minimum median day of emergence of October 30th that is far too late in the year for survival of MPB eggs and pupae. A more thorough assessment which takes into account the exposure of these life stages to freezing temperatures would be worth exploring, and very possibly make the date of October 30th even less feasible.

Changes in temperature due to climate change have the potential to affect insect seasonality differently across latitudes, and while previous research has shown that northern and southern MPB populations have different developmental rates, particularly in the teneral adult stage, a complete phenological was not present due to the absence of teneral adult stage parameters. The parameterized teneral adult curve in this thesis, in addition to the oviposition model which incorporates varying fecundity, allows a complete cohort-based phenological model to predict the southern MPB life cycle. This phenological model

indicates that southern MPB populations have adapted to warmer temperatures and are unlikely to successfully complete a bivoltine life cycle, and that there are significant differences between the southern and northern MPB teneral adult stage. The model presented in this thesis can be used for forest management and prediction as changing climate continues to affect MPB and other insect populations.

Bibliography

Amman, G. D. (1972). Some Factors Affecting Oviposition Behavior of the Mountain Pine Beetle1. *Environmental Entomology*, *1*(6), 691–695. https://doi.org/10.1093/ee/1.6.691

Armendáriz-Toledano, F., Torres-Banda, V., & Zúñiga, G. (2017). The Current Status of *Dendroctonus ponderosae* Hopkins (Coleoptera: Curculionidae: Scolytinae) in Mexico. *The Coleopterists Bulletin*, *71*(3), 565–570. https://doi.org/10.1649/0010-065X-71.3.565

Arora, V. K., Peng, Y., Kurz, W. A., Fyfe, J. C., Hawkins, B., & Werner, A. T. (2016). Potential near-future carbon uptake overcomes losses from a large insect outbreak in British Columbia, Canada. *Geophysical Research Letters*, *43*(6), 2590–2598. https://doi.org/https://doi.org/10.1002/2015GL067532

Bentz, B. J., Logan, J. A., & Vandygriff, J. C. (2001). Latitudinal variation in *Dendroctonus ponderosae* (Coleoptera: Scolytidae) development time and adult size. *The Canadian Entomologist*, *133*(3), 375–387. https://doi.org/10.4039/Ent133375-3

Bentz, B. J., Duncan, J. P., & Powell, J. A. (2016). Elevational shifts in thermal suitability for mountain pine beetle population growth in a changing climate. *Forestry*, *89*(3), 271–283. https://doi.org/10.1093/forestry/cpv054

Bentz, B. J., Logan, J. A., & Amman, G. D. (1991). Temperature-dependent development of the mountain pine beetle (Coleoptera: Scolytidae) and simulation of its phenology. *The Canadian Entomologist*, *123*(5), 1083–1094. https://doi.org/10.4039/Ent1231083-5

Bentz, B. J., & Powell, J. A. (2014). Mountain Pine Beetle Seasonal Timing and Constraints to Bivoltinism: A Comment on Mitton and Ferrenberg, "Mountain Pine Beetle Develops an Unprecedented Summer Generation in Response to Climate Warming." *The American Naturalist*, *184*(6), 787–796. https://doi.org/10.1086/678405

Bleiker, K. P., & Smith, G. D. (2019). Cold Tolerance of Mountain Pine Beetle (Coleoptera: Curculionidae) Pupae. *Environmental Entomology*, *48*(6), 1412–1417. https://doi.org/10.1093/ee/nvz116

Bleiker, K. P., Smith, G. D., & Humble, L. M. (2017). Cold Tolerance of Mountain Pine Beetle (Coleoptera: Curculionidae) Eggs From the Historic and Expanded Ranges. *Environmental Entomology*, *46*(5), 1165–1170. https://doi.org/10.1093/ee/nvx127

Bonhomme, R. (2000). Bases and limits to using 'degree day' units. *European Journal of Agronomy*, *13*(1), 1–10. https://doi.org/10.1016/S1161-0301(00)00058-7

Brière, J.-F., Pracros, P., Le Roux, A.-Y., & Pierre, J.-S. (1999). A Novel Rate Model of Temperature-Dependent Development for Arthropods. *Environmental Entomology*, *28*(1), 22–29. https://doi.org/10.1093/ee/28.1.22

Burnham, K. (2002). *Model selection and multimodel inference: A practical information-theoretic approach*. Springer.

Cobbold, C. A., & Powell, J. A. (2011). Evolution stabilises the synchronising dynamics of poikilotherm life cycles. *Bulletin of Mathematical Biology*, *73*(5), 1052–1081. https://doi.org/10.1007/s11538-010-9552-1

Cole, W. E. (1962). The effects of intraspecific competition withing mountain pine beetle broods under laboratory conditions. *Res. Note 97. Ogden, UT: USDA Forest Service Intermountain Forest and Range Experiment Station.*

Corbett, L., Withey, P., Lantz, V., & Ochuodho, T. (2015). The economic impact of the mountain pine beetle infestation in British Columbia: Provincial estimates from a CGE analysis. *Forestry An International Journal of Forest Research*, 1–6. https://doi.org/10.1093/forestry/cpv042

Davidson, J. (1944). On the Relationship between Temperature and Rate of Development of Insects at Constant Temperatures. *Journal of Animal Ecology*, *13*(1), 26–38. https://doi.org/10.2307/1326

Dowle, E. J., Bracewell, R. R., Pfrender, M. E., Mock, K. E., Bentz, B. J., & Ragland, G. J. (2017). Reproductive isolation and environmental adaptation shape the phylogeography of mountain pine beetle *Dendroctonus ponderosae*. *Molecular Ecology*, *26*(21), 6071–6084. https://doi.org/https://doi.org/10.1111/mec.14342

Embrechts, P., & Hofert, M. (2013). A note on generalized inverses. *Mathematical Methods of Operations Research*, *77*(3), 423–432. https://doi.org/10.1007/s00186-013-0436-7

Gilbert, E., Powell, J., Logan, J., & Bentz, B. (2004). Comparison of three models predicting developmental milestones given environmental and individual variation. *Bulletin of Mathematical Biology*, *66*(6), 1821–1850. https://doi.org/10.1016/j.bulm.2004.04.003

Giroday, H.-M. C. d. l., Carroll, A. L., & Aukema, B. H. (2012). Breach of the northern Rocky Mountain geoclimatic barrier: Initiation of range expansion by the mountain pine beetle. *Journal of Biogeography*, *39*(6), 1112–1123. https://doi.org/https://doi.org/10.1111/j.1365-2699.2011.02673.x

Hansen, E. M., Bentz, B. J., Powell, J. A., Gray, D. R., & Vandygriff, J. C. (2011). Prepupal diapause and instar IV developmental rates of the spruce beetle, *Dendroctonus rufipennis* (Coleoptera: Curculionidae, Scolytinae). *Journal of Insect Physiology. 57(10): 1347-1357.*, 1347–1357. Retrieved April 20, 2021, from https://www.fs.usda.gov/treesearch/pubs/39259

Hopper, K. R. (1999). Risk-Spreading and Bet-Hedging in Insect Population Biology. *Annual Review of Entomology*, *44*(1), 535–560. https://doi.org/10.1146/annurev.ento.44.1.535

Ives, A. R. (1989). The Optimal Clutch Size of Insects When Many Females Oviposit Per Patch. *The American Naturalist*, *133*(5), 671–687. https://doi.org/10.1086/284944

Janz, N. (2002). Evolutionary ecology of oviposition strategies. In. T. M. M. Hilker (Ed.), *Chemoecology of insect eggs and egg deposition.* (pp. 349–376). Blackwell.

Logan, J. (2013). *Applied mathematics*. Wiley.

Logan, J. A., Bolstad, P., Bentz, B. J., & Perkins. (1995). Assessing the effects of changing climate on mountain pine beetle dynamics. *Proceedings of a Joint IUFRO Working Party Conference (ed. by FP Hain, SM Salom,WF Ravlin,TL Payne & KF Raffa)*, 86–108.

Logan, J. A., Wollkind, D. J., Hoyt, S. C., & Tanigoshi, L. K. (1976). An Analytic Model for Description of Temperature Dependent Rate Phenomena in Arthropods 1. *Environmental Entomology*, *5*(6), 1133–1140. https://doi.org/10.1093/ee/5.6.1133

Logan, J. A., & Bentz, B. J. (1999). Model Analysis of Mountain Pine Beetle (Coleoptera: Scolytidae) Seasonality. *Environmental Entomology*, *28*(6), 924–934. https://doi.org/10.1093/ee/28.6.924

Logan, J. A., & Powell, J. A. (2001). Ghost Forests, Global Warming, and the Mountain Pine Beetle (Coleoptera: Scolytidae). *American Entomologist*, *47*(3), 160–173. https://doi.org/10.1093/ae/47.3.160

Logan, J. A., Régnière, J., & Powell, J. A. (2003). Assessing the impacts of global warming on forest pest dynamics. *Frontiers in Ecology and the Environment*, *1*(3), 130–137. https://doi.org/10.1890/1540-9295(2003)001[0130:ATIOGW]2.0.CO;2

McManis, A. E., Powell, J. A., & Bentz, B. J. (2018). Developmental parameters of a southern mountain pine beetle (Coleoptera: Curculionidae) population reveal potential source of latitudinal differences in generation time. *The Canadian Entomologist*, *151*(1), 1–15. https://doi.org/10.4039/tce.2018.51

McManis, A. E., Powell, J. A., & Bentz, B. J. (2019). Modeling mountain pine beetle (*Dendroctonus ponderosae*) oviposition. *Entomologia Experimentalis et Applicata*, eea.12783. https://doi.org/10.1111/eea.12783

Meddens, A. J. H., Hicke, J. A., & Ferguson, C. A. (2012). Spatiotemporal patterns of observed bark beetle-caused tree mortality in British Columbia and the western United States. *Ecological Applications*, *22*(7), 1876–1891. https://doi.org/https://doi.org/10.1890/11-1785.1

Powell, J. A., & Bentz, B. J. (2009). Connecting phenological predictions with population growth rates for mountain pine beetle, an outbreak insect. *Landscape Ecology*, *24*(5), 657–672. https://doi.org/10.1007/s10980-009-9340-1

Powell, J. A., & Logan, J. A. (2005). Insect seasonality: Circle map analysis of temperature-driven life cycles. *Theoretical Population Biology*, *67*(3), 161–179. https://doi.org/10.1016/j.tpb.2004.10.001

Régnière, J., Powell, J., Bentz, B., & Nealis, V. (2012). Effects of temperature on development, survival and reproduction of insects: Experimental design, data analysis and modeling. *Journal of Insect Physiology*, *58*(5), 634–647. https://doi.org/10.1016/j.jinsphys.2012.01.010

Reid, R. W., & Gates, H. (1970). Effect of temperature and resin on hatch of eggs of the mountain pine beetle (*Dendroctonus ponderosae*). *The Canadian Entomologist*, *102*(5), 617–622. https://doi.org/10.4039/Ent102617-5

Sahota, T. S., & Thomson, A. J. (1979). Temperature induced variation in the rates of reproductive processes in *Dendroctonus rufipennis* (Coleoptera: Scolytidae): A new approach to detecting changes in population quality. *The Canadian Entomologist*, *111*(9), 1069–1078. https://doi.org/10.4039/Ent1111069-9

Sambaraju, K. R., Carroll, A. L., & Aukema, B. H. (2019). Multiyear weather anomalies associated with range shifts by the mountain pine beetle preceding large epidemics. *Forest Ecology and Management*, *438*, 86–95. https://doi.org/10.1016/j.foreco.2019.02.011

Soderberg, D. N., Mock, K. E., Hofstetter, R. W., & Bentz, B. J. (2021). Translocation experiment reveals capacity for mountain pine beetle persistence under climate warming. *Ecological Monographs*, *91*(1). https://doi.org/10.1002/ecm.1437

Thomas, C. D., Cameron, A., Green, R. E., Bakkenes, M., Beaumont, L. J., Collingham, Y. C., Erasmus, B. F. N., de Siqueira, M. F., Grainger, A., Hannah, L., Hughes, L., Huntley, B., van Jaarsveld, A. S., Midgley, G. F., Miles, L., Ortega-Huerta, M. A., Townsend Peterson, A., Phillips, O. L., & Williams, S. E. (2004). Extinction

risk from climate change. *Nature*, *427*(6970), 145–148. https://doi.org/10.1038/nature02121

APPENDICES

APPENDIX A

MPB Field Data

Julian Day	Tree 1	Tree 2	Tree 3
216	0	9	33
218	0	4	7
221	0	0	81
222	0	1	46
224	0	5	61
226	0	39	60
229	0	73	27
231	0	20	24
233	0	11	19
236	0	1	2
238	0	1	2
240	0	2	0
244	0	0	0

Table A.1: Attack data from three trees in Lockett Meadows, Cococino National Forest, AZ, 2015.

Julian day	Tree 1	Tree 2	Tree 3
214	0	0	0
217	0	0	0
221	0	0	0
223	1	0	0
228	41	0	0
231	79	8	0
234	40	24	0
236	37	23	0
238	20	11	0
242	18	7	0
244	1	4	0
249	5	2	0
252	0	1	0
257	0	1	0

Table A.2: Attack data from three trees in Lockett Meadows, Cococino National Forest, AZ, 2016.

Julian Day	1N	1S	2N	2S	3N	3S
210	0	0	0	3	2	0
215	0	0	0	1	0	0
218	0	0	0	0	0	0
222	1	2	5	3	0	0
224	7	0	4	1	2	0
229	14	7	6	29	23	19
232	51	1	3	33	0	0
235	34	6	41	8	4	1
237	12	1	3	4	1	0
239	37	2	36	2	6	0
243	39	4	25	1	5	0
245	15	4	11	0	2	0
250	1	0	15	1	0	0
253	0	0	0	0	0	0

Table A.3: Emergence data from three trees in Lockett Meadows, Cococino National Forest, AZ. Trees were attacked in 2015 and observance was observed in 2016.

Juliday Day	1N	1S	2N	2S	3N	3S
192	0	0	0	0	0	0
195	0	1	0	1	0	0
199	0	0	1	0	0	0
202	0	0	2	0	0	0
206	0	0	0	2	0	0
212	1	5	0	0	0	0
213	0	0	0	0	0	0
215	3	2	0	0	0	1
216	0	2	0	0	0	0
219	6	7	0	0	0	0
221	5	5	0	0	0	0
223	17	7	0	0	0	0
225	15	5	0	0	0	0
227	5	0	0	0	0	0
229	0	3	0	0	0	0
231	0	6	0	0	0	0
233	0	1	0	0	0	1
235	0	0	0	0	0	1
244	0	0	0	0	0	2

Table A.4: Emergence data from three trees in Lockett Meadows, Cococino National Forest, AZ. Trees were attacked in 2016 and observance was observed in 2017.

APPENDIX B

Code for Major Models

B.1   Southern MPB Oviposition Model Code

```
function [y] = ovipos(NUMFEMALES,TAUS,PHLOEM_TEMPS,START_DAY)
%     Creates MPB oviposition PDF for an Arizona population with given
%     temperature, population inputs, with terms accounting for the
%     accumulation of variance across temperatures. This model is derived
%     from the McManis et al (2019) oviposition rate model. Parameters for
%     getrates() are the Southern MPB population oviposition parameters
%     in this thesis.
%
%     Number of attacking females given as a row vector (NUMFEMALES).
%     Length should beequal and corresponding to TAUS.
%
%     Attack days (TAUS) given as a row vector in Julian days corresponding
%     to NUMFEMALES.
%
%     START_DAY is first Julian day of PHLOEM_TEMPS records.
%
%     PHLOEM_TEMPS is phloem temperatures as column vector given in C
%     degrees for each hour of a year, starting at midnight on START_DAY.
%     Vector should extend at least 45 days past TAUS(end).
%
%     %% Example command use %%
```

```
%
%          numfemales = [9 4 1 5 39 73 20 11 1 1 2];
%          taus = [216 218 222 224 226 229 231 233 236 238 240];
%          phloem = ones(1,17520).*25;
%          startday = 168;
%          output = ovipos(numfemales,taus,phloem,startday)
%
%
%% Define variables and Initialize Matrices


%Oviposition parmaters
p =[0.0913    0.0309    6.6000    30.9000    1.3613    1.9889]
% d value for calculation of t0
d = 1;
eggfree = 1;
%Sigma from McManis et al. 2019 paper
q= 0.32;
%Creating uniform vector of f-values
fvalues = linspace(0.05,0.95,19);
%Creating vector of taus from input TAUS
taus = TAUS;
%Vector for number of females created from NUMFEMALES for weighting PDFs
numfemales = NUMFEMALES;
%Initializing matrices
all = [];
final = [];


%% Creating time/temp vector that begins at START_DAY
```

```
%defining dt

dt=(1/24);

%First day of time is start date for phloem temps

tmin= START_DAY;

%Last day is day of last attack plus 45 days

tmax=TAUS(end)+45;

%nt is number of blocks needed

nt=(tmax-tmin)/dt+1;

%Time separated in units of days but in increments of hours

t=linspace(tmin,tmax,nt);

%Eliminate last block that is extra

t(end)= [];

 %Create vector of phloem temps for tmin-tmax above

T = PHLOEM_TEMPS(1:length(t));


%% Calculate rates, cumulative rates, t0 (delay time)

%Calculate oviposition rates

rates = getrates(T,p(1,:));

%Get cumulative sum of rates

cumrates = dt.*cumtrapz(rates);

%Taking the integral that will be later used for delay times

int = cumtrapz(getrates_t0(T)).*dt;

%Define taus for the tau loop

usetau = TAUS;


%Begin loop which creates PDFs for each tau

for m = 1:length(usetau)

    tau = usetau(1,m);
```

```matlab
%Find index of tau in t
tau_index=find(t>=tau,1);
%Find the index value for end of egg-free distance excavation
endeggfreeindex = find((int - int(tau_index))>=eggfree,1);
%Use that index to find the day t0 ends, subtract tau to get t0
t0 = t(endeggfreeindex)-tau;


%Calculate cumulative rates R with delay time removed
if isempty(endeggfreeindex)== 1
    R = 0;
    t0 =0;
else
     R=max(0,cumrates-cumrates(endeggfreeindex));
end %End of R calculation
% Loop calculating PDFs for uniform f for current tau
    %Loop to calculate PDFs for uniform f vector
    for k = 1:length(fvalues)
        %Use specific f for loop
        f = fvalues(k);
        %Create tt to avoid division by zero below
        tt=max(dt,(t-tau-t0));
        %Epsilon used in PDF calculation
        eps = (R+log(f))./tt;
        %Derivative of epsilon used in PDF calcuation
        deps = (t>t0+tau).*abs(-(R+log(f))./(tt.^2)+(rates./tt) );
        %PDF calculation
        PDF =(1/sqrt(2.*pi.*q.*q)).*exp(((-1./(2.*q.*q)).*(eps.^2))).*deps;
        %Normalization of PDF
```

```
        nPDF = PDF./trapz(PDF*dt);

        %Placing PDF for specific f in a matrix

        all(k,:)=nPDF;

    end %of calculation for uniform f vector


    %Sum down columns to get resultant P(some egg)

    p_egg=sum(all);

    %Normalize PDF

    p_egg=p_egg./(trapz(p_egg*dt));

    %Place PDF for this tau in final matrix

    final(size(final,1)+1,:) = p_egg;


end %of tau loop

%% Weighting and normalization of PDF for input tree

%Weighting by number of starting NUMFEMALES

tree = diag(numfemales(1,:))*final;

%Summing PDF for all taus

tree = sum(tree);

%Normalizing PDF

tree = tree./(trapz(tree)*dt);

%% Reshape PDF from hours to days and correctly size vector for vfpredmodel

%Reshape vector into matrix where each column is a day

treematrix = reshape(tree,24,tmax-tmin);

%Sum to get PDF in terms of days

treeday = dt*sum(treematrix);

%Create vector of length required for vfpred

treeinput = zeros(1,730);

%Place final PDF in vector
```

```
treeinput(1:(length(treeday)))=treeday;


[y] = treeinput;                                %Define output


function [rates] = getrates(T,p)
% Rates function as seen in Régnière et al (2012) and McManis et al (2009).
% T is temperature vector
% p is vector of parameters from McManis thesis pg 62 (2018)
% p(1) = omega
% p(2) = Psi
% p(3) = Tb
% p(4) = Tm
% p(5) = DeltaB
% p(6) = DeltaM
[rates] = max(0, p(2).*((exp(p(1).*(T-p(3))))-(((p(4)-T)./(p(4)-p(3)))...
.*exp(((-1*p(1)*(T-p(3)))./p(5)))-(((T-p(3))./(p(4)-p(3)))...
.*exp((p(1).*(p(4)-p(3)))-((p(4)-T)./p(6)))))));


function [rates] = getrates_t0(tmps)
% Rates function as seen in Régnière et al (2012) and McManis et al (2009).
% T is temberature vector
% p is vector of parameters from McManis et al, (2018)
% b(1) = omega
% b(2) = Psi
% b(3) = Tb
% b(4) = Tm
% b(5) = DeltaB
% b(6) = DeltaM
```

```
b = [0.0632    0.1773    5.8992   29.6069  2.5514   2.7269];

[rates] = max(0, b(2).*((exp(b(1).*(tmps-b(3))))-(((b(4)-tmps)...

./(b(4)-b(3))).*exp((-1*b(1)*(tmps-b(3)))./b(5)))-(((tmps-b(3))...

./(b(4)-b(3))).*exp((b(1).*(b(4)-b(3)))-((b(4)-tmps)./b(6)))))));
```

B.2 Southern MPB Phenology Model Code

```
function [y]=vfpredmodel(NUMFEMALES, TAUS, START_DAY, PHLOEM_TEMPS)
%       Predict MPB phenology for an Arizona population with given
%       temperature, population inputs, with terms accounting for
%       the accumulation of variance across temperatures and life
%       stages.
%
%       Number of attacking females given as a row vector
%       (NUMFEMALES). Length should be equal and corresponding to
%       TAUS.
%
%       Attack days (TAUS) given as a row vector in Julian days
%       corresponding to NUMFEMALES.
%
%       START_DAY is first Julian day of PHLOEM_TEMPS records.
%
%       PHLOEM_TEMPS is phloem temperatures as column vector given
%       in C degrees for each hour of a year, starting at midnight
%        on START_DAY. Vector should be 2*24*365=17520 hrs long.
%
%       Example command use:
%           numfemales = [9 4 1 5 39 73 20 11 1 1 2];
%           taus = [216 218 222 224 226 229 231 233 236 238 240];
%           phloem = ones(1,17520).*25;
%           startday = 168;
%           time2=[startday:(startday+729)];
%           pout=vfpredmodel(numfemales, taus, startday, phloem);
%           figure
```

```
%           plot(time2,pout)
%           legend('Oviposition','Egg','L1','L2','L3','L4', ...
%           'Pupae','Adult Emergence')
%
%% Input Parameters %%


%Matrix of rates parameters for southern population
global p        %Set p to global so it can be used by ovipos()
% p = [omega    Psi         Tb          Tm          DeltaB      DeltaM]
%     except for p(8,:), teneral adult
p =[0.0913      0.0309      6.6000      30.9000     1.3613      1.9889
    %Oviposition
    0.2045      0.0326      6.0251      31.9309     0.5410      5.5031
    %Eggs
    0.1517      0.0521      4.6029      31.7661     0.0117      5.4256
    %First Instar
    0.1374      0.0431      5.9791      31.8337     0.0413      4.4534
    %Second Instar
    0.1856      0.0170      6.0115      31.2656          0      4.3079
    %Third Instar
    0.1694      0.0545      14.9990     31.4364          0      5.2947
    %Fourth Instar
    0.1658      0.0166      6.3504      30.8041          0      3.5426
    %Fifth Instar
%   r_max       T_b         T_m
    0.0197      11.3539     27.2079     NaN         NaN         NaN];
    %Teneral adult (Brière curve)
```

```
% Set variance parameters

sigma=[ 0.032              %Oviposition

       0.038               %Eggs

       -0.2182             %First Instar

       0.1524              %Second Instar

       0.165               %Third Instar

       0.1354              %Fourth Instar

       0.0673              %Pupae

       0.0009];            %Teneral Adult


%Calculation of nus from sigma

nus= (sigma.^2)./2;


%% Defining time vectors %%

tmps=PHLOEM_TEMPS;

%Define temperature as input temperature

nh=24;

%Number of hours in a day

ndays=365+365;

% 2*365 = 730, 2 years of time

nt=nh*ndays;

%Total number of hours in 730 days

tmin=START_DAY;

%Smallest time is start day of phloem temps

tmax=ndays+tmin;

%Max day is two years from start date

dt=(tmax-tmin)/nt;

%Time step (1hr)
```

```
tmps=reshape(tmps,nh,ndays);

%Reshape temperatures so each column is a whole day of data

treal=linspace(tmin,tmax-(tmax-tmin)/ndays,ndays);

%Real time vector that begins at tmin

tcalc=treal-tmin;

%Time vector that starts at zero - convenient for setting up

%convolution matrix

tol=1e-8;

%Tolerance used for numerical calculations




%% Lifestage calculations


%Use oviposition model for first input

pout=zeros(8,ndays);

%Initialize matrix for output of emergence distributions

pinput = ovipos(NUMFEMALES,TAUS,PHLOEM_TEMPS,START_DAY);

%Call oviposition model for initial input

pout(1,:)= pinput;

%First distribution is ovipositing adults (istg=1)


%Calculate rates and integrate variabilities for each stage

for istg=2:8

    %get rates for current stage:
        %eggs
    if (istg == 2)
        rates = getrates(tmps, p(2,:));
```

```
    %L1
elseif (istg == 3)

    rates = getrates(tmps, p(3,:));

    %L2
elseif (istg == 4)

    rates = getrates(tmps, p(4,:));

    %L3
elseif (istg == 5)

    rates = getrates(tmps, p(5,:));

    %L4
elseif (istg == 6)

    rates = getrates(tmps, p(6,:));

    %Pupae
elseif (istg == 7)

    rates = getrates(tmps, p(7,:));

    %Adult emergence/teneral adult
else (istg == 8);

    rates=(briere(tmps,p(8,:)));


end %of calculating rates for current stage


rates=sum(rates);
% add up developmental increment for this day by summing over
% hours in the day (down columns)
crates=dt*cumtrapz(rates);
% cumulative rates over days for this stage
crates1=1-crates;
% to make the calculation efficient
```

```
nu=nus(istg);

% variance for this stage


%pre-calculate some factors which will be used over and over

%in loop for efficiency

texp(2:ndays)=1./(4*nu*tcalc(2:ndays));

%1/denominator of exp of Green's function

tden(2:ndays)=1./sqrt(4*nu*pi*tcalc(2:ndays).^3);

%1/sqrt(stuff) of Green's function



% the following loop  integrates the contribution of variance

% for non-constant temperatures by summing along diagonals

% in an upper triangular matrix


for i=1:ndays-1


    i1=i+1:ndays;


    % pttau is the Green's function which weights the

    % contributions of variances and development

    pttau=exp(-texp(i1-i+1).*(crates1(i1)+crates(i)).^2).*tden(i1-i+1);


    %because of singularity in pttau it is wise to normalize

    wts=trapz([0 pttau]);

    if (wts<tol)

        % don't normalize those pttaus which are just small

        wts=1;
```

```
        end % of normalization


        pout(istg,i1)=pout(istg,i1)+pttau*pinput(i)/wts;


    end % of integrating variance


    pinput=pout(istg,:);
    % input for next life stage is end of last stage


end % of life stage calculations
y=pout; %Output


%% Functions called by vfpredmodel %%
%%%%%%%%%%%%%%%%%%%%%%%%%%%%%%%%%%%%


function [y] = ovipos(NUMFEMALES,TAUS,PHLOEM_TEMPS,START_DAY)
%     Creates MPB oviposition PDF for an Arizona population with given
%     temperature, population inputs, with terms accounting for the
%     accumulation of variance across temperatures. This model is derived
%     from the McManis et al (2019) oviposition rate model. Parameters for
%     getrates() are the Southern MPB population oviposition parameters
%     in this thesis.
%
%     Number of attacking females given as a row vector (NUMFEMALES).
%     Length should beequal and corresponding to TAUS.
%
%     Attack days (TAUS) given as a row vector in Julian days corresponding
%     to NUMFEMALES.
```

```
%
%      START_DAY is first Julian day of PHLOEM_TEMPS records.
%
%      PHLOEM_TEMPS is phloem temperatures as column vector given in C
%      degrees for each hour of a year, starting at midnight on START_DAY.
%      Vector should extend at least 45 days past TAUS(end).
%
%      Example command use: Using the same inputs as vfpredmodel(), the PDF
%      can be plotted using a time vector created similiarly to lines 196
%      to 201.
%
%% Define variables and Initialize Matrices
    global p
% d value for calculation of t0
d = 1;
eggfree = 1;
%Sigma from McManis et al. 2019 paper
q= 0.32;
%Creating uniform vector of f-values
fvalues = linspace(0.05,0.95,19);
%Creating vector of taus from input TAUS
taus = TAUS;
%Vector for number of females created from NUMFEMALES for weighting PDFs
numfemales = NUMFEMALES;
%Initializing matrices
all = [];
final = [];
```

```
%% Creating time/temp vector that begins at START_DAY
%defining dt
dt=(1/24);
%First day of time is start date for phloem temps
tmin= START_DAY;
%Last day is day of last attack plus 45 days
tmax=TAUS(end)+45;
%nt is number of blocks needed
nt=(tmax-tmin)/dt+1;
%Time separated in units of days but in increments of hours
t=linspace(tmin,tmax,nt);
%Eliminate last block that is extra
t(end)= [];
 %Create vector of phloem temps for tmin-tmax above
T = PHLOEM_TEMPS(1:length(t));


%% Calculate rates, cumulative rates, t0 (delay time)
%Calculate oviposition rates
rates = getrates(T,p(1,:));
%Get cumulative sum of rates
cumrates = dt.*cumtrapz(rates);
%Taking the integral that will be later used for delay times
int = cumtrapz(getrates_t0(T)).*dt;
%Define taus for the tau loop
usetau = TAUS;


%Begin loop which creates PDFs for each tau
for m = 1:length(usetau)
```

```
tau = usetau(1,m);

%Find index of tau in t

tau_index=find(t>=tau,1);

%Find the index value for end of egg-free distance excavation

endeggfreeindex = find((int - int(tau_index))>=eggfree,1);

%Use that index to find the day t0 ends, subtract tau to get t0

t0 = t(endeggfreeindex)-tau;


%Calculate cumulative rates R with delay time removed

if isempty(endeggfreeindex)== 1

    R = 0;

    t0 =0;

else

     R=max(0,cumrates-cumrates(endeggfreeindex));

end %End of R calculation


% Loop calculating PDFs for uniform f for current tau

   %Loop to calculate PDFs for uniform f vector

   for k = 1:length(fvalues)

       %Use specific f for loop

       f = fvalues(k);

       %Create tt to avoid division by zero below

       tt=max(dt,(t-tau-t0));

       %Epsilon used in PDF calculation

       eps = (R+log(f))./tt;

       %Derivative of epsilon used in PDF calcuation

       deps = (t>t0+tau).*abs(-(R+log(f))./(tt.^2)+(rates./tt) );

       %PDF calculation
```

```
        PDF =(1/sqrt(2.*pi.*q.*q)).*exp(((-1./(2.*q.*q)).*(eps.^2))).*deps;

        %Normalization of PDF

        nPDF = PDF./trapz(PDF*dt);

        %Placing PDF for specific f in a matrix

        all(k,:)=nPDF;

    end %of calculation for uniform f vector


    %Sum down columns to get resultant P(some egg)

    p_egg=sum(all);

    %Normalize PDF

    p_egg=p_egg./(trapz(p_egg*dt));

    %Place PDF for this tau in final matrix

    final(size(final,1)+1,:) = p_egg;


end %of tau loop

%% Weighting and normalization of PDF for input tree

%Weighting by number of starting NUMFEMALES

tree = diag(numfemales(1,:))*final;

%Summing PDF for all taus

tree = sum(tree);

%Normalizing PDF

tree = tree./(trapz(tree)*dt);


%% Reshape PDF from hours to days and correctly size vector for vfpredmodel

%Reshape vector into matrix where each column is a day

treematrix = reshape(tree,24,tmax-tmin);

%Sum to get PDF in terms of days

treeday = dt*sum(treematrix);
```

```
%Create vector of length required for vfpred
treeinput = zeros(1,730);
%Place final PDF in vector
treeinput(1:(length(treeday)))=treeday;


[y] = treeinput;                                    %Define output



function [rates] = getrates(T,p)
% Rates function as seen in Régnière et al. (2012)
% and McManis et al. (2018).
% T is temperature vector
% p is vector of parameters from McManis et al. (2018)
% p(1) = omega
% p(2) = Psi
% p(3) = Tb
% p(4) = Tm
% p(5) = DeltaB
% p(6) = DeltaM
[rates] = max(0, p(2).*((exp(p(1).*(T-p(3))))-(((p(4)-T) ...
./(p(4)-p(3))).*exp((-1*p(1)*(T-p(3)))./p(5)))- ...
(((T-p(3))./(p(4)-p(3))).*exp((p(1).*(p(4)-p(3)))-...
((p(4)-T)./p(6)))))));


function [y] = briere(tmps,p)
%Brière curve for teneral adult rates
% p = p(8,:)
% p = (rmax, T_B, T_M)
```

```
%Example code:

% % p = [0.0197 11.3539 27.2079];

% % T = linspace(0,40,100);

% % output = briere(T,p);

% % plot(T,output)

m=2;  %for sqrt Brière

Tb=p(2); a=p(1); Tm=p(3);

% find the curve's max using Brière formula:

Topt=(2*m*Tm+(m+1)*Tb+ sqrt( 4*m^2*Tm^2+(m+1)^2*Tb^2- ...

4*m^2*Tb*Tm))/(4*m+2);

% value at max, to normalize the shape function to peak of 1

norm=Topt.*( Topt -p(2) ).*(( abs(1-(Topt./p(3))) ).^0.5);

% now the max rate is exactly the parameter a=p(1);

r = a.*tmps/norm.*( tmps -Tb ).*(( abs(1-(tmps./Tm)) ).^0.5);

output = r.*(tmps>=p(2)).*(tmps<=p(3));

% make sure output is zero outside developmental range

[y] = output;


function [rates] = getrates_t0(tmps)

% Rates function as seen in Régnière et al (2012) and McManis et al (2009).

% T is temberature vector

% b is vector of barameters from McManis thesis bg 62 (2018)

% b(1) = omega

% b(2) = Psi

% b(3) = Tb

% b(4) = Tm

% b(5) = DeltaB

% b(6) = DeltaM
```

```
b = [0.0632    0.1773    5.8992    29.6069   2.5514    2.7269];
[rates] = max(0, b(2).*((exp(b(1).*(tmps-b(3))))-(((b(4)-tmps)...
./(b(4)-b(3))).*exp((-1*b(1)*(tmps-b(3)))./b(5)))-(((tmps-b(3))...
./(b(4)-b(3))).*exp((b(1).*(b(4)-b(3)))-((b(4)-tmps)./b(6)))))));
```